# Potential and Limitations of MCM-41 in Dechlorination Reactions

by

Colin P. Guthrie

A thesis
presented to the University of Waterloo
in fulfillment of the
thesis requirement for the degree of
Master of Science
in
Earth Sciences

Waterloo, Ontario, Canada, 2006

I hereby declare that I am the sole author of this thesis. This is a true copy of the thesis, including any required final revisions, as accepted by my examiners.

I understand that my thesis may be made electronically available to the public.

## Abstract

The purpose of this thesis was to conduct preliminary research into the feasibility of using MCM-41 as a catalyst support material in the treatment of organochloride contaminated water. Specifically, the stability of MCM-41 in water and its efficiency as a Pd metal catalyst support in the degradation of trichloroethylene (TCE) was examined.

MCM-41 is a mesoporous siliceous material that was developed by scientists with the Mobile Corporation in 1992. Since its development, MCM-41 has been the subject of a great deal of research into its potential application in catalytic sciences. The material possesses two especially notable characteristics. First, the diameter of its pores can be adjusted between 2 and 10 nm depending on the reagents and procedure used in its synthesis. Second, MCM-41 has an exceptionally high surface area, often in excess of 1 000 $m^2/g$ in well-formed samples. Other researchers have succeeded in grafting a variety of different catalytic materials to the surfaces and pores of MCM-41 and reported dehalogenation reactions proceeding in the presence of hydrogen. Thus, MCM-41 shows promise in treating a variety of chlorinated volatile organic compounds (cVOCs), such as chlorinated benzenes, trichloroethylene (TCE), perchloroethylene (PCE) and some polychlorinated biphenyls (PCBs).

Preliminary stages of this research were devoted to synthesising a well-formed sample of MCM-41. The method of Mansour *et al.* (2002) was found to be a reliable and repeatable procedure, producing samples with characteristic hexagonal crystallinity and high surface areas. Crystallinity of all materials was characterized by small angle X-ray powder diffraction (XRD). Samples of MCM-41 prepared for this research exhibited a minimum of three distinct peaks in their XRD traces. These peaks are labelled 100, 110, and 200 according to a hexagonal unit cell. The 100 peak indicates that the sample is mesoporous. The 100, 110, and 200 peaks together indicate a hexagonal arrangement of the mesopores. An additional peak, labelled 210, was also observed in materials prepared for this research, reflecting a high degree of crystallinity. The position of the 100 peak was used to calculate the unit cell parameter - "a" - of the samples according to Bragg's Law. The value of the unit cell parameter corresponds to the centre to centre distance of the material's pores and thus the relative diameter of the pores themselves. The unit cell parameter of samples prepared for this research ranged from 4.6 nm

to 5.3 nm with an average value of 4.8 nm. Surface areas of prepared samples were determined by BET nitrogen adsorption analysis and ranged from 1 052 to 1 571 $m^2/g$ with an average value of 1 304 $m^2/g$. Field emission scanning electron microscope (SEM) images of a representative sample of MCM-41 revealed a particle morphology referred to as 'wormy MCM-41' by other researchers.

A sample of aluminum-substituted MCM-41 (Al-MCM-41) was also synthesized. The crystallinity of Al-MCM-41 was characterized by small angle XRD. The XRD trace of the material showed only one distinct peak centred at 2.1 degrees 2θ. The 110 and 200 peaks seen in MCM-41 were replaced by a shoulder on the right hand side of the 100 peak. The shape of this trace is typical of Al-MCM-41 prepared by other researchers and is indicative of the lower structural quality of the material, i.e. a less-ordered atomic arrangement in Al-MCM-41 compared to that of regular MCM-41. The unit cell parameter of the Al-MCM-41 sample was 4.9 nm. The surface area of the sample was determined through BET nitrogen adsorption analysis and found to be 1 304 $m^2/g$.

Attempts were made to synthesize an MCM-41 sample with enlarged pores. Difficulties were encountered in the procedure, specifically with regards to maintaining high pressures during the crystallization stage. Higher temperatures used during these procedures caused failure of the O-ring used in sealing the autoclave, allowing water to be lost from the reaction gel. Samples generated in these attempts were amorphous in character and were subsequently discarded.

A solubility study involving MCM-41 was undertaken to determine the stability of the material in water at ambient temperature and pressure. The experiment included several different solid/water ratios for the dissolution experiments: 1/200, 1/100, 1/75, 1/25. Results indicated that MCM-41 is metastable at ambient temperatures and more soluble than amorphous silica in water. The maximum silica concentration observed during the experiment was used to calculate a minimum Gibbs free energy of formation for MCM-41 of - 819.5 kJ/mol. The higher free energy value compared to quartz (- 856.288 kJ/mol) is indicative of the metastability of the material in water. Supersaturation with respect to amorphous silica was observed in samples prepared with relatively high concentrations of MCM-41. A subsequent

decrease in dissolved silica concentration with time in these samples represented precipitation of amorphous silica, driving the concentration downward towards saturation with respect to this phase (120 ppm). The equilibrium concentration of 120 ppm recorded in these samples represented 4.8 mg out of 200, 400, 500, and 1 600 mg of initial MCM-41 dissolving into solution in the solid/liquid ratios of 1/200, 1/100, 175, and 1/25, respectively. Supersaturation with respect to amorphous silica did not occur in experiments with very low solid/water ratios. It also did not occur in higher solid/water experiments from which the $SiO_2$ saturated supernatant was decanted and replaced with fresh deionized water after two weeks of reaction. The difference in dissolution behaviour is believed to result from deposition of a protective layer of amorphous silica from solution onto the MCM-41 surfaces, which reduces their dissolution rate. Thus, supersaturation with respect to amorphous silica is only manifested at early time and only when relatively large amounts of fresh MCM-41 are added to water.

The solubility experiment was repeated using samples of Al-MCM-41 to determine the effect of Al substitution on the stability of the MCM-41. Dissolution curves for the Al-MCM-41 samples revealed behaviour that was analogous to that of the silica-based MCM-41 at similar solid/water ratios. Substitution of Al into the structure of MCM-41 appeared to have no positive or negative effects on the stability of the material in water.

Solid MCM-41 material was recovered on days 28 and 79 of the solubility experiment and dried under vacuum. Solid material was also recovered from the Al-MCM-41 solubility experiment on day 79. These recovered samples were characterized by XRD and BET nitrogen adsorption analysis. An increase in background noise in the XRD plot of MCM-41 from the fresh to the 79 d sample indicated an increased proportion of an amorphous phase in the sample. The XRD plot of the 79 d sample of Al-MCM-41 also showed increased background noise corresponding to an increased proportion of an amorphous phase. The increased amorphous phase would have resulted from the continuous dissolution of the crystalline MCM-41 and reprecipitation as amorphous silica in the samples. BET surface area analysis of recovered MCM-41 compared to the freshly prepared material showed no significant change in surface area after 28 and 79 days in water. Analysis of the 79 d Al-MCM-41 indicated a 10% decrease in surface area relative to the as-prepared material. A set of SEM images were taken of the day 28 and 79 MCM-41 samples and compared to a sample of freshly prepared material.

No substantial change in morphology was observed in the day 28 sample when compared to the fresh material. Some change was noted in the day 79 sample particle morphology, with worm-like structures appearing to be better developed than in the as-synthesized material.

A series of palladized MCM-41 (Pd/MCM-41) samples with varying mass percent loadings of Pd was prepared to investigate the dehalogenation efficiency of Pd/MCM-41 in contact with TCE. TCE degradation was investigated in batch experiments. MCM-41 samples were prepared with calculated Pd loadings of 0.1, 1, and 5 mass %. The actual palladium content of the materials was determined using an EDAX-equipped SEM. The success of the loading technique was better at lower mass loadings of Pd, i.e. there was a greater deviation of actual Pd content from targeted or calculated contents at higher loadings of Pd. It was found that a procedure designed to yield 1% by mass Pd/MCM-41 produced an average loading of 0.95% Pd by mass. A procedure designed to produce a 5% Pd/MCM-41 sample resulted in an average loading of 2.6 mass %. These deviations were attributed to error inherent in the EDAX analysis and reduced effectiveness of the loading technique at higher Pd concentrations.

All batch experiment reaction bottles were prepared with solid/liquid ratios of 1/800. The various Pd/MCM-41 samples induced rapid dehalogenation reactions, with the maximum extent of TCE degradation occurring before the first sample was taken at 7 to 12 min and within 35 min in the case of 0.1% Pd/MCM-41. The 0.1% Pd/MCM-41 sample degraded 70% of total TCE in solution with an estimated degradation half-life of 14 min. The 1% Pd/MCM-41 sample degraded 92% of total TCE in solution with an estimated half life of between 3 and 6 min. The 5% Pd/MCM-41 sample degraded only 22% of total TCE in solution; degradation half-life could not be determined. The seemingly paradoxical result of lower degradation efficiency at higher Pd loadings is proposed to result from absorption of hydrogen from solution by Pd, which is unreactive relative to the dissolved hydrogen in solution. Production of reaction intermediates and daughter products was also lower in the 1% by mass Pd/MCM-41 experiment compared to the 0.1 and 5% by mass Pd/MCM-41. Analysis of degradation products results from the experiments indicated that TCE degrades to ethane in the presence of Pd/MCM-41 with relatively low concentrations of chlorinated daughter products resulting from a random desorption process. A batch experiment using pure silica MCM-41 was also conducted to determine if there was adsorption of TCE to the support material itself. A lack of

change in TCE concentration between the control sample and the MCM-41 sample during the experiment indicated no significant adsorption of TCE onto MCM-41.

The conclusion of this research is that although MCM-41 is relatively unstable in water, its high TCE degradation efficiency shows promise for its application in developing water treatment technologies. However, more research needs to be conducted to fully determine the potential use of MCM-41 in water treatment and to investigate ways to improve its long-term stability in water.

**Acknowledgements**

I thank my supervisor Dr. Eric J. Reardon for his guidance and considerable insight into many aspects of this project and science in general. My time under his supervision has vastly improved my abilities as a researcher, writer, and scientist.

I extend my appreciation to my thesis committee members Dr. Robert Gillham, Dr. Hartwig Peemoeller, and John Vogan for their suggestions and input into this work.

Thank you: Dr. Jamal Hassan and Dr. Firas K. Mansour for their help in synthesizing and understanding MCM-41; Lorretta Pinder and Dr. Gui Lai for their conversations with me about chlorinated compounds and TCE degradation; Wayne L. Nobel, Brian Ellis, Nina Heinig, Zhenhua He, and Ralph D. Dickhout for their assistance with the analytical aspects of this thesis; Mark Hall and Randy Fagan for their help in understanding the mysteries of geochemical laboratory research; and Sue Fisher for always being helpful and answering my many questions.

To my family, whose love, support, and advice over the years have made all the difference in my life.

The author wishes to acknowledge funding for this project provided by ETECH (Ontario Centre of Excellence), Envirometal Technologies Inc, NSERC (Natural Sciences and Engineering Research Council of Canada).

**Table of Contents**

**List of Tables**

**List of Figures**

# 1. INTRODUCTION

## 1.1 Background

Since the late 1970s an increasing amount of research has been devoted to the study and treatment of chlorinated compounds in groundwater. These compounds were traditionally used in many different industrial and domestic applications as industrial solvents, dry cleaning solvents, degreasers, refrigerants, pesticides, dielectric fluids, as well as in pulp and paper, rubber, and plastics manufacturing (Gainza, 2004; Narayanan, 1995; Walbridge, 1983; Hohener, 2003; Dua, 2002; Richardson & Zheng, 1999; Ewald, 1998; Lesage, 1991; Abramowicz, 1993). Chlorinated compounds of human origin found in aquifers number into the thousands and include, but are not limited to: trichloroethene (TCE), dichloroethene (DCE), polychlorinated biphenyl (PCB), perchloroethene (PCE), and dichloromethane (DCM). Great quantities of these chemicals were released into the environment both accidentally and through improper disposal techniques. This has allowed significant quantities of chlorinated compounds to infiltrate into the subsurface, contaminating the vadose zone and groundwater aquifers in many industrialized countries. In an article by Page (1981) and summarized in Pankow & Cherry (1996) it was reported that 388 out of 669 wells tested in New Jersey were contaminated by TCE; 835 of 1071 by 1,1,1-TCA; and 179 of 421 by perchlorate. A study by Soeteman *et al.* (1981) and summarized in Pankow and Cherry (1996) reported that 67% of wells sampled in the Netherlands were contaminated by TCE; 43% by carbon tetrachloride; and 19% by PCE. The persistence of volatile organic compounds in groundwater flow systems is an unfortunate tribute to their long-term chemical stability and mobility in aqueous systems. The prime concern over their presence in groundwater is negative human health effects even at ppb concentrations for some of the more toxic compounds when the groundwater is used for drinking water supplies (Cothern *et al.*, 1986; Crosta & Dotti, 1998). Remediating this type of contamination requires a carefully-designed treatment system, as natural degradation is - in many applications - a very slow process.

There are currently three widely used methods for treatment of chlorinated compounds in groundwater: 1. *in situ* treatment using a permeable reactive barrier (PRB) of zero-valent iron (Gavaskar, 1999; Phillips, 2003; Gusmao, 2004), 2. pump-and-treat methods where

groundwater is brought to the ground surface, treated, and re-injected into the aquifer (Mackay & Cherry, 1989; Mackay, 2000), and 3. biodegradation where bacteria convert chlorinated compounds to relatively innocuous products (Brar & Gupta, 2000; Kao & Lei, 2000). In all three cases, inclusion of a catalyst in the system design can greatly improve the efficiency of the dehalogenation reactions taking place. A catalyst is a material that enhances the rate of a reaction and is either not consumed or is regenerated at the end of the reaction sequence. The advantages of using a catalyst in groundwater treatment, when compared to the uncatalyzed reaction are that it enhances reaction rates, reduces residual concentrations of the parent compound being treated, and reduces production of undesirable daughter products. Catalysts used in groundwater remediation programs include nickel, platinum, copper, zinc, and palladium. Palladium catalysts, in particular, have been shown to be very effective in dehalogenation reactions involving many of the common chlorinated groundwater contaminants (Li & Klabunde, 1998; McNab & Ruiz, 1998; Prati & Rossi, 1999; Mackenzie *et al.*, 2006).

The surface area of the catalyst used in a treatment system is important to the overall efficiency of the reaction. In general, the greater the surface area of the catalyst in contact with reagents during a reaction, the greater the potential catalytic activity. Maximizing the exposed surface area can be accomplished by adhering nanometer-scale sized particles of the catalyst to a support material. Adhering gold particles to $CeO_2$ for the purpose of aerobic oxidation of aldehydes provides an example of this technique (Corma & Domine, 2005). A great deal of recent catalytic research has been focused on developing catalyst supports with the largest possible surface area. In the early 1990s, scientists at the Mobile Corporation patented a novel, siliceous material with several interesting properties. The material is referred to as MCM-41, which is variously known as ‘Mobil Crystalline Material’ or ‘Mobil’s Composition of Matter’. MCM-41 is characteristically composed of a hexagonal arrangement of siliceous mesopores (Beck *et al.*, 1992; Hammond *et al.*, 1999). Perhaps the most important property of MCM-41 is its extremely high surface area. The surface area of as-synthesized MCM-41 can often be in excess of 1 000 $m^2/g$ (Cheng *et al.*, 1997). This presents an exciting possibility of improving the effectiveness of contaminant treatment as few other catalyst support materials have such high surface areas. Additionally, the pore size of MCM-41 can be adjusted from between two and 10 nm, depending on the reagents and procedure used in its synthesis (Corma *et al.*, 1997)

or through post-synthesis treatments (Kruk & Jaroniek, 1999; Sayari *et al.*, 2005). Different metal cations may also be incorporated into the MCM-41 structure by substitution with the silicon cation in the material's silica tetrahedra (Borade & Clearfild, 1995; Ziolek *et al.*, 2004). Okumara *et al.* (2003) palladized the pores and internal surfaces of MCM-14 and reported catalytic hydrogenation and dehalogenation reactions proceeding in the presence of hydrogen. Thus, Pd/MCM-41 shows promise in technologies for treating cVOC contaminated water.

This thesis will evaluate the potential of MCM-41 as a support for a transition metal catalyst (palladium) in the treatment of water contaminated with chlorinated compounds. The long term goal of this research is to develop a water treatment technology using the Pd/MCM-41 catalyst in conjunction with zero-valent iron, which functions as an electron source (Figure 1.1). The thesis is divided into two separate chapters, each examining a different aspect of MCM-41 as it relates to potential water treatment technologies. The first presents information and results regarding the synthesis of MCM-41 and related materials along with the results of an experiment to determine MCM-41 and Al-MCM-41 solubility in water. The second chapter is concerned with the preparation and catalytic TCE degradation efficiency of Pd/MCM-41. Each of the two chapters includes a section-specific introduction, background information, experimental methods, and results and discussion.

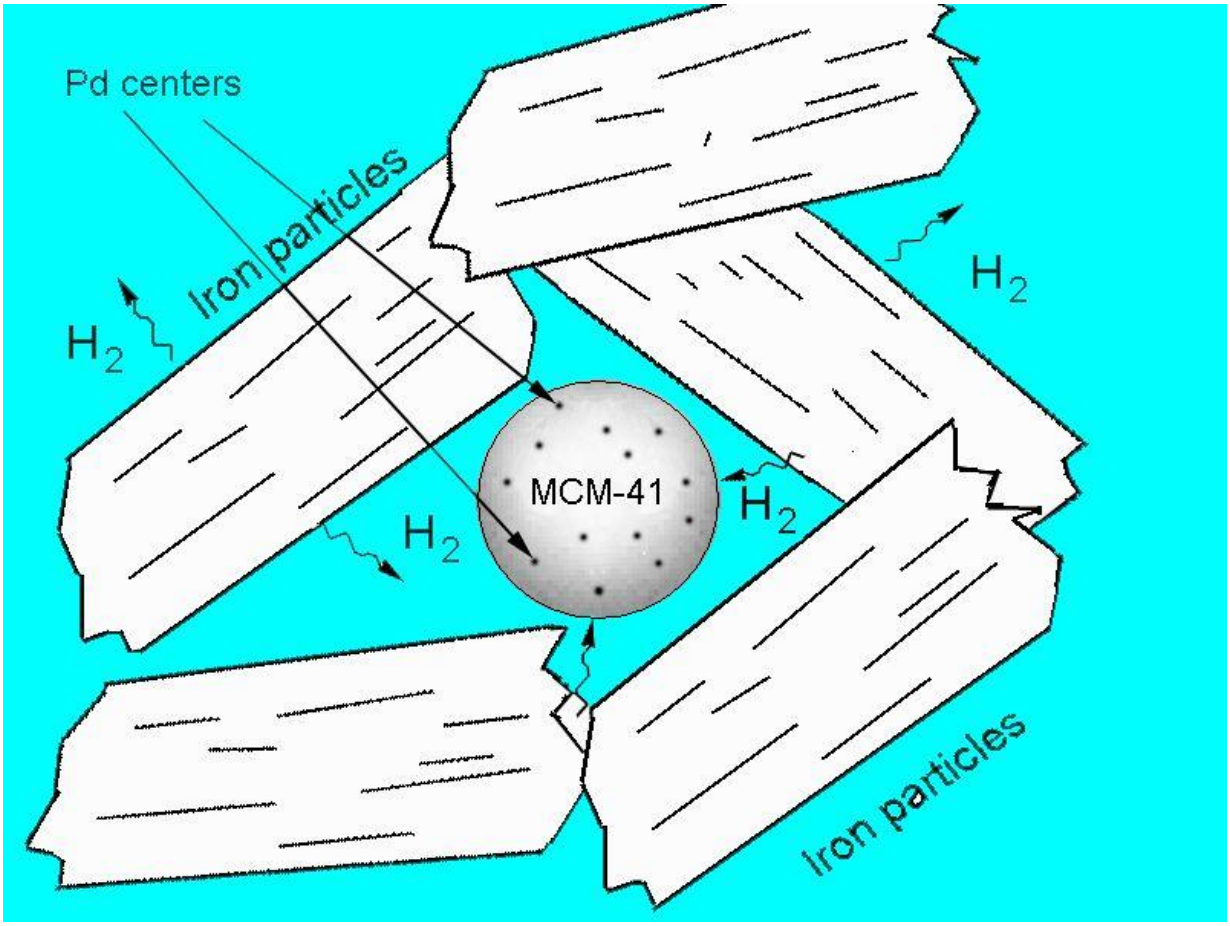


Figure 1.1: Representation of the Pd/MCM-41 catalyst and zero-valent iron technology (After Reardon, E. J. (2005) Presentation at the Waterloo/Dupont Iron Technology in Groundwater Remediation Meeting, Waterloo, March 30$^{th}$, 2005).

## 1.2 Thesis Objectives

This thesis was concerned with developing a new application for mesoporous MCM-41 in the context of catalytic reductive dechlorination reactions. The primary objectives of the research were to: 1) successfully synthesize MCM-41 and related materials; 2) determine the stability of MCM-41 in water and whether incorporation of Al into its structure improved its stability; 3) establish whether MCM-41 is a viable transition metal catalyst support for use in enhancing reductive dechlorination reactions by zero-valent iron; 4) add to research in the field of applying catalyst supports to improve current *in situ* or *ex situ* treatment methods of contaminants in groundwater.

The objectives were studied by:

- Refining procedures for synthesizing consistent batches of mesoporous, well-formed MCM-41 and Al-MCM-41.
- Conducting dissolution experiments on MCM-41 and Al-MCM-41 to determine their solubility characteristics and stability in aqueous solution.
- Refining procedures for loading Pd, a transition metal catalyst, on the surfaces and in the pores of previously synthesized MCM-41.
- Determining the effect of using an MCM-41 supported catalyst in conjunction with hydrogen in enhancing reductive dechlorination reactions.

## 2. MCM-41 AND ITS STABILITY IN WATER

### 2.1 Background

This section is concerned with the synthesis of MCM-41 materials and an investigation into the stability of MCM-41 and Al-MCM-41 under aqueous conditions at ambient temperature and pressure. If MCM-41 is to be used in groundwater treatment applications it should resist degradation by water. This chapter also serves as an introduction to the synthesis and unique characteristics of the MCM-41 material.

Studies related to MCM-41 began in 1992 when a group of scientists employed by the Mobile Corporation published a paper entitled "A New Family of Mesoporous Molecular Sieves Prepared with Liquid Crystal Templates" (Beck *et al.*, 1992). The paper described the synthesis and characterization of a new family of mesoporous molecular sieves to which they gave the name M41S. MCM-41 is a material belonging to this family. The material was an improvement over other mesoporous materials of the time, which were generally amorphous solids with irregularly spaced, non-uniform sized pores (Beck *et al.*, 1992). Freshly prepared MCM-41 presents as a loose, agglomerated white powder with low mechanical stability (Kumar *et al.*, 2001). It is the structure and properties of the material at the nanometre scale which have generated a great deal of interest in it and its many potential applications. The uniform size and shape of pores, large surface areas, and high thermal and hydrothermal stability are advantages of MCM-41 with respect to its potential use as a sorbent material and catalyst support (Koh *et al.*, 1997). There is some doubt as to whether MCM-41 possesses hydrothermal stability; an issue discussed in greater detail later in this section. It is also possible to substitute metal cations for silicon atoms within the silica tetrahedra of MCM-41's bulk structure, providing unique catalytic properties.

MCM-41 is a relatively straightforward material to produce under controlled laboratory conditions. The synthesis of the material is described in greater detail in Section 2.2.2. Beck *et al.* (1992) proposed that the process by which MCM-41 is formed during its synthesis follows a liquid crystal templating mechanism. The continuous solvent region in the synthesis gel – the deionized water – creates inorganic walls between the surfactant liquid crystal structures. The

resulting MCM-41 structure is defined by the organization of surfactant molecules into micellar liquid crystals which serve as structural templates. Two possible pathways for the formation of this final structure were described in the article: 1. Surfactant molecules were already ordered into the crystal structure – liquid crystal phase – before the addition of the silica source; 2. Addition of silica itself results in the formation and ordering of silica-encased surfactant micelles (Beck *et al.*, 1992; Holmes *et al.* 1998). Hammond *et al.* (1999) propose that the final structure of MCM-41 is controlled during synthesis by electrostatic charge matching between the organic surfactant (denoted as $S^+$ or $S^-$) and inorgranic precursor (denoted as $I^+$ or $I^-$). $S^+$ represents a quaternary ammonium ion in the case of MCM-41 synthesis. This matching may occur through direct ion pairing: $S^+ I^-$ or through triple ion formation: $S^+ X^- I^+$, where $X^-$ denotes the intermediate anion (Huo *et al.*, 1994).

A successful synthesis of MCM-41 produces a pure silica material composed by a hexagonal array of tubular channels of nearly uniform diameter, generally referred to as pores in the literature (Hammond *et al.*, 1999). Interconnections between the pores of MCM-41 are energetically unfavourable and the pore walls are made of an amorphous arrangement of silica tertrahedra (Kleestorfer *et al.*, 2001). A notable aspect of MCM-41 is that the diameter of the pores can be controlled through the carbon chain length of the surfactant used during synthesis (Letellier *et al.*, 2006; Kruk *et al.*, 1997; Horcajada *et al.*, 2004). Pore size may also be controlled through the addition of auxiliary organic reagents during synthesis (Beck *et al.*, 1992). Generally, the pore diameter of the material lies between values of 2 and 10 nm (Hammond *et al.*, 1999; Beck *et al.*, 1992). Post synthesis treatment of MCM-41 with organic compounds such as N,N-dimethylhexadecylamine has also been reported as a successful method for enlarging pore diameter (Kruk *et al.*, 1999; Sayari *et al.*, 2005). In their seminal article, Beck *et al.* (1992) reported that pore regularity decreases with increasing pore diameter. The relatively large pore size of MCM-41 can be compared with that of zeolites – another commonly used molecular sieve – which have diameters typically less than 1 nm (Kumar *et al.*, 2001; Mansour *et al.*, 2002).

The morphology of the MCM-41 particles depends on the reagents and synthesis procedure used. Particles in the form of hexagonal biscuits, hollow spheres, paintbrush bristles, wormy/rope-like masses, donuts, and half donuts have been described in various studies (Beck

*et al.*, 1992; Yuan, 2001; Han *et al.*, 2004; Gaydhankar, 2005). The surfaces of MCM-41 particles are dominated by silanol groups. These silanol groups may be classified as being one of three different varieties: single, $(SiO)_3Si\text{-}OH$; geminal, $(SiO)_2Si(OH)_2$; or hydrogen bonded, $(SiO)_3Si\text{-}OH\text{-}OH\text{-}Si(SiO)_3$. The surface density of these groups is approximately 2.5 to 3.0 groups/nm$^2$ and depends on the surfactant removal technique (Zhao *et al.*, 1997). Under ambient humidity levels, all silanol groups become involved in hydrogen bonding with water molecules (Trebosc *et al.*, 2005).

Perhaps the most important aspect of MCM-41 with regards to environmental catalysis is its exceptionally high surface area. In general, the greater the surface area of a catalyst contacting reagents during a catalytic reaction, the greater the efficiency of the reaction relative to the uncatalyzed reaction. Materials of the M41S family typically have surface areas greater than 700 m$^2$/g that enhance catalytic activity and adsorptive capacity (Beck *et al.*, 1992). Typically prepared MCM-41 can have surface areas in excess of 1 000 m$^2$/g (Cheng *et al.*, 1997; Mansour *et al.*, 2002; Run *et al.*, 2004; Zeng *et al.*, 2006). This may be compared to other catalytic materials and supports: between 535-648 m$^2$/g and 827 to 941 m$^2$/g for zeolites, depending on the material being characterized; 0.1 m$^2$/g to 54.2 m$^2$/g for hydroxyapatite; between 12 and 277 m$^2$/g for different forms of $Al_2O_3$; and 74 to 364 m$^2$/g for some bimetallic systems (Nam *et al.*, 1999; Saravanamurugan, 2006; Joschek *et al.*, 2000; Koutsopoulos, 2002; Liu, 2006; Lin *et al.*, 2004; Yu *et al.*, 1994; Fortuny *et al.*, 1999).

An additional advantage of MCM-41 is that the tetrahedrally-coordinated silicon atom in the silica tetrahedral composing the bulk of the material may be substituted for similarly sized and charged transition metal ions during synthesis or through post-synthesis impregnation. Metals successfully incorporated into MCM-41 include: Al, Cu, Fe, V, Ti, V, Cr, Mo, and Mn (Shen & Kawi, 2002; Long & Yang, 1999; Decyk, 2006; Zhang *et al.*, 1996). The substitution of metal cations into the MCM-41 structure creates a charge imbalance that is satisfied through incorporation of Na and H ions. The difference in size between these ions and the silicon they replace results in structural defects and a corresponding decrease in MCM-41 crystal quality (Shen and Kawi, 2002). Metal-substituted MCM-41 is useful in catalytic selective oxidation reactions and acid catalyzed reactions such as catalytic hydrocarbon reactions (Rajakovic *et al.*, 2003; Corma *et al.*, 1994; Kosslick *et al.*, 1999).

The material has been reported as having good stability below temperatures of 1 000 K and pressures of 100 MPa (Bai *et al.*, 2002). Other researchers are not so confident in their assessment of MCM-41 stability. Zheng *et al.* (2004) report poor hydrothermal stability and propose it results from the thinness and incomplete cross-linking of pore walls. Zhao *et al.* (1998) reported loss of structural features over three months of exposure to 60% humidity. The hydrothermal stability of MCM-41 may be improved through various methods including: improvement of sample crystallinity; minimization of surface silanol group density; pH adjustments and salt effects during synthesis; and finally, post synthesis restructuring procedures, which have been shown to be particularly effective (Mori *et al.*, 2002; Zheng *et al.*, 2004).

In summary, the adjustable pore size, large surface area per unit mass, and possibility of substituting metal cations for tetrahedrally-coordinated silicon atoms suggests MCM-41 is an ideal catalyst support material. Some doubt as to the stability of MCM-41 in water has been raised which would certainly limit the potential for its use in typical water treatment situations. The following sections of this chapter will describe the synthesis of MCM-41 and Al-MCM-41 and the results of experiments undertaken to determine their solubility in water.

## 2.2 Experimental Methods

### 2.2.1 Reagents

All reagents used for this research were of reagent grade quality. Nanopure® deionized water was used at all times with an average resistivity of 17.8 Mohms/cm. All prepared samples of MCM-41, Al-MCM-41, and Pd/MCM-41 were stored in tightly sealed Nalgene® LDPE and HDPE plastic bottles. MCM-41 samples were stored under air at ambient temperature, pressure, and humidity.

### 2.2.2 MCM-41 Preparation

The procedure used in producing batches of MCM-41 was based on the procedure of Mansour *et al.* (2002). Briefly, tetramethyl ammonium hydroxide pentahydrate (TMAOH) and cetyltrimethyl ammonium bromide (CTABr) were dissolved in 200 g of deionized water under gentle stirring at 300 K. Fumed silica powder was added once the opaque solution turned clear

and the resulting mixture was stirred and heated for 3 h. The final molar composition of the gel was 1.0 $SiO_2$, 0.19 TMAOH, 0.27 CTABr, 40 $H_2O$. Necessary masses of reagents were calculated on a basis of 200 g of water. The gel was covered with Parafilm and aged for 24 h at room temperature. The mixture was transferred to a stainless steel autoclave sealed with a Viton Teflon O-ring and heated for 68 h at 400 K. The reaction was stopped by quenching the autoclave under cold water for 30 min. The contents of the autoclave were transferred to plastic centrifuge bottles and washed, centrifuged, and decanted eight times or until conductance of the supernatant rinsate was less than 1 mS/cm. In practice, the rinsate conductance was generally less than 0.1 mS/cm. The slurry recovered from the centrifuge bottles was dried overnight at 320 K. Finally, the solid material was calcined for 8 h at 923 K to ensure complete removal of the organic template.

The mesoporosity and hexagonal structure of the various MCM-41 samples was verified by low angle x-ray diffraction analysis (XRD) between 1 and 10 degrees 2θ using a Bruker AXS D8 Advance X-ray diffractometer. Cell parameter "a" was calculated based on the 2θ position of the maximum intensity peak (100) on the XRD trace and Bragg's Law:

$$2d_{100}\sin\theta = n\lambda$$

$$a = (2/\sqrt{3}) * d_{100}$$

where n is an integer equal to 1 and the wavelength parameter λ is equal to 1.5418 Å. The value of the cell parameter is the pore centre-to-centre distance for the material and includes the pore radius and thickness of the pore walls (Beck *et al.*, 1992). As such, the value of the cell parameter corresponds to the relative pore diameter of the sample. Sample surface area was determined using a Micromeritics Gemini III 3275 Surface Area Analyzer following the Brunauer-Emmet-Teller isotherm (BET) nitrogen adsorption surface area technique. Morphology of a representative sample of the material was determined using a Leo 1530 Field Emission Scanning Electron Microscope (SEM).

### 2.2.3 Water Resistant MCM-41 Preparation

The phrase 'water resistant' refers to a sample of MCM-41 material that is relatively stable in water, i.e. possessing low solubility. An attempt was made to prepare a sample of water

resistant MCM-41 following the synthesis procedure described by Mori *et al.* (2002). The reagents and molar ratio were the same as those used in preparation of pure silica MCM-41, described in section 2.2.2. The only notable difference in the procedure was the temperatures and time intervals used during the gel aging stage of the synthesis. The reactant gel was placed in a stainless-steel autoclave sealed with a Viton Teflon O-ring and aged for 3 days at 308 K. The temperature was then increased to 413 K and the gel was allowed to age for an additional 3 days. The autoclave was then quenched under cold water for 30 min before being opened. The gel was removed from the autoclave and washed, centrifuged, and decanted eight times or until final conductivity of the rinsate was 1 mS/cm or less. A calcination was performed on the sample for 6 h at 873 K to remove any remnant of the organic template. The material was characterized by small angle X-ray diffraction.

### 2.2.4 Al-MCM-41 Preparation

A sample of aluminum substituted MCM-41 (Al-MCM-41) with a Si/Al molar ratio of 10 was prepared. The material was synthesized using a procedure based on those of Borade & Clearfield (1995) and Long & Yang (1999). Briefly, solution "A" was made by dissolving TMAOH in 100 g of deionized water to which was then added fumed silica powder. Solution "B" was made by dissolving NaOH in 100 g of deionized water to which was added CTACl and $Al_2O_3 \cdot Na_2O$. Both solutions were stirred for 15 min at which point solution A was slowly added to solution B followed by an additional 15 min of stirring. The final molar composition of the gel was 1.0 $SiO_2$, 0.05 $Al_2O_3$, 0.23 CTMACl, 0.11 $Na_2O$, 0.089 TMAOH, 125 $H_2O$. Necessary masses of reagents were calculated on a basis of 200 g of water. The mixture was transferred to a stainless steel autoclave sealed with a Viton Teflon O-ring. The autoclave was heated for 48 h at 373 K before the reaction was stopped by quenching with cold water for 30 min. The gel was transferred to plastic centrifuge bottles and washed, centrifuged, and decanted eight times. The recovered solid was allowed to dry overnight at 323 K followed by calcination under air for 10 h at 833 K to remove the organic template. The relevant properties of the material were examined using XRD and BET nitrogen adsorption surface area analyses.

### 2.2.5 Silica Dissolution Experiment Involving MCM-41

A series of plastic sample bottles were prepared in duplicate containing samples with solid/liquid ratios of regular MCM-41 and deionized water of 1/200 and 1/100. A sample blank was also prepared by filling a sample bottle with deionized water. An earlier experiment following the same procedure examined the solubility of MCM-41 at higher concentrations in water using solid/liquid ratios of 1/75 and 1/25. This earlier experiment also included sample bottles prepared with solid to liquid ratios of 1/200 and 1/100, which allowed the repeatability of the experiment to be verified.

The sample bottles were tightly sealed with threaded screw caps and mounted in a wheel configuration in an isotemperature bath. A schematic of the wheel and isotemperature bath setup is presented in figure 2.1. An aquarium heater was suspended in the bath and was controlled by a computer/data acquisition system to ensure a constant temperature of 298 K ± 0.1 K. An aquarium pump was directed at the horizontally-secured sample bottles to keep the wheel in rotation. This rotation ensured that MCM-41 particles would contact all of the solution in the sample bottle.

The samples and reaction blanks were analyzed for silica concentration as $SiO_2$ using a Pharmacia LKB Novaspec II spectrophotometer and the molybdate blue method. The experiment lasted 79 days and samples were taken at various intervals throughout the experiment. On day 18 of the experiment, the 1/200 and 1/100 solid to liquid ratio samples were allowed to settle for 30 min and the supernatant solution was decanted and the bottles refilled with fresh deionized water. This was done to determine if initial dissolution behaviour would be repeated. The duration of the earlier dissolution experiment using 1/200, 1/100, 1/75, and 1/25 solid to liquid ratios was 28 days and samples were taken at various points throughout the experiment.

Reaction bottles were left stationary and upright for 30 min before sampling to allow settling of any solid particles suspended in solution. Samples were taken by decanting 3 to 4 ml of the supernatant solution into a plastic syringe and passing it through a 0.2 μm Acrodisc® filter into a plastic 10 ml sample vial. The vials were tightly sealed with screw caps and stored at room temperature until being analyzed for $SiO_2$ concentration. A portion of the solid MCM-41

material was recovered on days 28 and 79 and dried under vacuum over a saturated KCl solution (80% relative humidity) at the end of the experiment. The properties of the recovered material were examined using XRD, BET nitrogen adsorption surface area, and SEM analyses and compared to those of freshly prepared MCM-41.

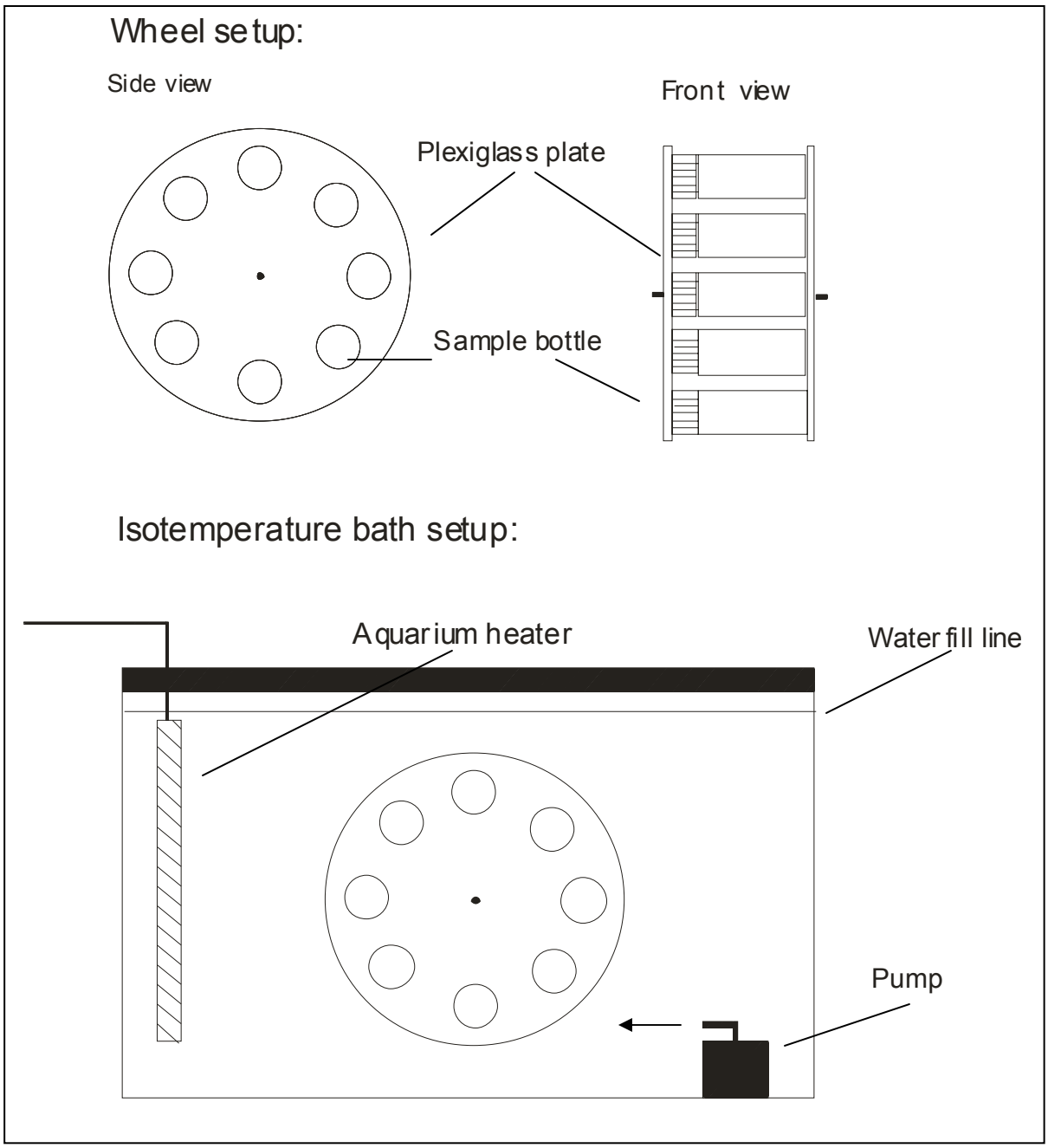


**Figure 2.1: Schematic illustrating the wheel and isotemperature bath setup for the dissolution experiments.**

### 2.2.6 Silica Dissolution Experiment Involving Al-MCM-41

Another series of sample bottles were prepared using Al-MCM-41 and deionized water and arranged in wheel configuration as in the MCM-41 solubility experiment described in Section 2.2.5. Sample bottles were prepared with solid to liquid ratios of 1/200, 1/100, and 1/75. This experiment was undertaken to determine the effect on stability of Al cation substitution into MCM-41 relative to regular MCM-41. Shen & Kawi (2002) proposed that Al incorporation into MCM-41 improved the material's resistance to degradation by hydrothermal treatments with steam at 873 K and boiling water.

The duration of the experiment was 79 d, with samples taken at intervals throughout the experiment. Sampling was performed using the same procedure as described for the regular MCM-41 dissolution experiment. A portion of solid Al-MCM-41 was recovered on day 79 of the experiment and dried under vacuum over a saturated KCl solution (80% relative humidity). The properties of the recovered material were examined by XRD and BET nitrogen adsorption surface area analyses and compared to those of the freshly prepared Al-MCM-41.

## 2.3 Results and Discussion

### 2.3.1 Pure Silica MCM-41

Four different samples of pure silica MCM-41 were prepared for this research. No problems were encountered during the syntheses and the physical properties of the final materials were comparable. It was found that maintaining pressure within the autoclave during the gel aging stage of the procedure was absolutely necessary to obtain a well-formed sample with high surface area. Loss of pressure during the gel aging stage resulted in samples of amorphous character. The final material produced by the procedure presents as a very fine white powder.

The four samples are identified as Aug. 29-05, Oct. 13-05-A, Oct. 13-05-B, and Aug. 22-06 and their relevant physical properties are presented in table 2.1. Results of the characterization of an Al-MCM-41 sample are also included in the table and described in greater detail in section 2.3.3. The samples identified as Oct.13-05-A and Oct. 13-05-B are of the same batch but were separated after the autoclave portion of the synthesis procedure due to an overflow of the reaction gel from the beaker inside the autoclave. Sample A was gel from within the beaker

while sample B was material that overflowed into the autoclave itself. They are labelled as two separate samples because characterization showed them as having slightly different physical properties.

**Table 2.1: Summary of MCM-41 samples' physical properties.**

| Sample ID | 2 θ of 100 peak | d100 | a (Angstroms) | a (nm) | surface area ($m^2$/g) |
|---|---|---|---|---|---|
| Aug. 29-05 | 2.24 | 39.4 | 46.4 | 4.6 | 1 090 |
| Oct. 13-05-A | 2.22 | 39.8 | 46.8 | 4.7 | 1 052 |
| Oct. 13-05-B | 2.18 | 40.5 | 47.6 | 4.8 | 1 571 |
| Aug. 22-06 | 1.97 | 44.8 | 52.7 | 5.3 | 1 504 |
| Al-MCM-41 | 2.13 | 41.4 | 48.7 | 4.9 | 1 304 |

Results of the XRD analysis for samples Aug. 29-05, Oct. 13-05-A, Oct. 13-05-B, and Aug. 22-06 were plotted as intensity versus $2\theta^o$. The XRD trace of Aug. 29-05 is presented as a representative plot in figure 2.2. Traces for the other samples may be found in Appendix A. The peaks of the plots are labelled according to a hexagonal unit cell. The lack of background noise and the presence of distinct, narrow peaks on the plots are evidence of a high degree of crystallinity in the samples. In all four of the plots, the presence of the 100 peak indicates that the sample is mesoporous. The 100, 110, and 200 peaks considered as a whole indicate that the pores are in a hexagonal arrangement. In addition, all four samples exhibit the 210 peak, the presence of which indicates an exceptionally high degree of crystallinity in the material (Mansour *et al.*, 2002). Calculation of the unit cell parameters indicated pore centre to centre distances of between 4.6 and 5.3 nm.

BET nitrogen adsorption surface area analysis indicated that the surface areas of the four MCM-41 samples ranged between 1 052 to 1 571 $m^2$/g with an average of 1 304 $m^2$/g.

A calculation was undertaken to estimate the proportion of silanol groups present at the surface in a given sample of the MCM-41 material (Appendix B). The calculation yielded a conservative estimate of 25% of the total silanol groups in MCM-41 being exposed at the surface. The surface density of silanol groups in MCM-41 has a strong influence on the adsorption behaviour of polar molecules such as $H_2O$ (Zhao *et al.*, 1997). Silanol groups also influence MCM-41's interactions with various other compounds such as acid groups, metal

complexes, and organic solvents such as methanol (Alvaro *et al.*, 2005; Sakthivel *et al.*, 2006; Takamuku *et al.*, 2005).

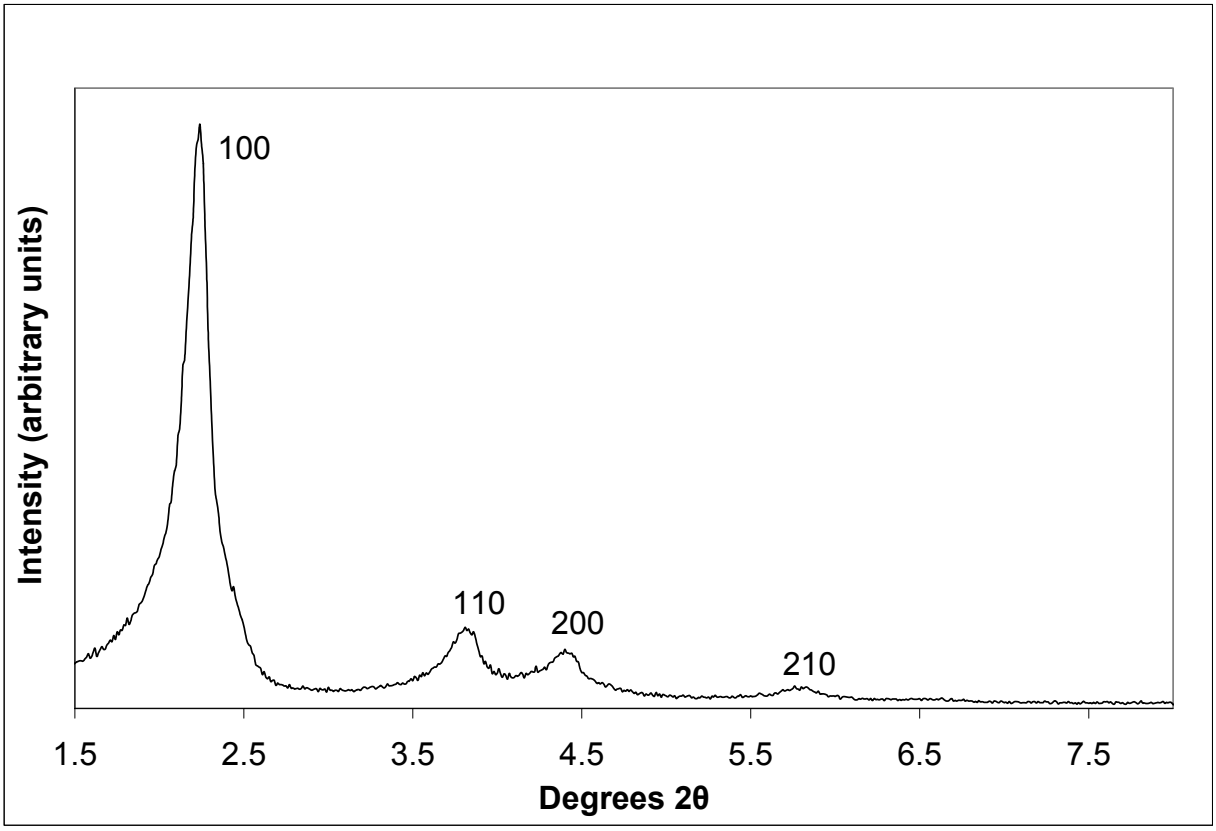


**Figure 2.2: XRD pattern of calcined Aug. 29-05 MCM-41.**

### 2.3.2 Water Resistant MCM-41 Preparation

Whether it is possible to produce an MCM-41 sample that is more stable in water following the Mori *et al.* (2002) procedure is questionable. The procedure and reactants are similar to those of the Mansour *et al.* procedure. The one notable difference in Mori *et al.*'s procedure was the temperature and time interval employed in the gel aging stage. It is possible that increased aging time and use of two different temperatures during this stage can yield a sample with a higher degree of crystallinity. If these temperatures and longer gel aging result in a higher degree of crystallinity in the material, this may in turn render the material more resistant to dissolution by water. Kittaka *et al.* (2005) support the findings of Mori *et al.*, proposing that the improved water-resistance of the material may result from a decrease in Na molecule

contamination in the MCM-41 lattice. Minimizing contamination would reduce imperfections in the MCM-41 structure resulting from inclusion of Na atoms and thus improve the material's crystallinity. However, a cursory citation search did not find any articles describing a successful synthesis of an MCM-41 sample that was more water resistant than standard MCM-41 following the procedure of Mori *et al.*

An attempt to synthesize a water resistant form of MCM-41 was unsuccessful. Upon opening the autoclave following the gel aging stage of the synthesis, the gel was found to be significantly more viscous than gels of other, successful MCM-41 preparation procedures. Regardless, the gel was collected, washed, centrifuged, and decanted 8 times.

Results of the XRD analysis showed only one identifiable peak. The poor quality of the XRD trace (not presented) indicated an amorphous sample lacking the hexagonal and mesoporous character of MCM-41. The synthesis was not repeated due to time constraints.

One possible reason for the failure in the synthesis of this particular sample would be a loss of pressure from the autoclave during the gel aging stage. This could result in evaporation of water and organic compounds from the autoclave, causing the gel to have the high viscosity observed upon opening the autoclave. As mentioned previously, maintaining high pressure within the autoclave during the gel aging stage was found to be crucial in obtaining a high surface area, mesoporous, and hexagonal MCM-41 sample.

### 2.3.3 Aluminum Substituted MCM-41 Preparation

One sample of Al-MCM-41 was synthesized for use in the silica dissolution experiment described in section 2.2.6. The purpose of the experiment was to determine if a more stable form of MCM-41 would result. The structure of the sample was determined using XRD analysis while the surface area was determined using the BET nitrogen adsorption technique. The relevant properties of this sample are listed along with those of the pure silica MCM-41 samples in table 2.1.

The XRD trace of the sample is presented in figure 2.3. The plot has only one discernible peak, labelled 100 as in the regular MCM-41 samples. The other two peaks that are characteristic of regular MCM-41 are replaced by a shoulder on the right hand side of the 100 peak. This

shoulder may represent an increased proportion of an amorphous phase in the sample. The XRD plot of this sample is consistent with Al-MCM-41 XRD plots published by other authors (Corma *et al.*, 1994; Kosslick *et al.*, 1999; Rahiala *et al.*, 1999). The pore centre to centre distance of the sample was calculated as being 4.9 nm. Results of a BET nitrogen adsorption analysis indicated a surface area of 1 304 $m^2/g$. It is concluded that this is a well-formed sample of the Al-MCM-41 material.

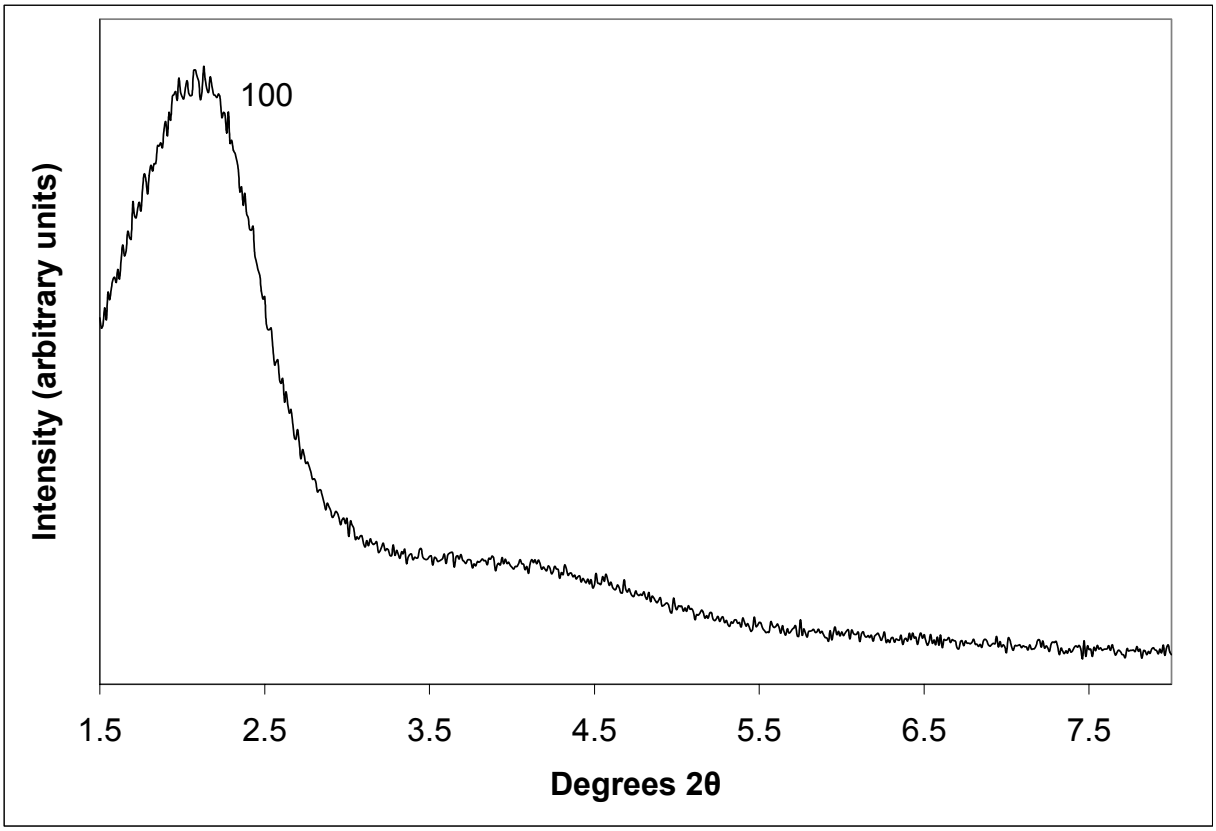


**Figure 2.3: XRD trace of calcined Al-MCM-41.**

The lesser crystallinity of Al-MCM-41 relative to MCM-41 has been proposed to result from the size differences between the Si atom and the Al atom that replaces it as well as an enhancement of Na and H atoms in the structure to satisfy the charge imbalance caused by substitution of $Al^{3+}$ for $Si^{4+}$. The size difference results in structural defects and a corresponding decrease in the material's crystallinity (Shen and Kawi, 2002). This also provides an explanation as to why the 110 and 200 peaks are replaced in the XRD trace by a

single amorphous shoulder on the right hand side of the 100 peak and the increase in background noise relative to traces for regular MCM-41.

### 2.3.4 Silica Dissolution Experiment Involving Pure Silica MCM-41

The results of the dissolution experiments are presented in figures 2.4 and 2.5 as plots of concentration in ppm silica versus time. All dissolution experiments were conducted using portions of the Aug. 29-05 sample of MCM-41. All samples with the exception of blanks and the 1/100 samples were prepared in duplicate. Concentration data for samples and duplicates are presented in Appendix C. The average percent difference between sample and duplicate concentrations was 5%. Under ideal circumstances, analysis of the sample blank would yield $SiO_2$ concentrations of 0 ppm. Analysis of the blank showed $SiO_2$ concentrations ranging between 1 and - 6 ppm. Much of this variability likely results from spectrophotometer instrument drift and error inherent in the sampling and analysis techniques.

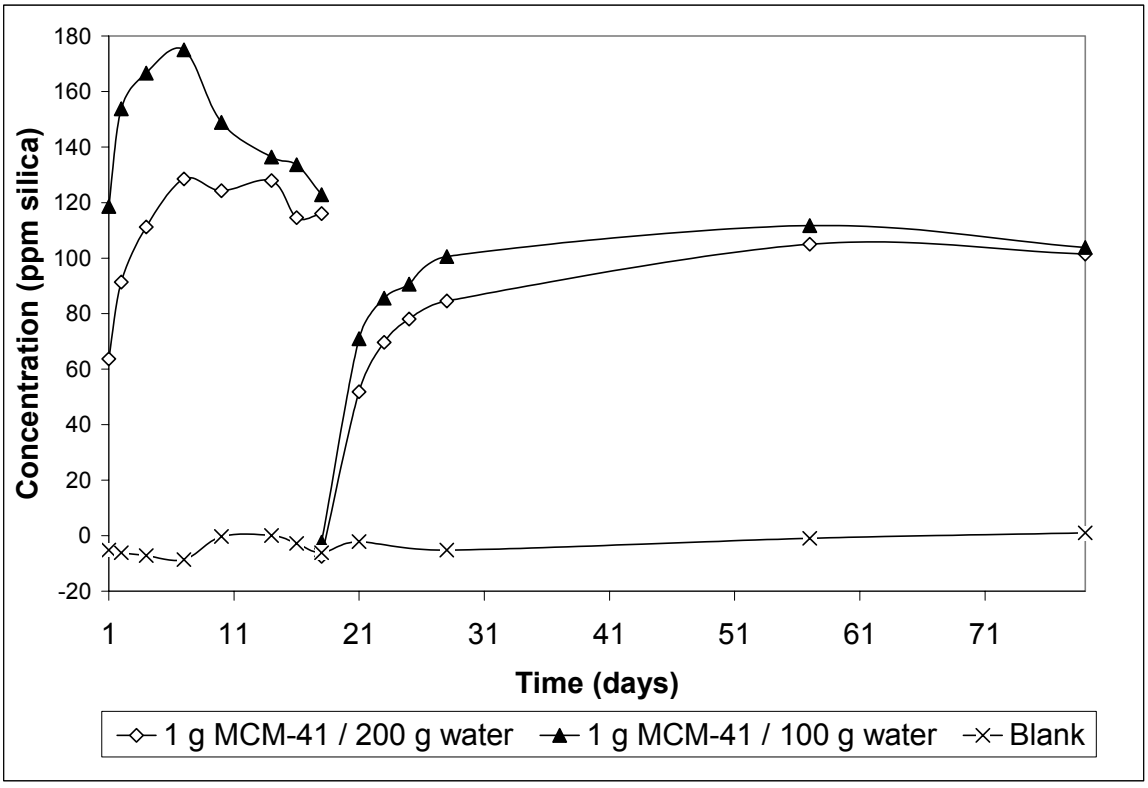


**Figure 2.4: Silica concentration results of the MCM-41 solubility experiment showing effect of decanting and replacing supernatant solution.**

Figure 2.4 shows concentration versus time results for pure silica MCM-41 at solid to liquid ratios of 1/100 and 1/200. The $SiO_2$ concentration increases rapidly at both solid to liquid ratios representing rapid dissolution of MCM-41. The 1/200 sample approaches a maximum concentration of approximately 128 ppm within 7 d. This concentration indicates that 3% or 6 mg of the initial 250 mg of MCM-41 in the sample bottle had dissolved. The concentration of this sample then decreases slightly to a concentration of 115 ppm within 18 d. This indicates that 2% or 5 mg of the initial mass of MCM-41 had dissolved. The 1/100 sample reached a maximum concentration of 175 ppm within 7 d. This concentration indicates that 2% or 7 mg of the initial 400 mg of MCM-41 dissolved. The concentration then decreases towards a value of 122 ppm within 18 d indicating that 1% or 5 mg of the initial mass of MCM-41 had dissolved. The long term concentration value of 115 to 122 ppm corresponds to the reported solubility of amorphous silica (Ksp = $10^{-2.7}$) which is 120 ppm (Stumm & Morgan, 1996).

The maximum concentrations and subsequent decrease in concentration observed at these higher solid to liquid ratio indicates that MCM-41 has higher solubility than amorphous silica and thus is less stable. If the flux of silica dissolving from the MCM-41 surface is high relative to the precipitation of amorphous silica, then it would be possible for the silica concentration in the bulk solution to attain values exceeding amorphous silica saturation. Note that the near surface region of the solution could attain saturation with respect to amorphous silica before the bulk solution, allowing amorphous silica precipitation before the bulk solution exhibits saturation with respect to amorphous silica. Therefore the attainment of Si concentrations higher than amorphous silica saturation may only be observed at early times and at high MCM-41/water ratios.

The effect of decanting and replacing the saturated solution on day 18 of the experiment may also be seen in figure 2.4. Both samples exhibit a rapid increase in $SiO_2$ concentration to a value of approximately 100 ppm. This concentration indicates that 2% and 1% of the initial mass of MCM-41 in the 1/200 and 1/100 dissolved, respectively. Interestingly, the dissolution behaviour of the samples after decanting and refilling differs from the initial dissolution behaviour in that the amorphous silica supersaturation stage does not occur. The dissolution curve trends steadily upward towards a concentration of between 110 and 120 ppm. It is proposed that this is due to precipitation of amorphous silica onto the MCM-41 particles during

the initial period of reaction, creating a less soluble, protective layer on the MCM-41 particle surfaces. The other explanation is that the initial high silica concentrations are due to the dissolution of ultrafine silica particles that may have initially been present in the MCM-41 material and that the solubility of MCM-41 is actually the same as amorphous silica. However, given the very different structure of MCM-41 relative to amorphous silica, it would be highly coincidental, and therefore unlikely, that the two substances would have the same Gibbs free energy and thus the same solubility. Thus it is concluded that MCM-41 is in fact more soluble and less stable than amorphous silica. A minimum estimate of the Gibbs free energy of formation of MCM-41 was undertaken based on the maximum silica concentration observed in the dissolution experiment (175 ppm = 2.92 x $10^{-3}$ mol/kg, figure 2.4). Free energies of formation of $H_4SiO_4^o$ and $H_2O$ used in the calculation were -1 308 000 and -23 7141 J/mol, respectively (Robie *et al.*, 1978). It was assumed that the activity of $H_4SiO_4^o$ in solution was equal to its molality (i.e. activity coefficient equal to 1.0) and the activity of water and MCM-41 are equal to 1.0. The dissolution of MCM-41 can be described by the following reaction:

$$2H_2O_{(l)} + SiO_{2(s)} = H_4SiO_4^o{}_{(aq)}$$

Therefore,

$Ksp = [H_4SiO_4^o] / [H_2O]^2[SiO_{2(s)}] = 2{,}92 \times 10^{-3} = 10^{-2.54}$

$\Delta G^o_R = -RTlnK = -5606logK = 14\ 239.24$ J/mol

$\Delta G^o_R = \Delta G^o_{f\,(H4SiO4o)} - 2\,\Delta G^o_{f\,(H2O)} - \Delta G^o_{f(MCM\text{-}41)}$

$\Delta G^o_{f(MCM\text{-}41)} = -\ 819.479$ kJ/mol

Therefore, the minimum Gibbs free energy of formation of MCM-41 would be - 819.5 kJ/mol, which may be compared to - 856.3 kJ/mol for quartz as reported by Robie *et al.* The high free energy of formation for MCM-41 yielded by this calculation is an alternate indicator of its intrinsic instability in water at ambient temperatures.

The observations made during the first 18 d of the experiment, including the stage of supersaturation with respect to amorphous silica were supported by the results of an earlier MCM-41 solubility experiment. This earlier experiment lasted 28 d and used solid to liquid

ratios of 1/200, 1/100, 1/75, 1/25, and a blank. The results of this experiment are presented in figure 2.5 as a plot of concentration versus time. The dissolution behaviour of the 1/200 and 1/100 solid to liquid ratio samples was analogous to the behaviour of similar ratio samples in the later experiment. The 1/100 bottle was not sampled past the fourth day due to a constraint in the available amount of freshly prepared MCM-41. The observed behaviour of the samples with solid to liquid ratios of 1/75 and 1/25 is similar to that of the 1/100 sample in that they reach a concentration representing supersaturation with respect to amorphous silica before recrystallization reduces the concentration to approximately 120 ppm. Three data points of the 1/25 sample are presented. Other samples taken from this reaction bottle produced concentration results that were inadmissible because their concentrations were higher than the highest silica standard used and were beyond the linear portion of the spectrophotometer calibration curve. Regardless, the three points demonstrate dissolution behaviour comparable to that of the other relatively high solid to liquid ratio samples.

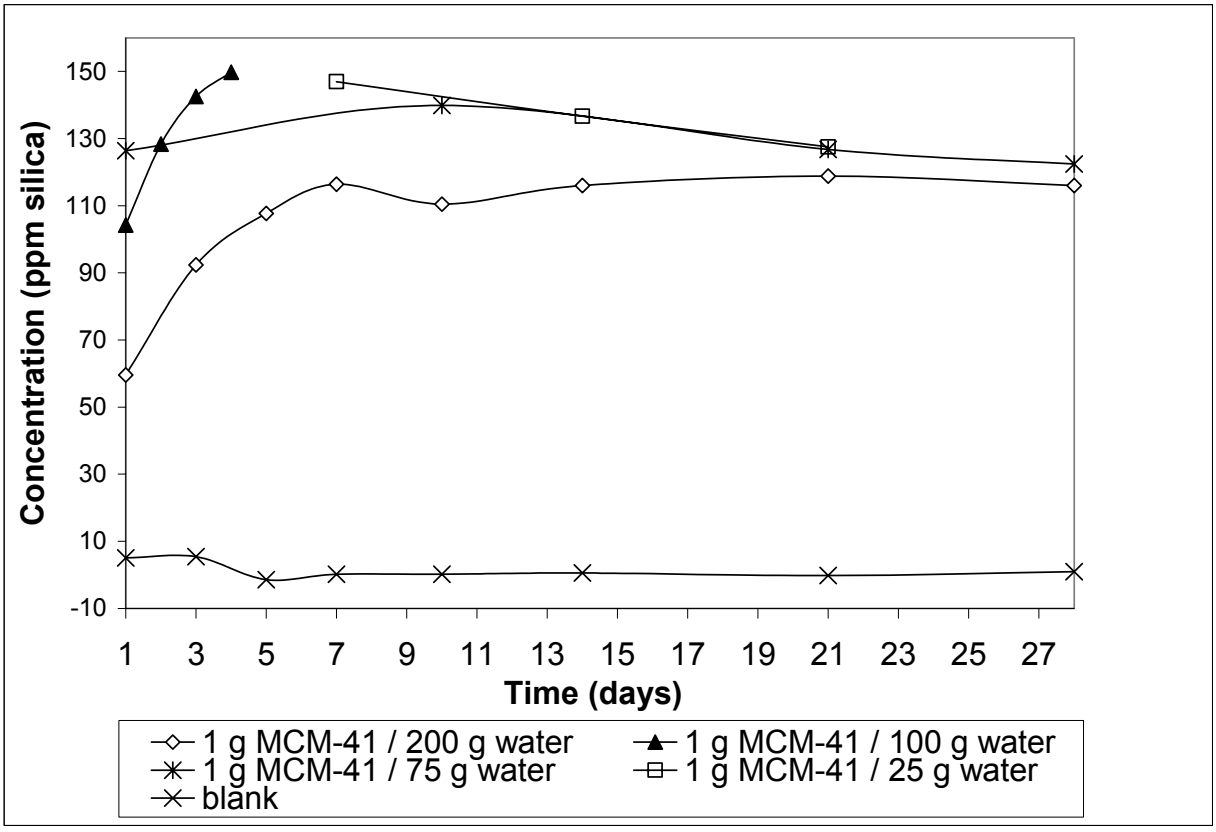


**Figure 2.5: Silica concentration results from the MCM-41 solubility experiment.**

Solid material was recovered at the end of both experiments and dried under vacuum over a saturated KCl solution (80% relative humidity). The dried material was characterized using XRD, BET surface area, and SEM analyses to determine the physical effect of MCM-41 being in contact with water for 28 and 79 d. The results of the XRD analyses are presented in figure 2.6. An increase in background noise from the freshly prepared MCM-41 to the day 79 sample is clear in the comparative plots. The increase in noise is due to an increased proportion of an amorphous phase in the sample. This amorphous phase is proposed to be amorphous silica that was precipitated as MCM-41 dissolved as described above. The relative positions of the 100, 110, and 200 peaks on the XRD trace do not change, indicating that mesoporosity and hexagonal character of the material is not adversely affected by contact with water. The 210 peak, which is visible in the XRD trace of the freshly prepared MCM-41, is indistinct in the day 79 sample. The results of BET nitrogen adsorption analysis indicated surface areas of 1 090, 1 043, and 1 162 $m^2/g$ for the as-prepared, 28 d, and 79 d samples, respectively. The change of 1 090 to 1 043 $m^2/g$ is a decrease in surface area of 4%. The change in surface area from 1 090 to 1 162 $m^2/g$ between the as prepared and day 79 samples represents an increase of 7%. These changes are insignificant given the typical 10% reproducibility in BET measurements. Therefore, BET surface area results indicate that there is no significant change to surface area in MCM-41 samples exposed to water over intervals of up to 79 days. SEM images taken of the 3 samples are presented in figure 2.7. There was no clear change in morphology observed when comparing the freshly prepared sample and the 28 d sample. The material in the 79 d image shows a change in particle morphology – wormy textures appear to be better developed than in the freshly synthesized material.

It is concluded based on these results that MCM-41 is metastable at ambient temperatures and more soluble than amorphous silica in water. Precipitation of previously dissolved MCM-41 as amorphous silica may promote the development of a protective layer of amorphous silica on the material's surface. The solubility of MCM-41 allowed a calculation of its minimum Ksp and Gibbs free energy of formation, which was found to exceed the free energy of quartz by 4%.

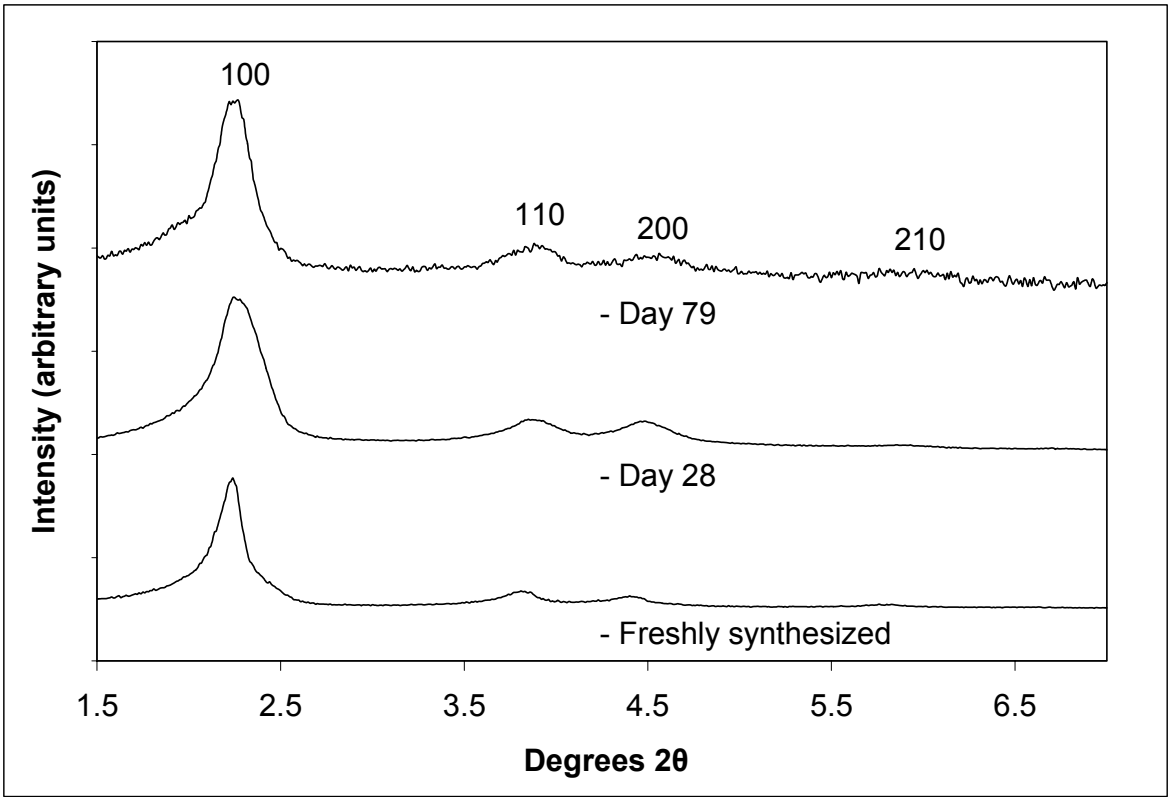


**Figure 2.6: Comparative XRD trace exhibiting differences between materials recovered on days 28 and 79 of the dissolution experiment and as-prepared MCM-41.**

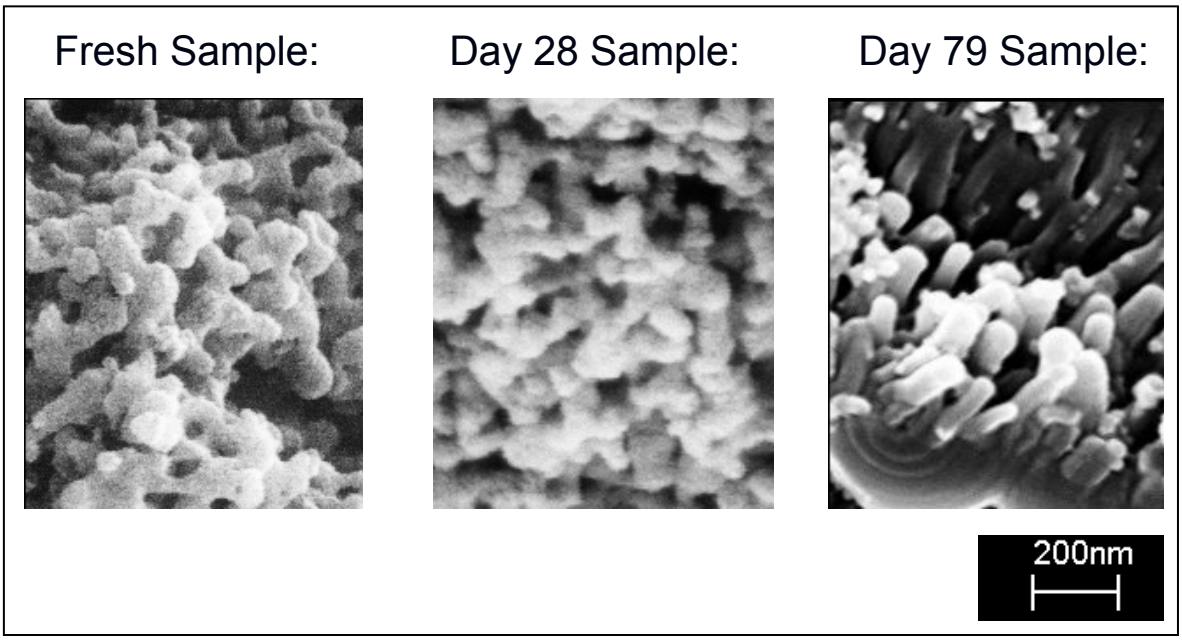


**Figure 2.7: Comparison of SEM image of as-prepared MCM-41 to images taken of materials recovered on days 28 and 79 of the dissolution experiment.**

### 2.3.5 Silica Dissolution Experiment Involving Al-MCM-41

The results of the Al-MCM-41 dissolution experiment are presented in figure 2.8 as a plot of concentration in ppm $SiO_2$ versus time in days. Concentration data for samples and duplicates are presented along with the regular MCM-41 data in Appendix C. Both samples and their duplicates are in reasonable accordance. The percent differences between them are generally less than 5%. The sample blank analysed during the Al-MCM-41 dissolution experiment was the same as that used in the pure silica MCM-41 experiment. Please refer to Section 2.3.4 for a discussion of the experimental error suggested by the variability of the sample blank concentration results.

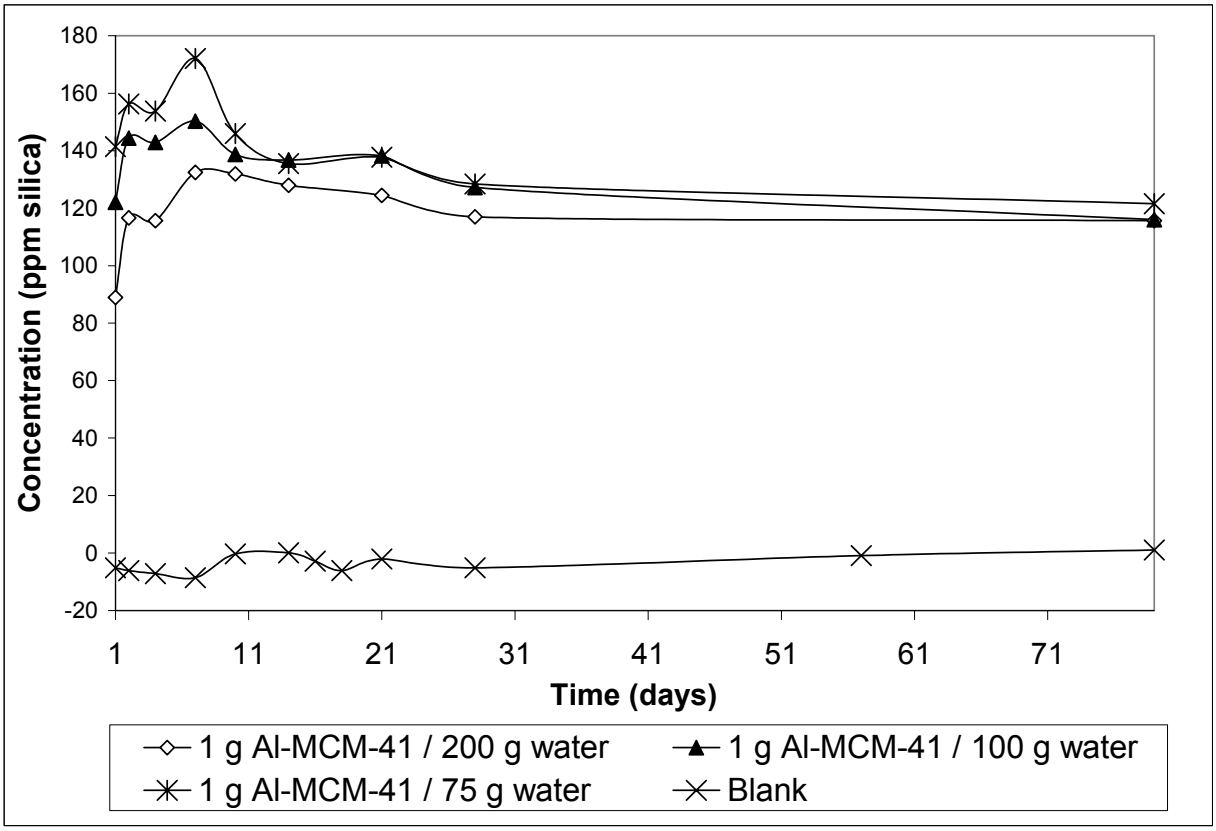


**Figure 2.8: Silica concentration results from the Al-MCM-41 dissolution experiment.**

The results of the Al-MCM-41 dissolution experiment are analogous to those of the pure silica MCM-41 solubility experiment at similar solid/liquid ratios. All three solid to liquid ratios achieved a maximum concentration within 7 days. The 1/200 solid/liquid sample reached a

maximum concentration of 133 ppm, which corresponds to the dissolution of 3% or 5 mg of the initial 201 mg of Al-MCM-41. The maximum concentration of 150 ppm attained by the 1/100 sample corresponds to the dissolution of 1% or 6 mg of the initial 402 mg of Al-MCM-41. The maximum concentration of 172 ppm attained by the 1/75 sample corresponds to the dissolution of 1% or 7 mg of the initial 533 mg of Al-MCM-41. Between days 7 and 79, all three of the samples approached a long term equilibrium concentration of approximately 120 ppm. This final equilibrium concentration represented 2, 1, and 1% or approximately 5 mg of the initial 201, 402, and 533 mg of Al-MCM-41 dissolving in the 1/200, 1/100, and 1/75 solid/liquid samples, respectively. The achievement of the maximum concentration in all three solid/liquid samples represents a stage of active dissolution of MCM-41 and attainment of supersaturation with respect to amorphous silica. The decrease in concentration from the maximum towards a value of approximately 120 ppm – saturation with respect to amorphous silica – represents a stage where the precipitation rate of amorphous silica outstrips the dissolution rate of MCM-41, i.e. the metastable MCM-41 is recrystallising to the more stable amorphous silica. It is possible that given enough time in contact with amorphous silica saturated water, all of the MCM-41 material would recrystallize as amorphous silica.

Solid material was recovered from the sample upon completion of the experiment and dried under vacuum over a saturated KCl solution (80% relative humidity). The sample was characterized using XRD and BET nitrogen adsorption surface area analyses and compared with the results of the freshly prepared material. The result of the XRD analysis of the 79 d sample is presented in figure 2.9. This plot may be compared to that of the freshly prepared material presented in figure 2.3. The general appearance of both plots is similar. The 100 peak and the shoulder immediately to the right are easily identified in both samples. The height of the shoulder in the day 79 sample is larger relative to the 100 peak than in the freshly calcined sample. There is also an increase in the amount of background noise in the 79 d sample plot. These two features indicate an increase in the proportion of amorphous silica in the sample. The origin of the amorphous silica is by precipitation from solution as the more soluble MCM-41 tries to come to equilibrium with the solution. This can be described as a *through-solution recrystallization* of the MCM-41. The recrystallization of MCM-41 is proposed to be a

continuous process occurring once water in the near surface regions of Al-MCM-41 attains a degree of supersaturation with respect to amorphous silica.

Results of the BET nitrogen adsorption analysis indicated that the surface area of the 79 d sample of Al-MCM-41 was 1 175 $m^2/g$. When compared to the surface area of the as-prepared material (1 304 $m^2/g$) the surface area of the recovered sample represents a percentage decrease of slightly less than 10%.

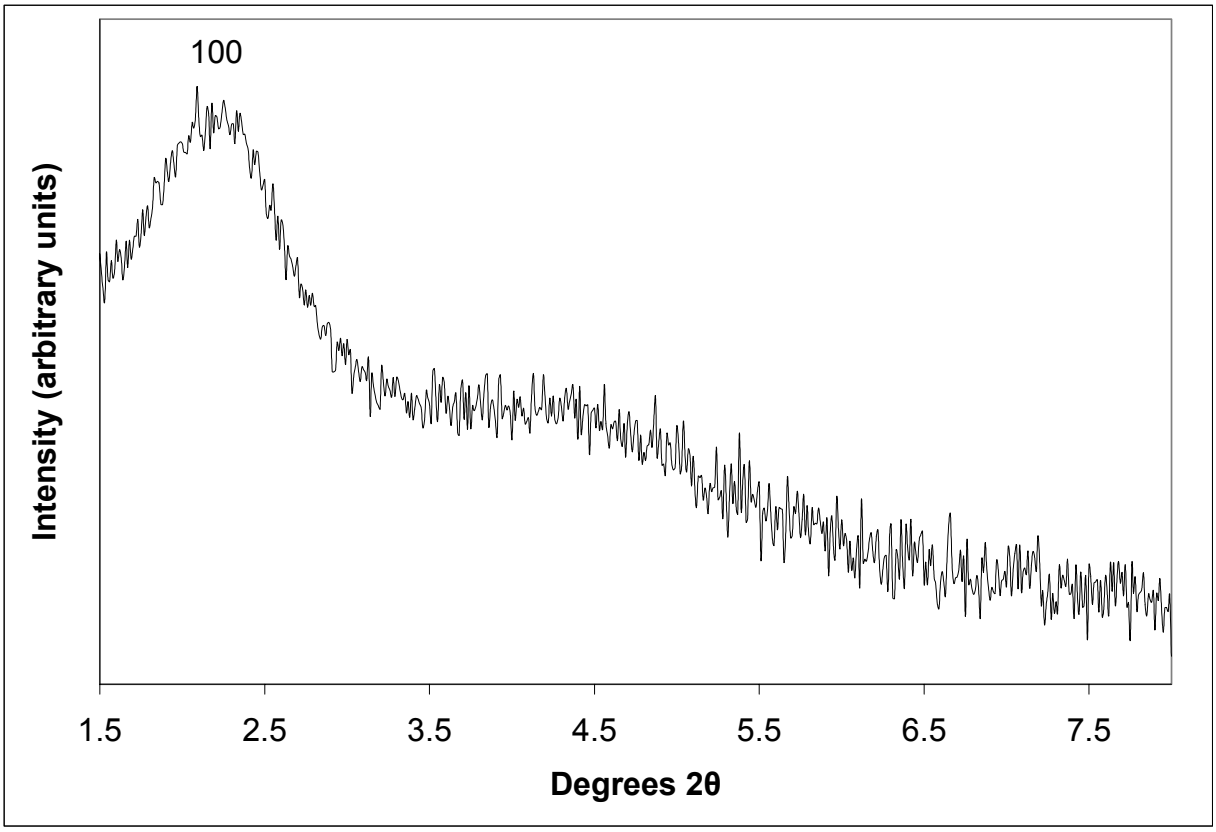


**Figure 2.9: XRD trace of Al-MCM-41 recovered on day 79 of the dissolution experiment.**

The results of this experiment suggest that incorporation of Al cations into the structure of MCM-41 does not have a significant effect in enhancing the material's stability in water at ambient temperatures. Both the initial dissolution behaviour and the long- term equilibrium concentrations of $SiO_2$ in water in contact with Al-MCM-41 were similar to the results of the pure silica MCM-41 experiment. Additionally, analyses of the material recovered after the

experiment indicated an increased proportion of an amorphous phase and loss of surface area approximating that of regular MCM-41 following similar water contact times.

### 2.4 Conclusions

MCM-41 is a siliceous material composed of a hexagonal arrangement of mesopores. Samples of material were synthesized under high pressure in an autoclave at 400 K. Maintaining pressure in the autoclave during this stage of the synthesis was found to be vital in producing well-formed samples with high surface area. Any loss of pressure represented failure of the O-ring, allowing water to escape the autoclave and hindering formation of the MCM-41 structure. An attempt to produce a water-resistant form of MCM-41 using a longer time interval and higher temperature during the autoclave stage of the synthesis was unsuccessful due to O-ring failure and loss of pressure from the autoclave. Aluminum-substituted MCM-41 was successfully produced using $Al_2O_3 \cdot Na_2O$ as an aluminum source.

Results of the dissolution study indicated that MCM-41 is metastable at ambient temperatures and more soluble than amorphous silica in water. Precipitation of previously dissolved MCM-41 as amorphous silica promoted development of a protective layer on the material's surface. Concentration results allowed a calculation of MCM-41's minimum Ksp and a minimum Gibbs free energy of formation of - 819.5 kJ/mol. This exceeds that of quartz by 4%. Concentration versus time results for an aluminum-substituted MCM-41 dissolution experiment revealed similar stability and dissolution behaviour as regular MCM-41. It is concluded from the solubility results and physical characterization of the material that incorporation of Al into the MCM-41 structure during sample synthesis does not improve the stability of MCM-41 in water.

# 3. PALLADIZED-MCM-41 AND TRICHLOROETHYLENE DEGRADATION

## 3.1 Background

The previous chapter of this thesis discussed MCM-41, its different forms, and its stability in water. This section is concerned with the results and interpretation of a preliminary investigation into MCM-41 as a palladium catalyst support material. The ability of Pd/MCM-41 to degrade trichloroethylene was investigated through several TCE degradation batch experiments. If Pd/MCM-41 or other metal catalyst MCM-41 systems are to be used in water treatment applications determining their efficiency in degrading chlorinated compounds is an important preliminary step. In addition, the reaction pathway of TCE degraded by Pd/MCM-41 will be discussed. The reaction pathway influences the form and concentration of chlorinated daughter products produced as TCE degrades. Mobility and toxicity of these daughter products can be equal to and higher than TCE, meaning that their production during treatment is generally as undesirable as the TCE contamination itself.

Current *in situ* treatment of chlorinated compounds in groundwater often involves the use of a zero-valent iron permeable reactive barrier (PRB) (Gavaskar, 1999; Day *et al.*, 1999). The disadvantage of purely iron PRBs is the relatively low reactivity of iron, requiring long contact times with contaminants (Schuth *et al.*, 2000). The long contact times required in PRB design can lead to incomplete degradation of contaminants under non-ideal circumstances. Use of a catalyst in conjunction with zero-valent iron PRB or in *ex situ* treatment technologies can lead to a more rapid and complete degradation of contaminants. Treatment methods that completely transform chlorinated compounds into products of lesser toxicity are preferable over other techniques, such as air stripping and adsorption as the destruction of the contaminants produces no secondary waste stream (Schreier and Reinhard, 1995).

Incorporation of transition metal catalysts into treatment systems shows promise for improving current treatment methods as they can dehalogenate a variety of chlorinated compounds at ambient conditions (Lowry and Reinhard, 1999). Dechlorination of halogenated compounds by metal catalysts takes place on active sites on the catalyst surface in a pseudo-first order reaction, producing relatively low amounts of reaction intermediates (Xu *et al.*, 2005).

MCM-41's potential use as a catalyst support offers advantages over other systems due to its exceptionally high surface area and reduced likelihood of forming a surface passivation layer – a challenge in the use of bimetallic catalysts such as Pd/Fe (Zhang *et al.*, 1998). Successful palladization of MCM-41 has also been reported by other researchers (Koh *et al.*, 1997; Mukhopadhyay *et al.*, 2002; Gonzalez-Arellano *et al.*, 2004; Panpranot *et al.*, 2004a; Panpranot *et al.*, 2004b; Behrens & Spittel, 2005; Marin-Astorga *et al.*, 2005). The procedure used in this research was that of Koh *et al.* (1997) and was found to have reasonable repeatability of Pd contents. Other researchers have also successfully loaded MCM-41 with other transition metal catalysts including Ti, V, Cr, Mn, Fe, Co, Ni, Cu, Nb, and Mo (Zhang *et al.*, 1996; Lensveld *et al.*, 2001; Shen & Kawi, 2002; Lim *et al.*, 2003; Rajakovic *et al.*, 2003; Ziolek *et al.*, 2004; Decyk, 2006). Palladium is an effective catalyst for treatment of halogenated compounds because chlorinated ethenes adsorb to Pd particles and are not released until dechlorination is complete (Kim & Carraway, 2003), thus reducing the accumulation of chlorinated daughter products.

Halogenated compounds are in an oxidized state relative to their non-halogenated counterparts. An example would be comparing the relatively oxidized TCE molecule to its degradation product - ethylene, which is in a reduced state. It is for this reason that the treatment pathway of chlorinated compounds is often referred to as a reductive dehalogenation reaction. The $H_2$/Pd catalytic system has been noted for inducing almost complete degradation of halogenated compounds; the following overall reaction has been proposed (adapted from McNab & Ruiz, 1998):

$$C_2HCl_3 \text{ (TCE)} + 3H_2 \rightarrow C_2H_4 + 3H^+ + 3Cl^-$$

This reaction may be thought of as a simplified or summarized version of TCE degradation as it does not indicate the various reaction pathways, and the formation of intermediates and daughter products that may be produced as chlorine atoms are successively removed from TCE. Arnold & Roberts (2000) present a more detailed degradation pathway of TCE in the presence of zero-valent iron rather than a dissolved hydrogen solution. They subdivide the pathway into different categories of reaction: hydrogenolysis, $\beta$-elimination, $\alpha$-elimination, and hydrogenation reactions. These pathways are presented in figure 3.1 and discussed in greater

detail in section 3.3.4.2. Degradation of TCE generally proceeds along a combination of these reaction pathways, depending on the reaction conditions.

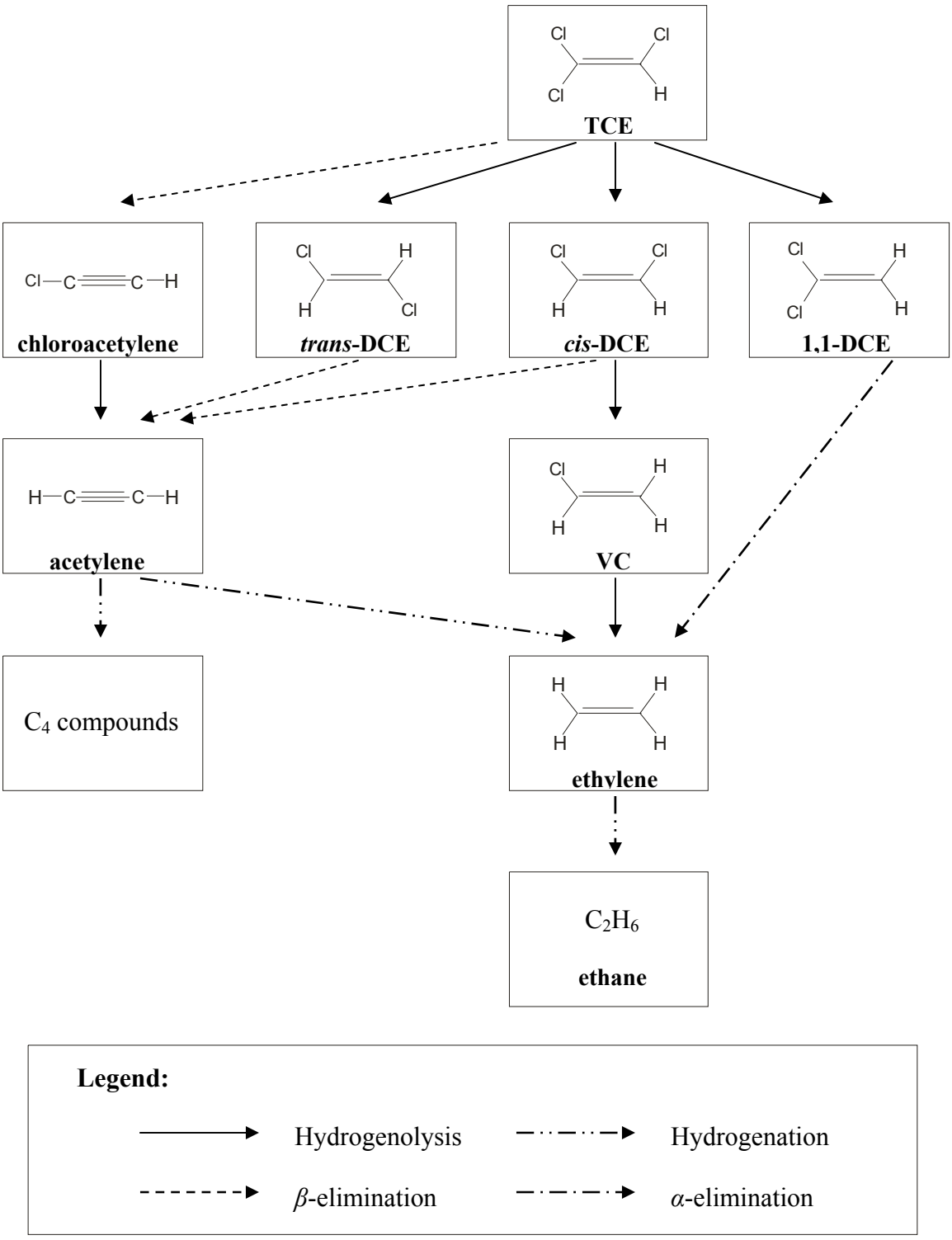


**Figure 3.1: Proposed pathways for TCE degradation (adapted from Arnold & Roberts, 2000).**

## 3.2 Experimental Methods

### 3.2.1 Pd/MCM-41 Preparation

Palladized MCM-41 (Pd/MCM-41) with different palladium loadings was synthesized following the procedure of Koh *et al.* (1997). $Pd(NH_3)_4Cl_2 \cdot H_2O$ was the palladium source and was added to the MCM-41 sample as an aqueous solution. The $Pd^{2+}$ cations in solution were oxidized and deposited as PdO nanoclusters on the MCM-41 surface when the sample was dried under air. An ammonium exchange performed on the MCM-41 sample prior to addition of the palladium source facilitated the oxidation of $Pd^{2+}$ via the reduction of $NH_4^+$ to $NH_3$. Briefly, the ammonium exchange was performed by adding between 0.5 and 2 g of as-prepared MCM-41 to 100 ml of a 2 M $NH_4Cl$ solution. The mixture was gently stirred for 15 min at room temperature. The mixture was then transferred to plastic centrifuge bottles and washed, centrifuged, and decanted eight times or until conductivity of the supernatant solution was less than 0.1 mS/cm. The solution was decanted and the solid MCM-41 was recovered and dried overnight at 393 K. Different mass percent loadings of Pd on MCM-41 were achieved by dissolving appropriate masses of $Pd(NH_3)_4Cl_2 \cdot H_2O$ into small volumes of deionized water – approximately 5 ml. This palladium solution was added dropwise to the dried MCM-41 following an incipient wetness technique; a technique suitable for impregnation by species that interact weakly with the support surface (Haber *et al.*, 1995). The samples were dried overnight at 393 K and calcined under air for 3 h at 593 K. The success of the Pd-loading procedure and Pd content by mass of the samples were determined using an EDAX-equipped SEM.

### 3.2.2 Hydrogen Uptake

A hydrogen uptake experiment was conducted to determine the moles of hydrogen absorbed by the palladium present in a sample of Pd/MCM-41. A Pd/MCM-41 sample with a calculated Pd content of 2% was prepared using a portion of the Aug. 29-05 MCM-41 and used in the uptake experiment. The experiment was repeated using 5% Pd/MCM-41 prepared using a portion of the Oct. 13-05-B MCM-41. A control sample of unpalladized MCM-41 was included in the experiment.

Masses of 0.5 g of Pd/MCM-41 and MCM-41 samples were weighed out and placed in separate glass syringes. Air was expelled from the syringe while taking care not to expel MCM-41 particles at the same time. The syringe was then injected with 10 ml of hydrogen gas. Absorption of the gas occurred quickly and approximately 10 min was allowed for the reaction to go to completion. The volume of gas taken up by the palladized and pure silica material was recorded. After the initial 10 min, an additional 10 ml of hydrogen gas was added to the syringe to determine if any further hydrogen uptake occurred, and if so these values were recorded.

### 3.2.3 Enlarged Pore MCM-41 Preparation

Various attempts were made to synthesize a sample of MCM-41 with larger pore sizes than those of the materials prepared following the procedure described in section 2.2.2. Enlarging the pores of MCM-41 is considered relevant to TCE degradation as it is proposed that pore size influences Pd particle size and access of TCE molecules to inner surfaces of the material.

The synthesis procedure was based on that of Corma *et al.* (1997) where it was reported that samples with larger pore sizes could be prepared by varying the concentration of $CTA^+$ (CTABr) in the synthesis gel. The authors report that they obtained a uniform, well-crystallized mesoporous material possessing enlarged pores by using a $CTMA^+/SiO_2$ molar ratio of between 0.09 and 0.15. They also used a crystallization temperature of 443 K during the autoclave step of the MCM-41 synthesis procedure. The use of higher crystallization temperatures to obtain samples with enlarged pore diameters is also described in a paper by Cheng *et al.* (1997). The remainder of the synthesis procedure was the same as that of regular MCM-41 described in section 2.2.2.

The attempt to synthesize an MCM-41 sample with enlarged pores was performed using a reaction gel with a molar composition of 1.0 $SiO_2$; 0.1 CTMABr; 0.14 TMAOH; 26.2 $H_2O$. Necessary amounts of reagents were calculated on a basis of 200 g of water. The $CTMA^+/SiO_2$ molar ratio value of 0.1 is within the optimal range as reported by Corma *et al.*

### 3.2.4 Batch Experiment

Batch reaction experiments were performed to determine the efficiency of TCE degradation by Pd/MCM-41 in a hydrogen saturated solution. Samples loaded with 0.1, 1, and 5% palladium by mass were used in these experiments. The experiment also included batch reactions using unpalladized MCM-41 to determine if there was adsorption of TCE onto the support material itself.

A hydrogen saturated solution was prepared in advance by bubbling hydrogen gas through a sparger into a 4 l Erlenmeyer flask of deionized water for 4 h. At 1 atm pressure and 298 K, this produces a dissolved hydrogen concentration of 0.000863 mol/l (Randall & Failey, 1927). After 4 h, approximately 1 l of the solution was decanted from the flask into a smaller carboy to which was added a volume of TCE in methanol solution to obtain the desired concentration of 10 mg/l. This concentration corresponds to $4.58 \times 10^{19}$ molecules TCE/l requiring $1.37 \times 10^{20}$ electrons/l to be reduced to ethylene. The electron donor ($H_2$) in the hydrogen saturated solution would provide $1.04 \times 10^{21}$ electrons/l at the above stated solubility. Therefore, the hydrogen saturated solution provides an excess of electrons necessary to reduce the TCE in the sample bottles. The carboy was sealed with a rubber stopper and the solution was vigorously stirred for 15 min using a magnetic stir bar. Meanwhile, a 50 mg mass of the appropriate Pd/MCM-41 and MCM-41 materials were added to 40 ml glass reaction bottles. The reaction bottles were then filled to overflowing with the hydrogen saturated TCE solution and crimp-sealed with Teflon and rubber caps. All samples were prepared in duplicate. The solid/liquid ratio of the prepared sample bottles was 1/800. Control samples were also prepared with 40 ml of the hydrogen saturated TCE solution and crimp sealed. The time at which the bottles were sealed was recorded as time zero for the experiment. The bottles were kept in rotation during the experiment to ensure that MCM-41 and Pd/MCM-41 materials came into contact with all of the solution in the reaction bottle.

Batch experiments took place over 120 min with reaction samples, duplicates, and controls being sampled after 5, 10, 20, 35, 60, and 120 min. The actual time of sampling was recorded when sampling times deviated from the above time intervals. Each reaction bottle was centrifuged prior to sampling to separate the solid particles from solution. The sample bottles

were de-crimped and 10 ml of the supernatant solution was sampled using a 10 ml glass syringe. 10 ml glass sample bottles were filled to overflowing with the solution and crimp-sealed with Teflon and rubber caps. The sample bottles were stored under refrigeration at 290 K until they were analysed.

The samples were analyzed for TCE concentration using a Hewlett Packard 5890 Series II gas chromatograph equipped with a $Ni^{63}$ ECD detector and following a liquid-liquid extraction gas chromatograph analysis technique. The samples were analysed for VC, 1-1 DCE, and the *cis* and *trans* isomers of DCE using a Hewlett Packard 5890 gas chromatograph equipped with an Hnu photo ionization detector using an Hnu NSW-plot capillary column and following a PID gas chromatograph analysis technique. Samples taken during the 0.1% Pd/MCM-41 experiment were also analyzed for methane, acetylene, ethylene, and ethane using a Hewlett Packard 5790 gas chromatograph equipped with a flame ionization detector (FID) using a GS-Q plot capillary column. Chloride concentrations in the 0.1% Pd/MCM-41 experiment samples were determined using a Dionex ICS-2000 ion chromatograph equipped with an ion-effluent generator and conductivity detector. Analytical error of these techniques is generally accepted as being 10%. Error in the analysis results is also exacerbated by sample storage over long periods of time prior to analysis due to the high volatility of TCE and the possibility of further degradation in the presence of the hydrogen saturated solution.

### 3.3 Results and Discussion

#### 3.3.1 Pd/MCM-41

A portion of the Aug. 22-06 sample of MCM-41 was used to prepare a sample of 0.1% by mass Pd/MCM-41. Portions of the Oct. 13-05-A and Aug. 22-06 MCM-41 materials were used in preparing two separate samples of 1% by mass Pd/MCM-41. The Aug. 29-05 sample of MCM-41 was used to prepare a sample of 2% by mass Pd/MCM-41. Three sets of 5% by mass Pd/MCM-41 samples were prepared using portions of the Oct. 13-05-A, Oct. 13-05-B, and Aug. 22-06 MCM-41 samples. These percentages refer to the calculated Pd contents.

Actual palladium content of the samples was determined using an EDAX equipped SEM. The results of the analysis are presented in Appendix D. Analysis revealed that the average Pd

content of the 0.1% by mass loading procedure was 0.50%. Analysis of the 1% by mass samples revealed average Pd contents of 0.69 and 1.23% for the Oct. 13-05-A and Aug. 22-06 samples, respectively. Average Pd contents of the 5% by mass procedure were 3.07, 2.24, and 2.65% for the Oct. 13-05-A, Oct. 13-05-B, and Aug. 22-06 samples, respectively. The Pd content of the 2% Aug. 29-05 Pd/MCM-41 sample was not analyzed by EDAX. Standard deviations in the mass % Pd as indicated by the EDAX analysis were generally between 0.3 and 0.4%. Standard deviations of 0.62 and 1.28% were calculated for the 5% by mass Oct 13-05-B and Aug. 22-06 Pd/MCM-41 samples, respectively. All Pd/MCM-41 samples will be referred to by their prepared Pd contents rather than their EDAX analysed contents.

The deviation of the actual Pd contents from the calculated contents is primarily attributed to analytical error of the EDAX technique resulting from the very small surface areas analyzed by the technique (approximately 35 $nm^2$ or less). This surface area is too small to accurately account for 'patching' or discontinuous Pd coverage of these materials. The amount of Pd added relative to the surface area of the MCM-41 sample is extremely small, which would promote non-homogenous coating of the material by the metal. Some of the deviation is also attributed to mechanical losses of Pd during the loading procedure.

The EDAX analysis also revealed greater deviation of actual Pd contents from the calculated values in the 5% by mass loading procedure when compared to the 1% by mass procedure. This indicates that the Pd loading procedure is less effective at higher Pd concentrations. This deviation may be due to aggregation of Pd particles at higher loadings, resulting in an uneven dispersion of Pd over the surface of MCM-41. It should be noted that EDAX analysis of the 0.1% by mass Pd/MCM-41 sample is the least accurate of all the samples due to this mass percent being below the detection threshold of the technique – i.e. analysis identifies the presence of Pd, but Pd peaks at this content are indistinct relative to background noise. The Pd loading procedure was repeatable with a reasonable degree of constancy, regardless of the deviation of calculated Pd contents from actual contents.

Palladium particle sizes cannot be determined through EDAX analysis. Koh *et al.* (1997) describe a TEM analysis revealing well distributed Pd particles of 2 to 2.5 nm in diameter that are located within the pores of a sample of MCM-41. The unit cell parameter of Koh *et al.*'s

MCM-41 was 4.47 nm. The unit cell parameters of the Aug. 29-05, Oct. 13-05-A, Oct 13-05-B and Aug. 22-06 MCM-41 samples were 4.6, 4.7, 4.8, and 5.3 nm, respectively. Given the size of these unit cell parameters, it is likely that Pd was grafted within the pores as well as on the surface of MCM-41 with minimal pore blocking by the particles. It is impossible to make this conclusion with complete certainty without determining the actual Pd particle diameters, the thickness of the pore walls, and the pore diameter distribution of the material. Since blocking of pores would reduce the surface area of MCM-41, a BET analysis of Pd-loaded samples might provide more insight into the degree of pore blocking caused by the Pd-loading technique.

### 3.3.2 Hydrogen Uptake Experiment

There was no observed hydrogen uptake in the syringe containing the pure silica MCM-41. This indicated that the hydrogen absorbed by the Pd/MCM-41 materials in the other uptake experiments was absorbed by palladium and not the MCM-41 support material. All volumes of hydrogen gas reported for this experiment were accurate to ± 0.25 ml.

It was observed that 6.00 ml of hydrogen gas was taken up by the 2% Pd/MCM-41 material. The hydrogen uptake was instantaneous – i.e. absorption occurred as quickly as hydrogen could be injected into the syringe. It should be noted that hydrogen absorbed by palladium is absorbed as H atoms and not as $H_2$ (Kircheim *et al.*, 1988; Cobden *et al.*, 1999). The 6 ml of gas corresponds to $2.5 \times 10^{-4}$ moles of $H_2$, or $5.0 \times 10^{-4}$ moles of H at 298 K. It was calculated that there were $9.4 \times 10^{-5}$ moles of Pd present in the 2% Pd/MCM-41 sample based on the calculated Pd content. Therefore, the ratio of moles of H absorbed per mole of Pd in the sample was 5.3.

The 5% Pd/MCM-41 was calculated as containing $2.35 \times 10^{-4}$ moles of Pd based on the calculated Pd content. It was observed that this material absorbed 8.00 ml of hydrogen gas, which corresponds to $3.33 \times 10^{-4}$ moles of $H_2$ at 298 K. This represents 2.8 moles of H being absorbed for every mole of Pd present. A similar calculation was carried out using the EDAX reported average Pd content of 2.24%, yielding a ratio of 6.4 moles of H absorbed per mole of Pd. The ratio of 6.4 is more consistent with the results of the 2% Pd/MCM-41 experiment (percent difference of 17%) than the ratio of 2.8 calculated using the calculated Pd content of

the 5% Pd/MCM-41. The implication of this is that the actual Pd content of the 2% Pd/MCM-41 sample was likely relatively close to 2%. This is consistent with the Pd loading technique being more effective at lower Pd contents as suggested by EDAX analyses.

Hanneken *et al.* (2002) describe enhanced hydrogen solubility in nano-sized hydrogen palladium systems relative to systems containing larger palladium particles. This is in support of the observation that Pd/MCM-41 is capable of absorbing a relatively large volume of hydrogen relative to the mass of palladium present in the material. Hanneken *et al.* noted that the hydrogen taken up by the palladium in their material was preferentially located in the interfacial regions of the Pd particles rather than the internal regions. It has been reported that the increased hydrogen solubility in nano-sized palladium particles is due to enhanced hydrogen solubility at the grain boundaries (Eastman *et al.*, 1993). This is also supported by the findings of Sachs *et al.* (2001) who observed and modelled the enhanced solubility of hydrogen in small Pd clusters of 2 to 5 nm diameter.

### 3.3.3 Enlarged Pore MCM-41

Three separate attempts were undertaken to synthesize MCM-41 samples with enlarged pore diameters. Materials were characterized by XRD and BET nitrogen adsorption surface area analysis in the cases where the synthesis procedure was carried through to completion.

A strong odour of melted rubber and chemicals was noted during the crystallization stage of the first attempted synthesis. The odour indicated that pressure had been lost from the autoclave, likely due to failure of the O-ring. The material inside the autoclave was a white solid, whereas the material at this stage should present as a milky white gel. The sample was discarded.

A second sample was prepared and the synthesis was carried through to completion. XRD analysis indicated a prominent peak centred at a 2θ value of 2.48 $^{o}$. The second two peaks (110 and 200) that are characteristic of a well-formed MCM-41 sample were absent. The absence of these peaks indicated that the material did not possess hexagonal crystallinity. In addition, results of the BET nitrogen adsorption analysis of the sample indicated a surface area of only

366 $m^2/g$. The results of these analyses revealed that the sample was poorly formed and did not possess the characteristic physical properties of MCM-41. This sample was also discarded.

A final attempt to produce enlarged pore MCM-41 was made using the same molar ratio, crystallization temperature, and procedure as the first two attempts. A different autoclave was used during this synthesis. Upon completion of the crystallization stage of the procedure the autoclave was quenched with cold water and opened. The gel in the autoclave was noted as having a translucent brownish colour and a pungent metallic odour. The colour and odour of the gel suggested that a reaction between the synthesis gel and the steel of the autoclave occurred during the crystallization stage of the procedure. The small angle XRD trace of this sample also lacked the characteristic 110 and 200 peaks, suggesting that the sample did not possess the hexagonal pore arrangement of well-formed MCM-41. A BET analysis was not performed on this sample.

The lack of success in following this procedure raises some doubt as to whether enlarged pore MCM-41 can be synthesized by simply altering the $CTMA^+/SiO_2$ molar ratio and increasing the crystallization time and temperature. A cursory literature review found some examples of success in influencing the pore characteristics of MCM-41 by altering these two variables in the synthesis procedure. An article by Araujo *et al.* (2005) reported variations in the unit cell parameter depending on the time interval used during the crystallization stage. The authors described an increase in the unit cell parameter from 4.13 to 4.25 nm when the synthesis time is extended from 1 to 4 days. Although this represents a 3% increase in the unit cell parameter, the pore diameter of the material decreased with increased synthesis time. Araujo *et al.* attributed this decrease in diameter to a corresponding increase in the thickness of the pore walls with time of crystallization. Cheng *et al.* (1997) describe a procedure for producing MCM-41 with enlarged unit cells using higher synthesis temperatures. The increase in size of the unit cell parameter of their material was also accompanied by a thickening of the pore walls. The article also described the effect of using different $CTMA^+/SiO_2$ molar ratios. Samples possessing relatively low XRD peak intensities were prepared by the authors using a $CTMA^+/SiO_2$ molar ratio of 0.1, the same ratio as was used in the procedure of this research. A sample exhibiting less distinct XRD peak intensities would likely possess relatively poor crystallinity due to an increased proportion of an amorphous phase in the sample. The article

suggests that optimal relative XRD peak intensities are obtained using $CTMA^+/SiO_2$ molar ratios of between 0.25 and 0.30, significantly higher than the optimal range of 0.09 to 0.15 reported by Corma *et al.* (1997).

Researchers wishing to obtain MCM-41 samples with enlarged pore diameters may benefit from pursuing techniques other than simply varying the crystallization time interval and temperature. Several alternate methods of enlarging the pore diameter have been proposed by other researchers including: use of surfactants possessing different carbon chain lengths; the use of auxiliary organic compounds during synthesis; and post synthesis treatments of MCM-41 with auxiliary organic compounds (Kruk *et al.*, 1997; Jana *et al.*, 2004; Sayari *et al.*, 2005; Kruk *et al.*, 1999).

### 3.3.4 TCE Degradation Batch Experiments

#### 3.3.4.1 TCE Degradation Results

A tabulation of the analytical results for the degradation experiment is included in Appendix E. The error in the liquid-liquid extraction and PID gas chromatograph analysis techniques is approximately 10%. Additional experimental error is introduced due to volatilization of organic compounds during sample preparation, extraction, and storage. Additional degradation of TCE during storage is also a potential source of error as TCE can be degraded by the hydrogen present in the sample solution. It is unlikely that this latter error source contributes significantly to experimental error given the consistency in concentration results between samples and control samples. It was found that actual TCE concentrations were consistently lower than the calculated concentration of 10 mg/l. The value for the initial molar concentration of TCE ($C_o$) was calculated as the average concentration of TCE in the control samples. Degradation half-lives for TCE dehalogenation were estimated based on plotted results. Application of kinetic models to the data and calculation of half-lives were not possible due to most of the degradation occurring before the first timed samples were taken and the TCE degradation reactions reaching their maximum extent before complete dehalogenation had occurred.

Results of the batch experiment using unpalladized MCM-41 are presented in figure 3.2 as a plot of normalized mass versus time. TCE concentrations in control samples were relatively constant during the experiment. Normalized mass concentrations of TCE in the samples containing MCM-41 also stayed relatively constant, deviating from a C/Co equal to 1 by 15% or less. This deviation is attributed to analytical and experimental error as discussed in the preceding paragraph. The results suggest that MCM-41 did not induce any significant change in TCE concentrations. This indicates there is no adsorption of TCE to the MCM-41 material itself. Reaction intermediates and chlorinated daughters were not detected, indicating that there was no detectable degradation of TCE.

Normalized TCE concentration vs. time results for the 0.1% Pd/MCM-41 sample are presented in figure 3.3. TCE concentration in the control sample stayed relatively constant, yielding an average initial TCE concentration of 0.05 μM. The first timed sample was extracted at 6 min. At that time, 35% of initial TCE had been degraded. Inspection of the plot reveals a TCE degradation half-life of 14 min. Subsequent samples show a steady decrease in TCE concentration with time approaching a limit of $C/C_o$ equal to 0.3 representing 70% degradation of the initial TCE. The maximum extent of TCE degradation by 0.1% Pd/MCM-41 occurred within the first 35 min of the experiment. The final concentration of TCE was 0.015 μM. A plot of daughter product concentrations on an expanded y-axis is presented in figure 3.4. Normalized mass versus time curves of the daughter products exhibit a shape similar to the TCE degradation curve. A similarity in the form of the curves between the different daughter products is also notable and discussed in greater detail below. Maximum production of chlorinated daughters occurred during the first 14 min, with concentrations remaining constant after that point. The contribution of chlorinated daughter products and reaction intermediates to the carbon balance was calculated as the sum of their masses divided by the initial TCE concentration. Daughter products composed 7% of the carbon balance in the first timed sample (figure 3.5). These products contributed 3% to the carbon balance in the remainder of the samples. Gaseous products of TCE degradation including methane, ethylene, and ethane contributed between 38 and 84% of the carbon mass balance with an average contribution of 63%. The sum of all reaction products including undegraded TCE accounted for between 86 and 101% of the balance for the samples extracted at 14, 23, 35, and 60 minutes. Samples taken at 6 and 125 min indicated lower balances of 75 and 69%, respectively. Deviation of the

carbon balance from a value of 100% is attributed to analytical and experimental error as previously discussed. Results of the carbon balance showed that gaseous products were the dominant degradation products of TCE during the experiment and that ethane was the dominant gaseous product.

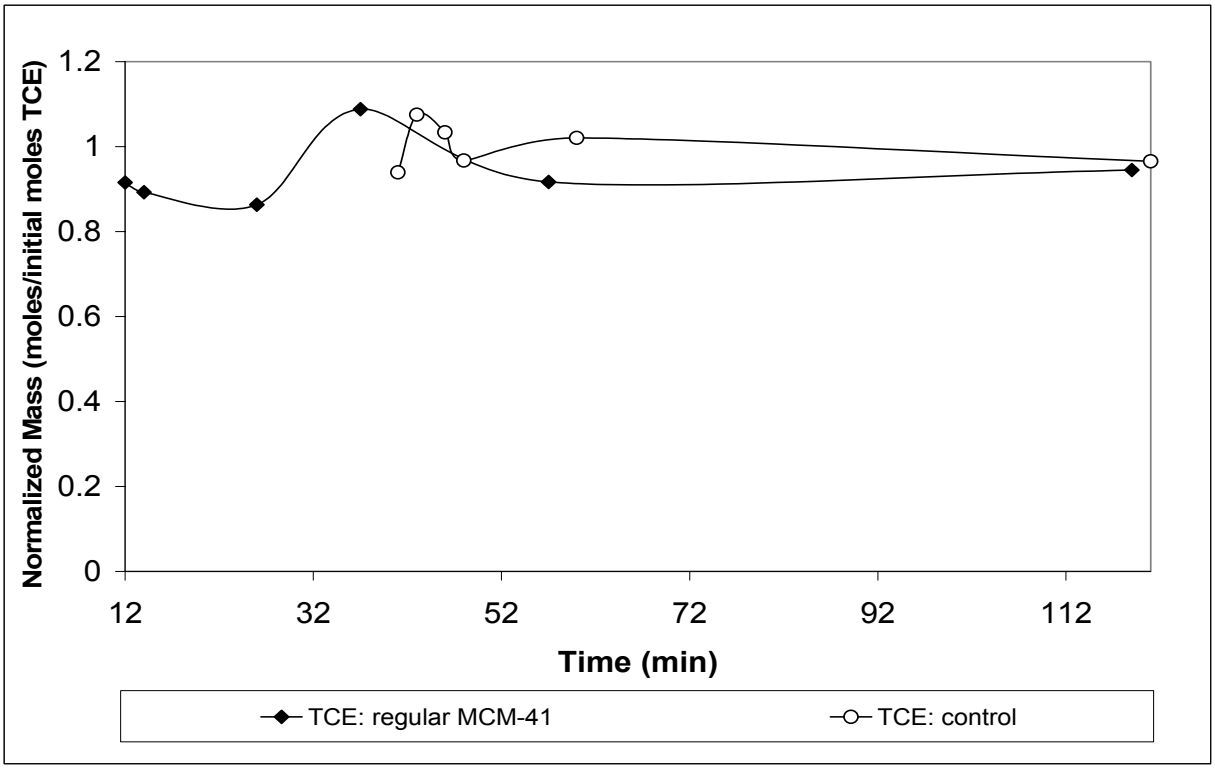


**Figure 3.2: Results of TCE degradation batch test using unpalladized MCM-41.**

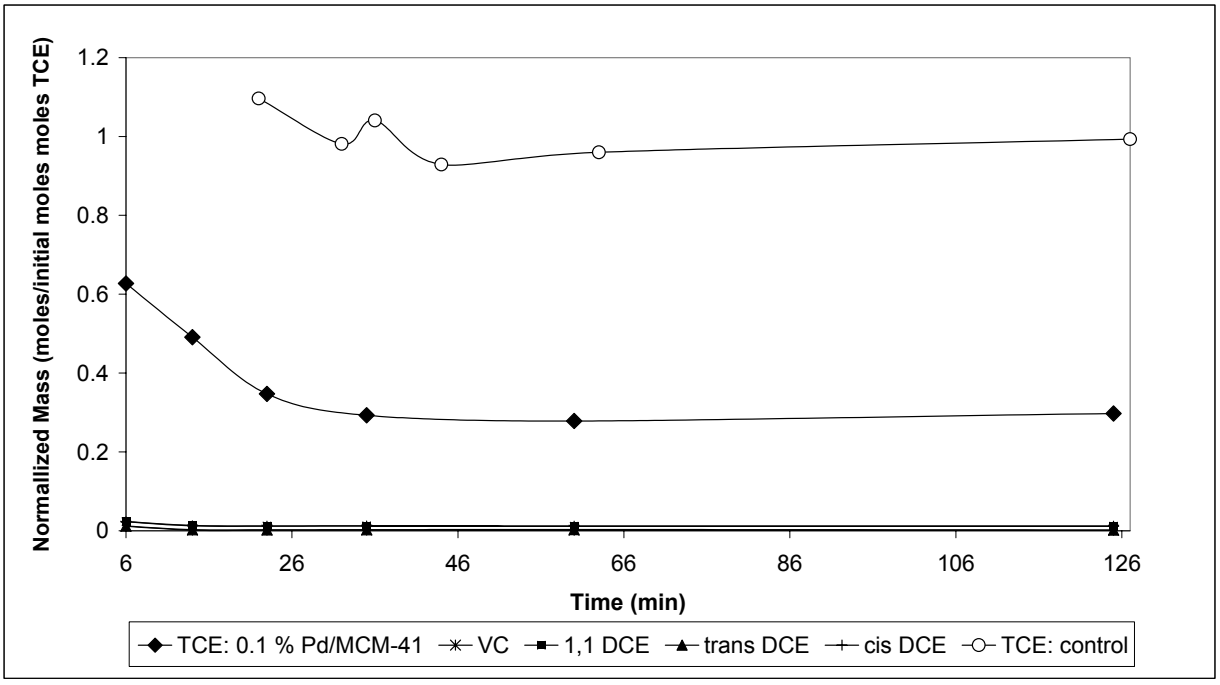


**Figure 3.3: Results of TCE degradation batch test using 0.1% Pd/MCM-41.**

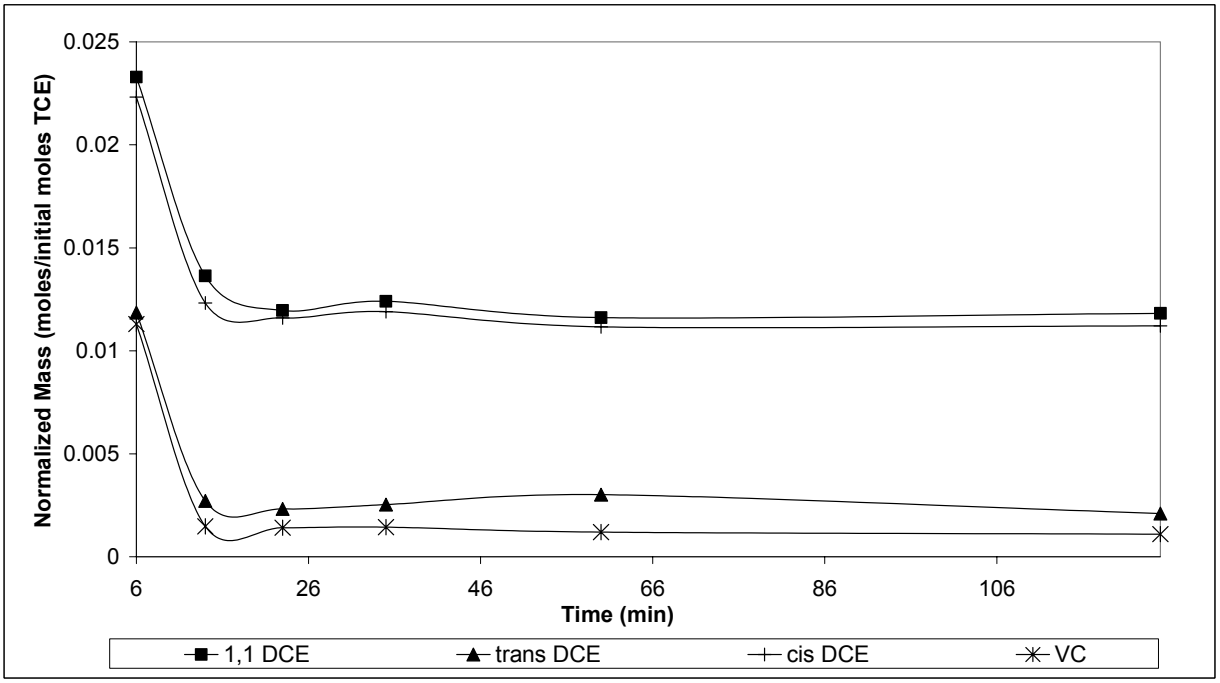


**Figure 3.4: Daughter product concentrations in 0.1% Pd/MCM-41 batch test with expanded vertical axis.**

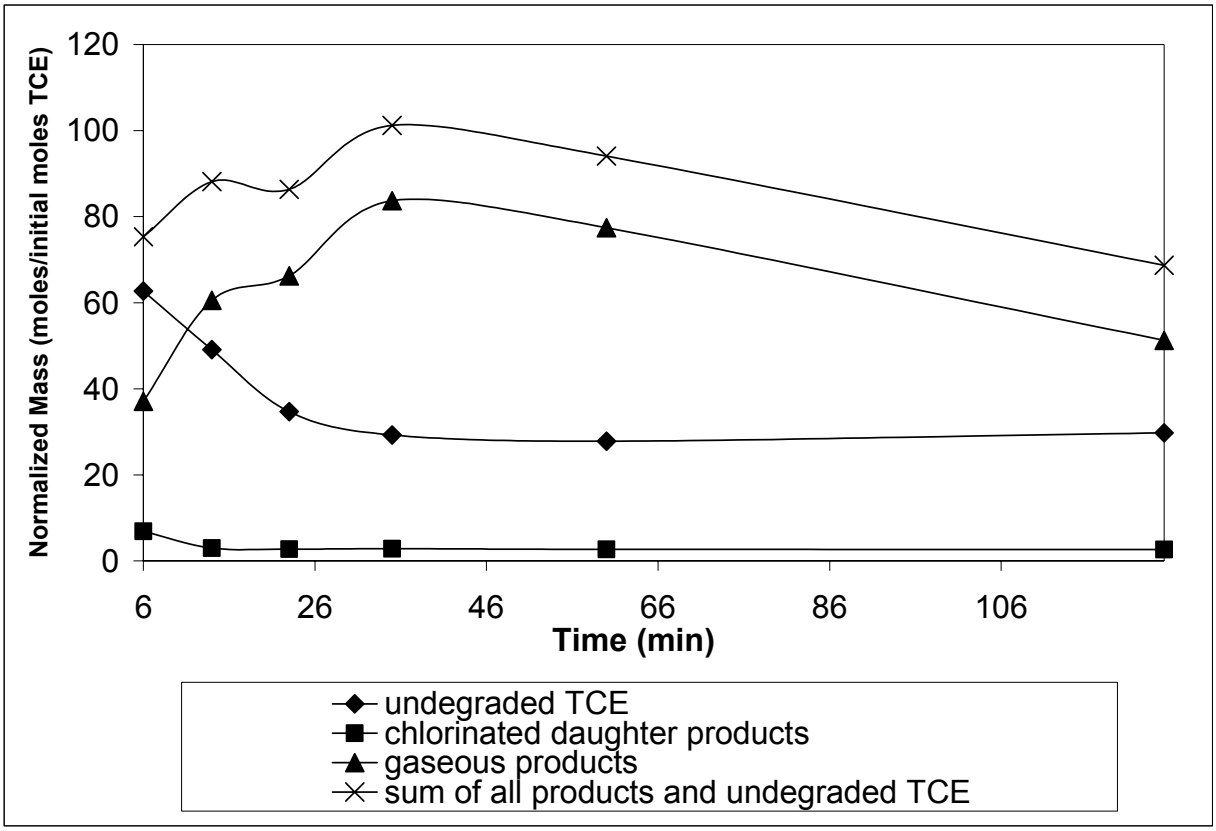


**Figure 3.5: Results of a carbon balance on TCE degradation products including undegraded TCE.**

Samples taken during the 0.1% Pd/MCM-41 experiment were also analyzed for chloride concentrations to allow the calculation of a chloride mass balance. The calculation indicated that the sum of moles of chloride as well as chloride contributions made by the undegraded TCE, VC, and DCE isomers in solution accounted for an average of 138% of the chloride balance (plot not included). This value is substantially higher than the 100% balance to be expected under ideal conditions. Additionally, the variation in the balance for individual samples was significant with a standard deviation of 66. The large variation in the chloride balance is due to a combination of analytical error, degradation and volatilization of TCE and daughter products from the samples between sampling and analysis.

TCE degradation results for the 1% Pd/MCM-41 are presented as a plot of normalized mass versus time in figure 3.6. TCE concentrations in the control samples stayed relatively constant throughout the experiment with less than 10% deviation from $C/C_o$ equal to one. Average

initial concentration of TCE was equal to 0.03 μM. The first sample of the reactive 1% Pd/MCM-41 was taken at 12 min. At 12 min, 79% of the initial TCE had already been degraded. Further degradation of TCE occurred from 12 to 125 min with 92% of initial TCE degraded in the final timed sample. The degradation half-life for TCE was estimated to be between 3 and 6 min. The final TCE concentration was approximately 0.003 uM. Values of $C/C_o$ did not reach a constant value within 125 min implying the possibility of further TCE degradation. It is recommended that future experiments involving 1% Pd/MCM-41 be extended over a longer time interval to determine the maximum extent of TCE degradation. A plot of chlorinated daughter production is presented in figure 3.7 on an expanded y-axis. An anomalous concentration of 0 normalized mass for all daughter products was identified at 32 min and excluded from the plot. This anomaly is likely the result of some solid particles of reactive Pd/MCM-41 being transferred from the 40 ml sample bottle to the 10 ml vial, thus allowing the degradation reaction to continue until all daughters had degraded. VC concentrations were below detection limits throughout the experiment. Concentrations of chlorinated daughter products all approach zero within 125 minutes. Samples extracted during the first 60 min of the experiment reveal relatively high daughter product concentrations. However, their normalized masses are still below 2% of initial TCE at maximum production. The shapes of the normalized mass versus time curves for the daughter products were similar. These samples were not analyzed for gaseous daughter products. Chlorinated daughter products contributed 3.6% of the carbon balance at maximum production during the experiment. Undegraded TCE composed an average of 15% of the balance. The remaining 80% of the carbon balance is likely contributed by the gaseous products of TCE degradation. However, this conclusion cannot be made with certainty in the absence of an analysis of the concentrations of these products.

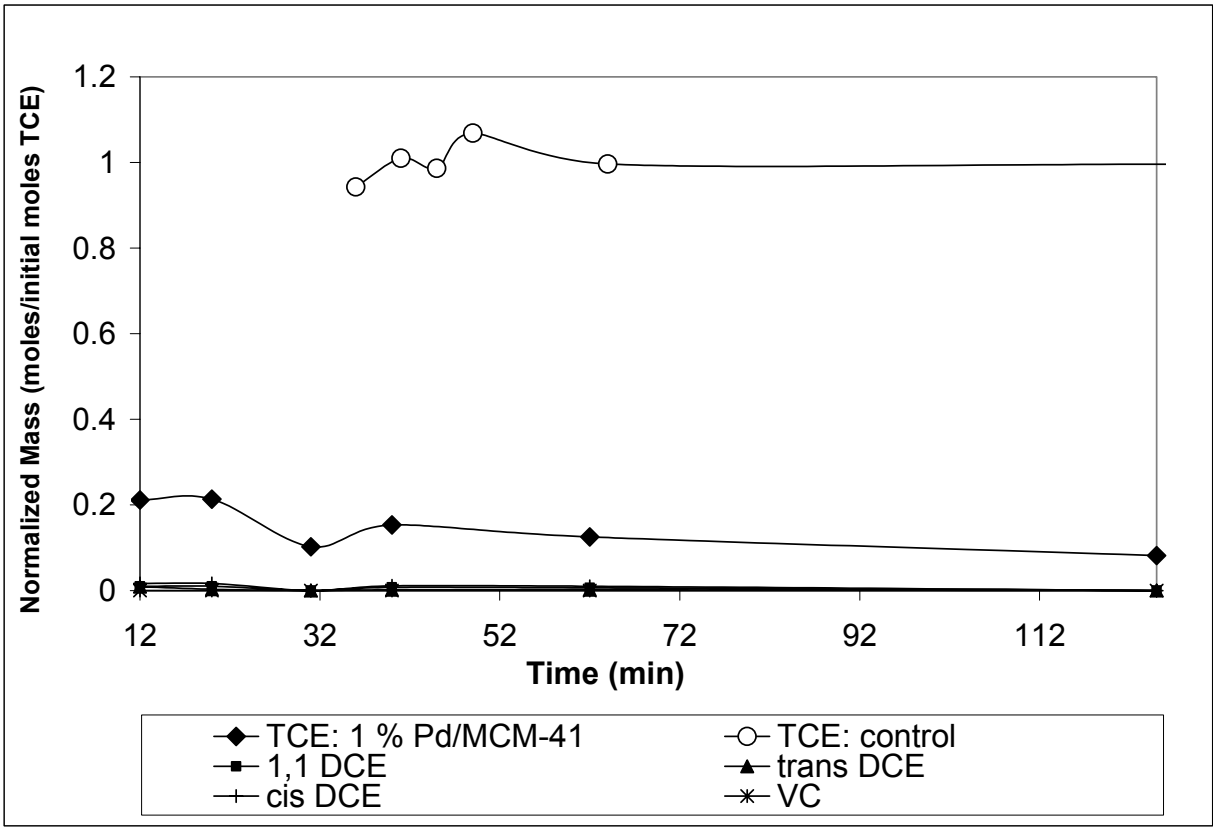


**Figure 3.6: Results of TCE degradation batch test using 1% Pd/MCM-41.**

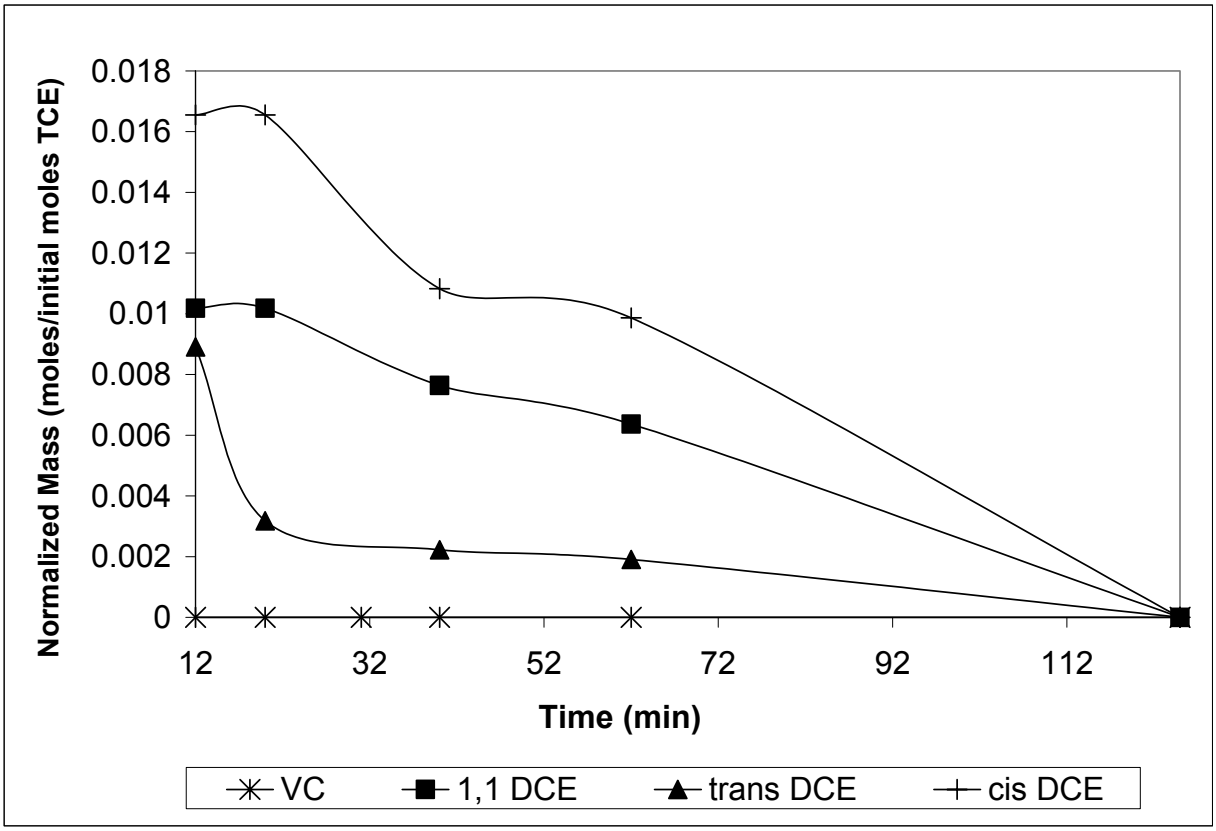


**Figure 3.7: Daughter product concentrations in 1% Pd/MCM-41 batch test with expanded vertical axis.**

Results of TCE degradation by 5% Pd/MCM-41 are presented in figure 3.8. Results of sample analyses for this experiment are presented up to 60 min. A sample was taken at 120 min but an error during analysis rendered the result unusable. TCE concentrations in the control sample remained relatively constant, yielding an average initial TCE concentration of 0.05 μM. A control sample taken at 43 min was calculated to be an extreme outlier and omitted from the plot and further calculations (Appendix E). The maximum extent of TCE degradation was 22%. Maximum extent of TCE degradation occurred within the first 17 to 28 min of the experiment. A degradation half-life for TCE in these samples could not be estimated although it is certain that it would be substantially greater than 60 min. It is unlikely that a successful analysis of the 120 min sample would have revealed any further TCE degradation by Pd/MCM-41. A plot of normalized concentrations versus time for daughter products is presented in figure 3.9 on an expanded y-axis. Vinyl chloride concentrations were below detection limits throughout the experiment. *trans* DCE, *cis* DCE, and 1,1-DCE, were produced

in increasing quantities between times 17 and 39 min. Maximum production of *cis* DCE and 1,1-DCE occurred at 39 min. Chlorinated daughter products contributed 3.6% of the carbon balance at their maximum extent. The shapes of the normalized mass versus time curves for the chlorinated daughters were similar. A notable result of this experiment was that undegraded TCE composed an average of 78% of the carbon balance, a relatively high proportion when compared to the 0.1 and 1% Pd/MCM-41 experiments. These samples were not analyzed for gaseous TCE degradation products. It is probable that gaseous products composed the bulk of the remaining 18% of the carbon balance; however, this conclusion cannot be made with certainty in the absence of an analysis for these products.

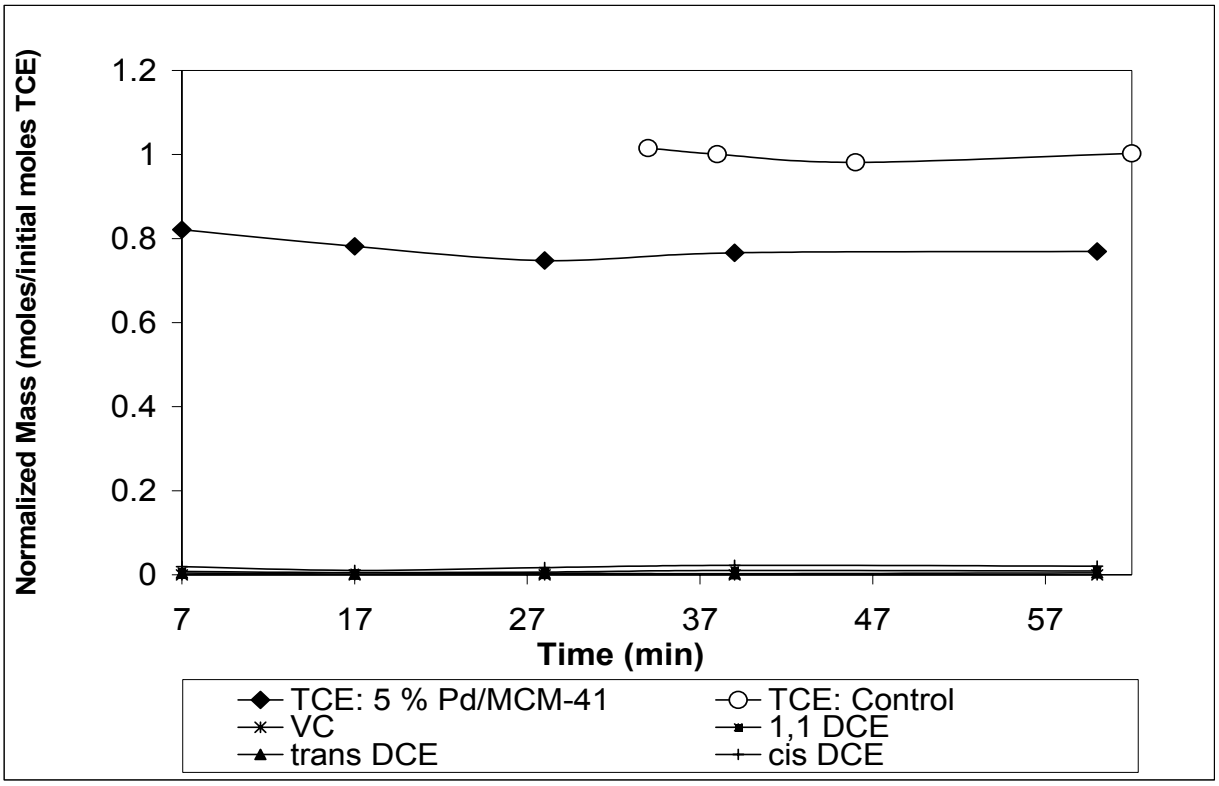


**Figure 3.8: Results of TCE degradation batch test using 5% Pd/MCM-41.**

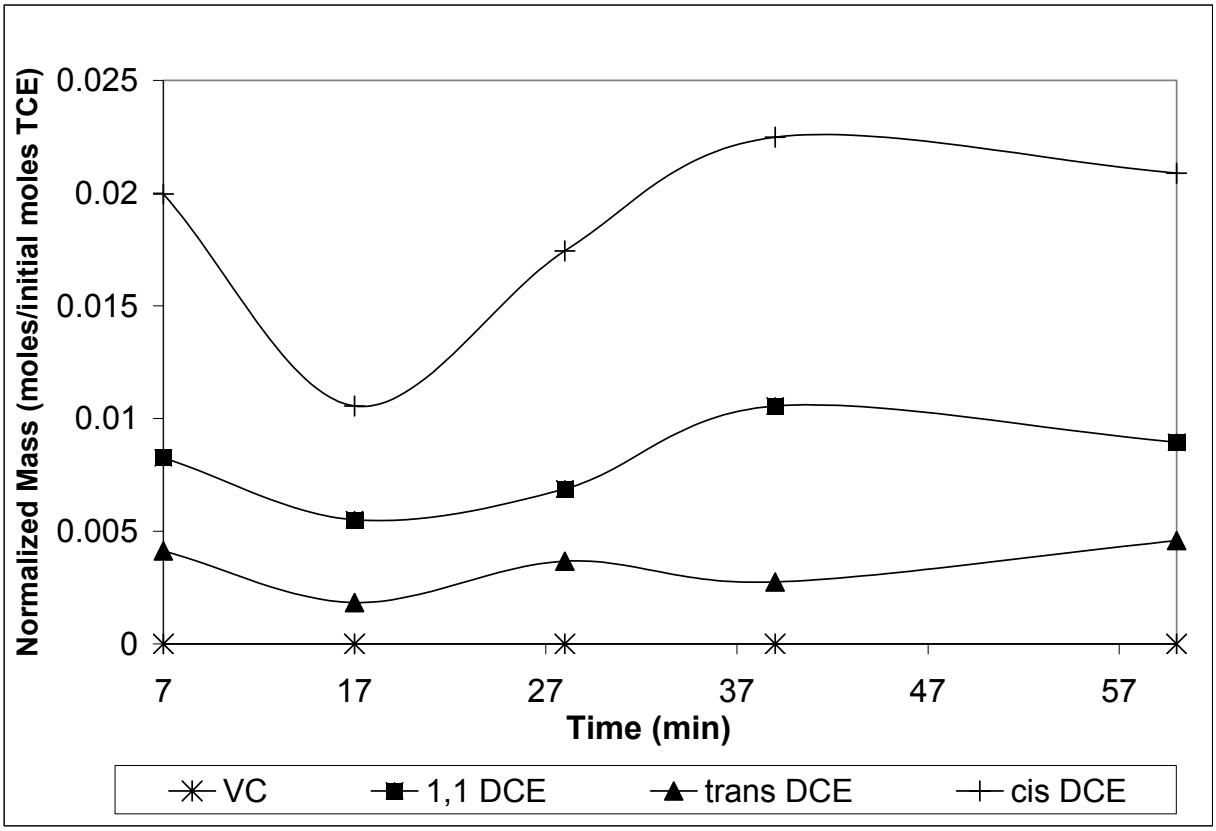


**Figure 3.9: Daughter product concentrations in 5% Pd/MCM-41 batch test with expanded vertical axis.**

In summary, it was found that the 0.1, 1, and 5% Pd/MCM-41 samples degraded 70, 92, and 22% of initial TCE, respectively. This effectiveness of degradation was mirrored by the reaction intermediates and daughter product concentrations where 0.1 and 5% Pd/MCM-41 produced higher concentrations of these products when compared to the 1% Pd/MCM-41. The 1% Pd/MCM-41 experiment also indicated zero concentrations of the daughter products within 120 min while the 0.1 and 5% Pd/MCM-41 materials produced them above detection limits. Therefore, there was increased degradation efficiency when Pd content was increased ten fold from 0.1 to 1%, but a loss in efficiency occurred when Pd content was increased from 1 to 5%. This paradoxical finding that increasing the amount of Pd present does not necessarily increase the material's capacity to degrade TCE suggests that there is an optimal Pd mass percent content of Pd/MCM-41 that lies between 0.1 and 5%. This conclusion is supported by Kim & Carraway (2003) who studied TCE degradation efficiency of Pd-coated zero-valent iron. They observed increased reaction rates with increasing Pd content up to a loading of 0.098%.

Loadings above this mass percent produced diminishing returns with regards to degradation efficiency. The authors attribute this loss in efficiency to complete covering of Fe by Pd, inhibiting Fe corrosion, and aggregation of Pd particles at higher loadings, effectively reducing the Pd surface area available for adsorption. This second explanation is applicable to the Pd/MCM-41 experiments as Pd particles may have agglomerated and become large enough to block the pores of MCM-41, effectively reducing access of TCE to Pd active sites. An alternate explanation for the decrease in degradation efficiencies is proposed to be extensive absorption of hydrogen by Pd in samples with higher mass % contents of Pd. A calculation based on the hydrogen uptake experiment described in section 3.3.3 indicated that there was sufficient Pd present in the 5% Pd/MCM-41 to absorb all of the available $H_2$ from the 40 ml of $H_2$-saturated solution (Appendix F). If only hydrogen dissolved in solution is capable of reacting with TCE, this may explain the lower efficiency of the 5% Pd/MCM-41 to degrade TCE. This is partly supported by an article by Lowry & Reinhard (2001) where decreased TCE transformation rates and increased production of halogenated reaction intermediates was observed below hydrogen concentrations of 100 μM.

A literature review was undertaken to compare the efficiency of the Pd/MCM-41 catalyst with the results of other researchers treating TCE with palladium and other catalyst systems. Degradation experiments in this research employed 50 mg of reactive material (0.1, 1, and 5% by mass Pd/MCM-41) in 40 ml of 10 mg/l TCE in hydrogen-saturated deionized water ($7.61 \times 10^{-2}$ mM). This represents a liquid to solid ratio of 800/1. Arnold & Roberts (2000) performed TCE degradation experiments using Fisher zero-valent iron (no palladium was present) in a solution containing 12 uM initial TCE concentration. They observed a degradation half-life of 55 h using 0.25 g of iron per 160 ml of solution with minimal production of chlorinated daughter products. In a TCE degradation experiment using a two-stage column reactor, McNab & Ruiz (1998) reported 100% TCE degradation in slightly more than 4 min using a 1% Pd on alumina beads catalyst system. Initial TCE concentrations were between 0.5 and 0.6 mg/l and no chlorinated degradation products were detected. The article by Kim & Carraway (2003) reported a TCE half-life of approximately 4 h and complete degradation in 25 h using a Pd/Fe catalyst with 0.047% Pd by mass. They did not detect reaction intermediates during the experiment. Lowry & Reinhard (1999) recorded 97% TCE degradation half-lives of approximately 4 to 6 min using 0.22 g/l of 1% Pd on aluminum.

Ethane was the only detected daughter product. A later article by Lowry & Reinhard (2001) reported a transformation half-life of 20 min for 140-180 μM TCE using 0.1 g/l of 1% by mass $Pd/Al_2O_3$ catalyst. They reported chlorinated reaction intermediates as composing 9.8% of the carbon mass balance. Lin *et al.* (2004) observed complete degradation of 7.5 mg/l TCE by 0.3 g of 0.25% by mass Pd on zero-valent iron within 5 min. Chlorinated daughter products accounted for 11.8% of degraded TCE. The article also includes a summary of degradation efficiency and daughter product concentrations resulting from experiments using other catalyst materials. They reported TCE degradation times of 6, 35, and 110 h for Ru/Fe, Pt/Fe, and Au/Fe with daughter products composing 0.5, 10.3, and 2.5% of degraded TCE, respectively. The efficiency of the Pd/MCM-41 materials used in this research is closest to the findings of Lowry & Reinhard (2001) as well as Lin *et al.* (2004) given the observed reaction rates and production of chlorinated daughter products. However, an unequivocal concluding as to which system is most efficient is not possible given the differences in reaction parameters between studies. Pd/MCM-41 also appears to be significantly more efficient than zero-valent iron alone or with other transition metal catalysts while producing daughter product concentrations that are on a par with other Pd catalyst materials.

#### 3.3.4.2 Identification of Reaction Pathway

An important aspect of TCE degradation experiments is to identify the degradation pathway. This is relevant to water treatment system design as the chlorinated daughter products (VC, 1,1-DCE, and DCE isomers) of TCE degradation may have higher toxicity and mobility in water than the TCE itself. It could be generally said that replacing one toxic contaminant with another is not an appropriate goal in treating contaminated water. The degradation pathway is determined through examining the concentrations of daughter products and gases produced as TCE is degraded. These concentrations are most easily compared through their contributions to the carbon balance. As a result of an NMR study of TCE adsorption onto Pd, Sriwatanapongse *et al.* (2006) proposed that there should be little to no production of reaction intermediates and chlorinated daughters under ideal conditions. They suggested that partially dehalogenated species remain adsorbed on the Pd surface until they react with excess hydrogen and desorb as ethane. The detection of chlorinated daughter products in experiments conducted for this research indicates that while there may be complete conversion of TCE before desorption as

ethane, there is also some degree of sequential dehalogenation taking place. In their much-referenced article, Arnold & Roberts (2000) propose possible reaction pathways for TCE reduction by zero-valent iron (figure 3.1). In the case of these experiments there are four groups of relevant reaction processes by which TCE may degrade to ethylene and ethane. The first group is composed of hydrogenolysis reactions where chlorine atoms are sequentially replaced by hydrogen atoms as TCE degrades to the DCE isomers, vinyl chloride, and finally to ethylene and ethane. The second group is composed of $\beta$-elimination reactions where two Cl atoms are removed from the TCE molecule, producing chloroacetylene with triple bonded C atoms. *Cis* and *trans* DCE may also degrade via a $\beta$-elimination pathway where two Cl atoms are removed, producing acetylene with triple bonded C atoms. Chloroacetylene then degrades to acetylene via a hydrogenolysis reaction. The third group is $\alpha$-elimination by which the two Cl atoms of the 1,1-DCE molecule are removed, producing ethylene. Finally, acetylene can sequentially degrade to ethylene and ethane via hydrogenation reactions. Hydrogenation involves the reduction of multiple bonds, as in the case of acetylene converting to ethylene. Efforts are generally made to avoid inducing sequential hydrogenolysis reactions in water treatment systems as these reactions can result in higher concentrations of chlorinated daughter products. In the case of sequential degradation, a combination of $\beta$-elimination and hydrogenation reactions is preferable as these processes degrade TCE to ethylene and ethane without producing accumulations of chlorinated daughter products.

Chlorinated daughter contributions to the carbon balance were 7.0, 3.6, and 3.6% at their maximum production in the 0.1, 1, and 5% Pd/MCM-41 experiments, respectively. Average contributions of daughter products to the carbon balances were 3.0, 1.7, and 3.0% in the 0.1, 1, and 5% Pd/MCM-41 experiments, respectively. Vinyl chloride was detected at a level of 1% of initial TCE concentration in the 0.1% Pd/MCM-41 experiment and was not detected in the 1 and 5% Pd/MCM-41 samples. The average contribution of gaseous products to the carbon balance was 63% in the 0.1% Pd/MCM-41 experiment. Samples from the 1 and 5% Pd/MCM-41 experiments were not analyzed for gas concentrations.

If degradation of TCE is occurring along a sequential dechlorination pathway, then $\beta$-elimination and hydrogenation are likely the dominant reactions, as evidenced by the gases contributing 63% of the carbon balance (Arnold and Roberts, 2000). The dominance of

ethylene and ethane over other gaseous degradation products provides further support for these reactions being the dominant pathways. However, the lack of production of acetylene above detection limits makes it difficult to definitively conclude that $\beta$-elimination is the dominant pathway in the case of these experiments. Additionally, as the Arnold and Roberts batch experiments included zero-valent iron, it is difficult to make a direct comparison of their results to those of this research. If the Pd catalyzed TCE degradation reaction was sequential – daughter products desorbing as they were produced – there would be production of total DCE at 32% of the carbon balance or more at some point during the experiment (Lowry & Reinhard, 1999). The maximum observed production of total DCE was 5.6%, occurring in the sample taken at 6 min. The sum of daughter product concentrations contributed less than 10% of the carbon balance at their maximum production levels in all experiments conducted for this research with average contributions of 3% and lower. It is also significant that the general shape of the normalized mass versus time plots of the various daughter products were similar to each other in each experiment. The similarities in shape of the plots suggest a random process of desorption of daughters before all chorine atoms of TCE had been replaced, rather than a sequential dechlorination process (Lowry & Reinhard, 2001).

It is concluded that complete dechlorination of TCE occurred before desorption as the gaseous products ethylene and ethane during the batch reactions conducted for this research. Detection of relatively low concentrations of chlorinated daughter products suggests random desorption of products before complete dechlorination had occurred rather than indicating a sequential degradation pathway. The lack of detection of acetylene in the 0.1% Pd/MCM-41 samples supports this conclusion as this compound is considered a reaction intermediate as TCE degrades to ethane along a $\beta$-elimination pathway (Kim & Carraway, 2003).

### 3.4 Conclusions

A series of Pd/MCM-41 samples were prepared at varying mass percent loadings of Pd. It was found that actual Pd content determined by EDAX analysis differed from the calculated Pd content. This difference increased with increasing Pd contents. Hydrogen uptake experiments using Pd/MCM-41 samples revealed 5.3 and 6.4 moles of H being absorbed for each mole of Pd present. Uptake occurred as quickly as hydrogen could be injected into the sample syringe.

Attempts to synthesize a sample of MCM-41 with enlarged pores were unsuccessful due to loss of pressure – and a corresponding loss of water from the reaction gel – from within the autoclave and reaction between the synthesis gel and the stainless steel autoclave during the crystallization stage of the synthesis.

Results of the batch TCE degradation experiments showed no degradation of TCE by regular MCM-41. This implies that changes in TCE concentrations in the reactive samples using Pd/MCM-41 resulted from degradation of TCE and not adsorption of the compound to the MCM-41 surface. The 0.1% Pd/MCM-41 degraded 70% of initial TCE with a degradation half-life of 14 min. Chlorinated daughters contributed 3% of the carbon balance. Gaseous products of TCE degradation contributed an average of 63% of the carbon balance. The 1% Pd/MCM-41 degraded 92% of initial TCE with a degradation half-life of between 3 and 6 minutes. Chlorinated daughter concentrations approached zero normalized mass units in 125 min contributing an average of 3.6% of the carbon balance. The 5% Pd/MCM-41 degraded 22% of initial TCE with a degradation half-life of between 2 and 3 min. Chlorinated daughters composed 3.6% of the carbon balance. The loss in efficiency between the 1 and 5% by mass Pd/MCM-41 samples is attributed extensive absorption of hydrogen by palladium particles. Degradation of TCE by Pd/MCM-41 compares favourably to other, similar catalyst systems and is a substantial improvement over the dehalogenation rates of zero-valent iron alone. Complete degradation of TCE by Pd/MCM-41 before desorbing as ethane is proposed to be the dominant degradation process with random desorption of chlorinated daughter products producing relatively low concentrations of 1,1-DCE, *cis* DCE, *trans* DCE, and VC during the batch experiments.

## 4. SUMMARY OF CONCLUSIONS

The synthesis of regular MCM-41 was found to be relatively straightforward, producing loose, white powders of exceptionally-high surface area. Various metals can be substituted for the tetrahedrally-coordinated silicon atom in MCM-41 with a corresponding decrease in structure quality with increasing metal content. A sample of Al-substituted MCM-41 was successfully synthesized but was found to be less crystalline than regular MCM-41.

MCM-41 was found to be metastable and more soluble than amorphous silica in water. Precipitation of amorphous silica from solution creates a protective layer of amorphous silica on the MCM-41 surface. A minimum Gibbs free energy of formation of MCM-41 was calculated to be - 819.5 kJ/mol, which is higher than that of quartz. Substituting Al into the MCM-41 structure had no effect on its solubility and thus its stability. Physical changes in MCM-41 in contact with water for a period of 79 days were an increased proportion of an amorphous phase present in the sample and a qualitative loss of a finer phase of material at the nanometer scale. There was no significant change in surface area of MCM-41 in contact with water for 79 days.

Palladization of MCM-41 can be achieved through a simple incipient wetness technique. Close agreement between calculated and actual Pd contents at lower mass percent loadings indicates that the procedure is more effective at lower Pd contents. Efficiency of TCE degradation by Pd/MCM-41 was examined in batch experiments with reaction bottles prepared with liquid/solid ratios of 800/1. MCM-41 samples with 0.1, 1, and 5 mass % loadings of Pd degraded 70, 92, and 22% of initial TCE concentrations in the presence of hydrogen. The decreased degradation between loadings of 1 and 5% was attributed to rapid absorption of hydrogen by palladium, which was then unavailable for reaction with TCE. Production of chlorinated daughters (1,1-DCE, DCE isomers, and VC) contributed 7, 3.6, and 3.6% of the carbon mass balance at their maximum production in the 0.1, 1, and 5% Pd/MCM-41 samples. Samples from the 0.1% Pd/MCM-41 experiment were also analyzed for gaseous products of TCE degradation. Ethane was produced at the highest concentrations relative to the other gaseous products. The small contribution of chlorinated daughter products and high contribution of gaseous products to the carbon balance, non-detection of acetylene, and

similarities in the shapes of the normalized mass curves of chlorinated daughter products suggest that complete degradation of TCE by Pd/MCM-41 before desorbing as ethane rather than degradation along a sequential pathway such as $\beta$-elimination.

The overall conclusion of this investigation is that although MCM-41 is thermodynamically unstable in water at ambient conditions, it exhibits exceptionally-high TCE degradation efficiencies when employed as a Pd catalyst support material in the presence of hydrogen. The TCE treatment efficiency is equivalent to and slightly higher than several other Pd catalyst technologies currently under investigation by other researchers. Considering Pd/MCM-41's ability to degrade TCE with relatively low production of undesirable chlorinated daughter products, further investigation into the material's application in water treatment systems is recommended.

## 5. RECOMMENDED FUTURE WORK

With regards to the high solubility of MCM-41 in water, further effort into synthesizing MCM-41 materials with different morphologies and pore sizes and determining their effect on stability in water is recommended. A longer term solubility experiment using regular MCM-41 could potentially investigate in greater detail the nature and extent of the MCM-41 recrystallization process from solution that is in contact with MCM-41. Future solubility experiments where fresh MCM-41 is added to water already at saturation with respect to amorphous silica may facilitate a better determination of the solution's silica concentration corresponding to the true solubility of MCM-41 and thus a better estimate of its Gibb's free energy of formation. .

Pd/MCM-41 showed high efficiency in degrading TCE. Future work would benefit from conducting different experiments to elaborate on this finding. The first recommendation would be a time-dependent TCE degradation batch test to determine if amorphous silica recrystallization from solution blocks TCE migration to reactive sites on the Pd surfaces. Other future studies would include: evaluation of the effect of MCM-41 pore size on TCE degradation efficiency; determining the optimal mass percent loading of Pd/MCM-41 for use in dehalogenation reactions; investigating the nature of the hydrogen uptake by Pd/MCM-41 in

greater detail; and evaluating the degradation efficiencies of other metal coatings, such as nickel. Most importantly, experiments addressing the ultimate goal of this research should be conducted, i.e. using a mixture of Pd/MCM-41 with zero-valent iron as the hydrogen source for the dehalogenation of TCE in column experiments (figure 1.1).

**APPENDIX A**

**Small angle XRD traces of MCM-41 samples prepared for this thesis.**

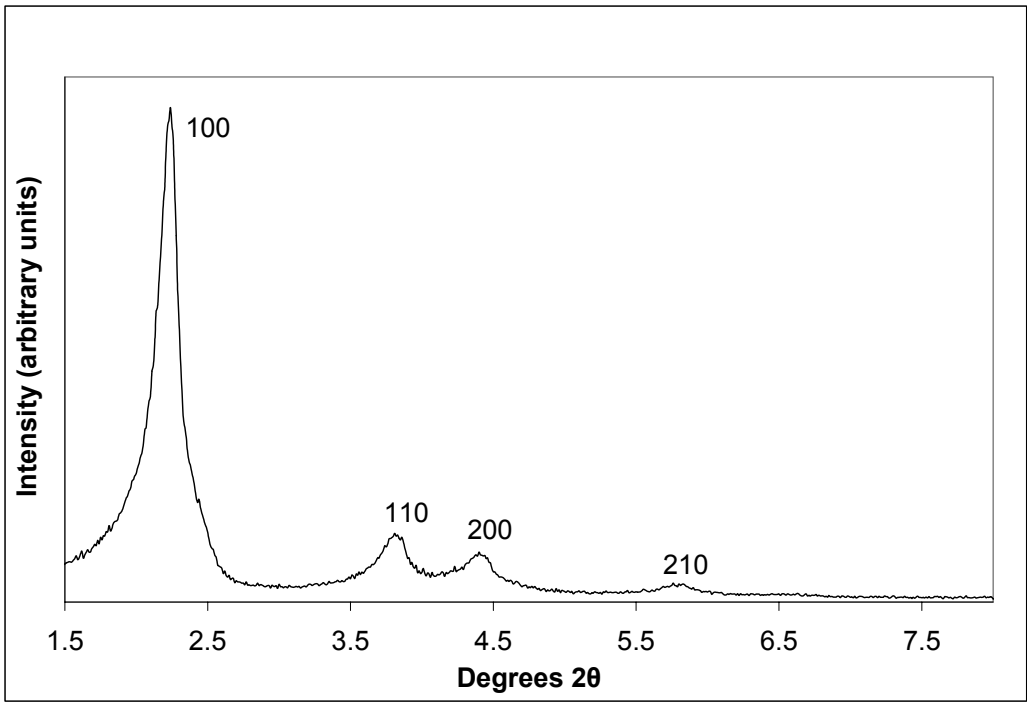


**Sample:** Aug. 29-05 MCM-41

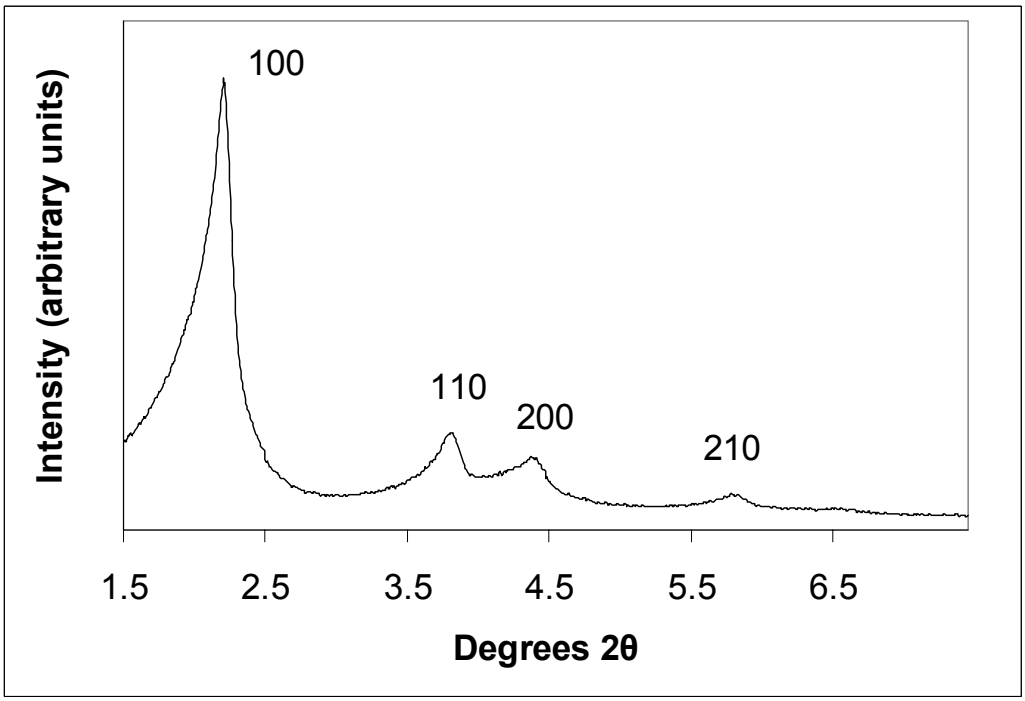


**Sample:** Oct. 13-05-A MCM-41

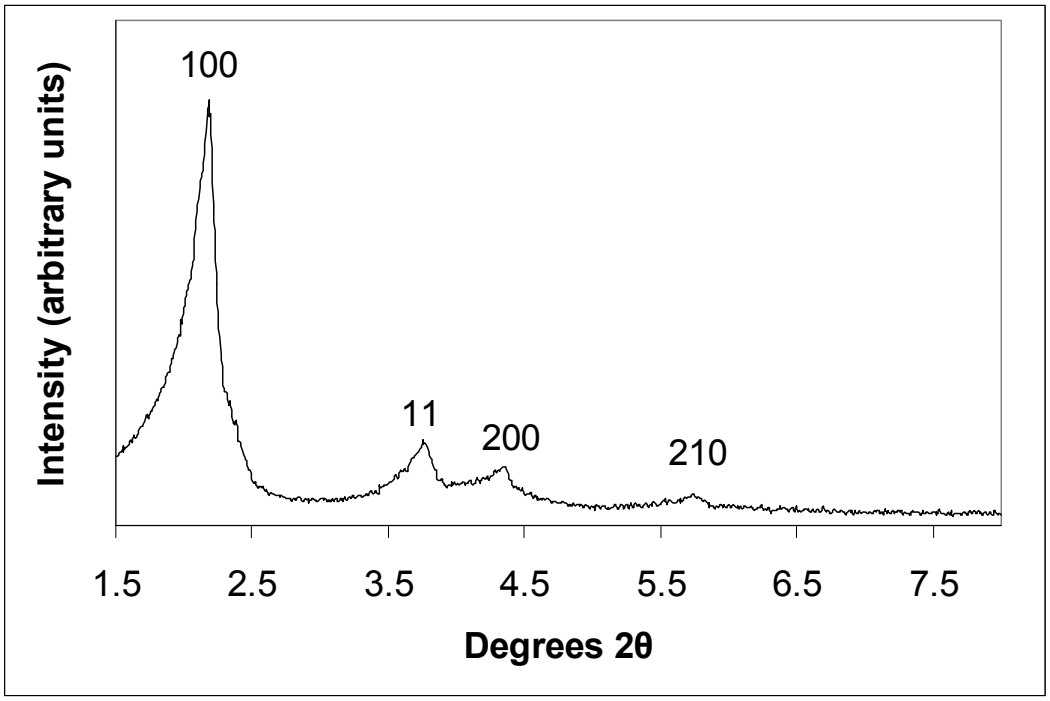


**Sample:** Oct. 13-05-B MCM-41

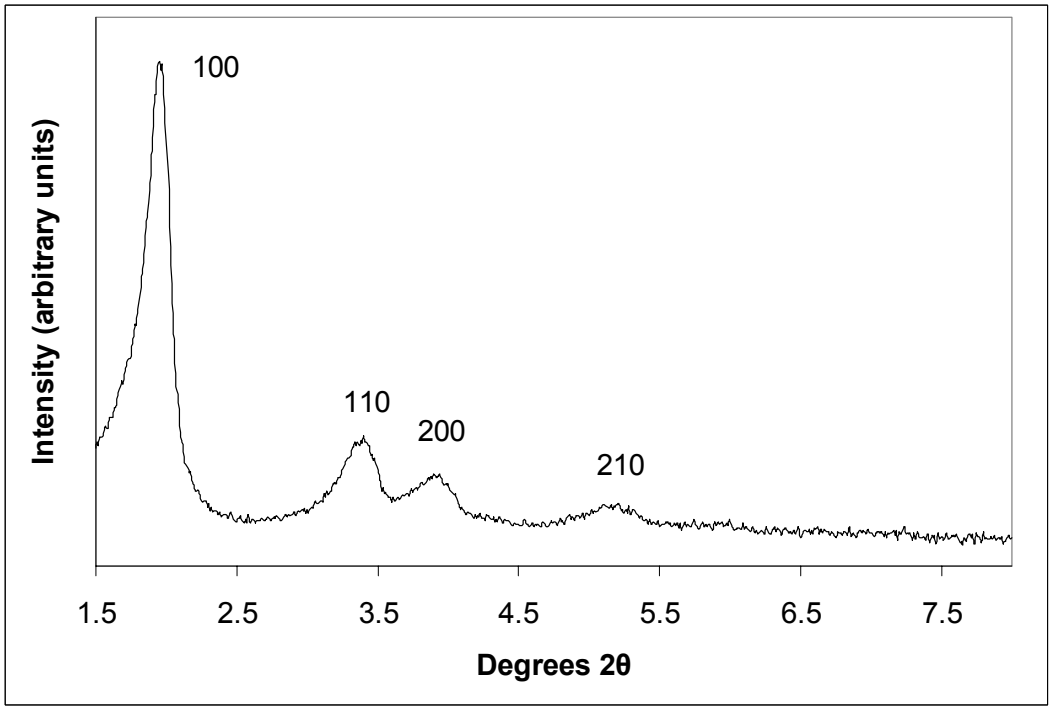


**Sample:** Aug. 22-06 MCM-41

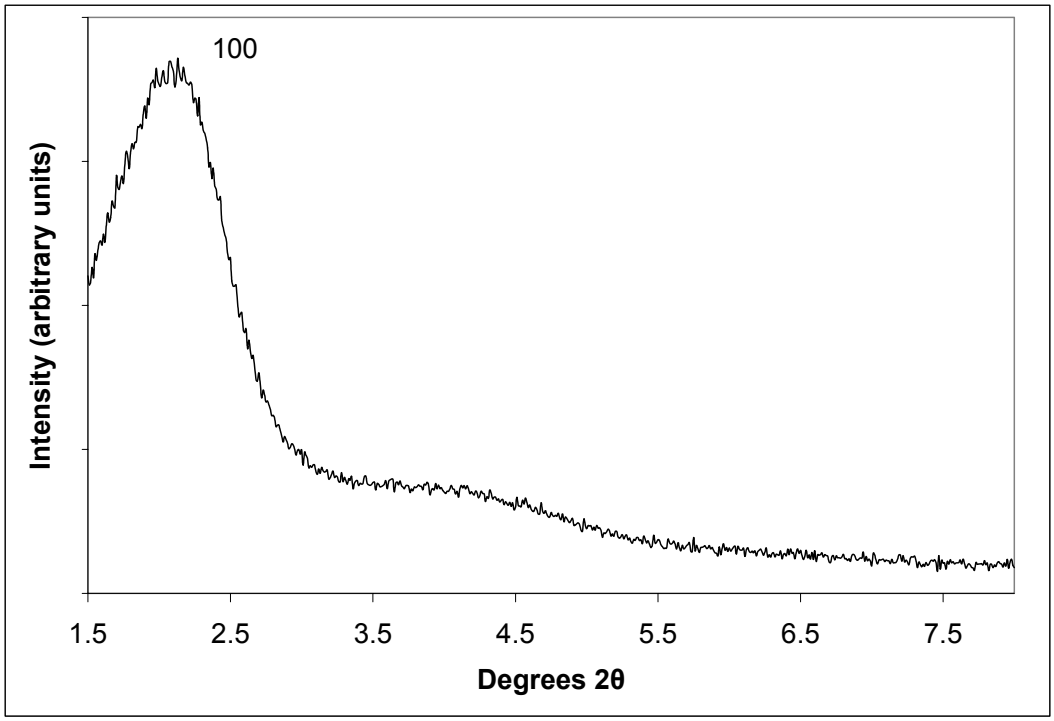


**Sample:** Al-MCM-41

## APPENDIX B

### Proportion of Silanol Groups Located at the Surface of MCM-41

A calculation was performed to estimate the proportion of silanol groups of MCM-41 that are located on the surface compared to the bulk of a representative sample. The calculation was done by assuming an MCM-41 formula mass of 60.0 g/mol, the formula mass of silica ($SiO_2$). Surface science research into MCM-41 conducted by Zhao *et al.* (1997) suggests that typical MCM-41 has 2.5 silanol groups per $nm^2$ of surface area. A surface area of 1 000 $m^2/g$ was used as a conservative estimate based on published characterizations of the material in addition to characterization results of materials prepared in this study.

(1 g MCM-41) / (60 g/mol) * NA = 1.0 X $10^{22}$ total atoms Si

(2.5 X $10^{18}$ Si groups / $m^2$) * (1 000 $m^2/g$) = 2.5 X $10^{21}$ surface Si groups/g

(2.5 X $10^{21}$ surface Si groups/g) / (1.0 X $10^{22}$ total atoms Si) * 100% = 25%

Therefore, it is estimated that 25% of all silanol groups present in a sample of MCM-41 are located at the surface of the material.

## APPENDIX C

### Silica concentration results from MCM-41 dissolution experiments:

| Solid/Liquid Ratio | Day Sampled | Concentration (ppm silica) |
|---|---|---|
| Blank | 1 | -5.1 |
| | 2 | -6.1 |
| | 4 | -7.1 |
| | 7 | -8.6 |
| | 10 | -0.3 |
| | 14 | 0.1 |
| | 16 | -2.8 |
| | 18 | -6.1 |
| | 21 | -2.1 |
| | 28 | -5.2 |
| | 57 | -0.9 |
| | 79 | 1.1 |
| 1/200 | 1 | 63.7 |
| | 2 | 91.4 |
| | 4 | 111.2 |
| | 7 | 128.5 |
| | 10 | 124.3 |
| | 14 | 127.9 |
| | 16 | 114.6 |
| | 18 | 116.0 |
| | 18 | -7.4 |
| | 21 | 51.9 |
| | 23 | 69.6 |
| | 25 | 78.1 |
| | 28 | 84.6 |
| | 57 | 105.0 |
| | 79 | 101.5 |
| 1/100 | 1 | 118.6 |
| | 2 | 153.8 |
| | 4 | 166.6 |
| | 7 | 175.0 |
| | 10 | 148.9 |
| | 14 | 136.4 |
| | 16 | 133.6 |
| | 18 | 122.8 |
| | 18 | -2.3 |
| | 21 | 71.0 |
| | 23 | 85.6 |
| | 25 | 90.6 |
| | 28 | 100.6 |
| | 57 | 111.7 |
| | 79 | 103.8 |

| Solid/Liquid Ratio | Day Sampled | Concentration (ppm silica) |
|---|---|---|
| 1/200 (duplicate) | 1 | 63.7 |
| | 2 | 93.4 |
| | 4 | 122.1 |
| | 7 | 142.4 |
| | 10 | 134.9 |
| | 14 | 133.0 |
| | 16 | 128.1 |
| | 18 | 130.0 |
| | 18 | -7.8 |
| | 21 | 49.4 |
| | 23 | 74.1 |
| | 25 | 74.9 |
| | 28 | 82.5 |
| | 57 | 109.3 |
| | 79 | 105.0 |

**Silica concentration results for earlier MCM-41 dissolution experiment:**

| Solid/Liquid Ratio | Day Sampled | Concentration (ppm silica) |
|---|---|---|
| Blank | 1 | 5.0 |
| | 3 | 5.4 |
| | 5 | -3.5 |
| | 7 | -1.9 |
| | 10 | -1.9 |
| | 14 | -1.5 |
| | 21 | -2.3 |
| | 28 | -1.1 |
| 1/200 | 1 | 59.6 |
| | 3 | 92.4 |
| | 5 | 107.8 |
| | 7 | 116.5 |
| | 10 | 110.6 |
| repeat analysis: | *10* | *146.9* |
| | 14 | 117.8 |
| | 21 | 120.7 |
| | 28 | 117.8 |
| 1/100 | 1 | 104.2 |
| | 2 | 128.3 |
| | 3 | 142.6 |
| | 4 | 149.7 |

| Solid/Liquid Ratio | Day Sampled | Concentration (ppm silica) |
|---|---|---|
| 1/75 | 1 | 126.4 |
| repeat analysis: | *1* | *164.4* |
| | 3 | 223.7 |
| | 5 | 220.9 |
| | 7 | 209.6 |
| | 10 | 142.4 |
| | 14 | 187.0 |
| | 21 | 128.9 |
| | 28 | 124.3 |
| 1/25 | 1 | 308.5 |
| | 3 | 254.8 |
| | 5 | 229.4 |
| | 7 | 149.8 |
| | 10 | 195.5 |
| | 14 | 181.4 |
| | 21 | 129.7 |
| | 28 | 192.7 |

**Silica concentration results from Al-MCM-41 dissolution experiment:**

| Solid/Liquid Ratio | Day Sampled | Concentration (ppm silica) |
|---|---|---|
| Blank | 1 | -5.1 |
| | 2 | -6.1 |
| | 4 | -7.1 |
| | 7 | -8.6 |
| | 10 | -0.3 |
| | 14 | 0.1 |
| | 16 | -2.8 |
| | 18 | -6.1 |
| | 21 | -2.1 |
| | 28 | -5.2 |
| | 57 | -0.9 |
| | 79 | 1.1 |
| 1/200 | 1 | 88.9 |
| | 2 | 116.6 |
| | 4 | 115.6 |
| | 7 | 132.5 |
| | 10 | 131.9 |
| | 14 | 127.9 |
| | 21 | 124.5 |
| | 28 | 117.0 |
| | 79 | 115.6 |

| Solid/Liquid Ratio | Day Sampled | Concentration (ppm silica) |
|---|---|---|
| 1/100 | 1 | 122.1 |
| | 2 | 144.4 |
| | 4 | 142.9 |
| | 7 | 150.3 |
| | 10 | 138.7 |
| | 14 | 136.8 |
| | 21 | 138.2 |
| | 28 | 127.2 |
| | 79 | 116.0 |
| 1/75 | 1 | 140.9 |
| | 2 | 156.2 |
| | 4 | 150.3 |
| | 7 | 168.1 |
| | 10 | 144.7 |
| | 14 | 132.2 |
| | 21 | 136.1 |
| | 28 | 149.3 |
| | 79 | 118.4 |
| 1/200 (duplicate) | 1 | 89.4 |
| | 2 | 110.2 |
| | 4 | 135.0 |
| | 7 | 140.9 |
| | 10 | 126.9 |
| | 14 | 130.0 |
| | 21 | 126.6 |
| | 28 | 119.4 |
| | 79 | 117.6 |
| 1/100 (duplicate) | 1 | 117.1 |
| | 2 | 144.9 |
| | 4 | 135.0 |
| | 7 | 162.7 |
| | 10 | 143.8 |
| | 14 | 135.5 |
| | 21 | 135.7 |
| | 28 | 163.7 |
| | 79 | 123.1 |
| 1/75 (duplicate) | 1 | 141.4 |
| | 2 | 156.2 |
| | 4 | 153.8 |
| | 7 | 172.1 |
| | 10 | 145.9 |
| | 14 | 135.5 |
| | 21 | 137.8 |
| | 28 | 128.4 |
| | 79 | 121.5 |

## APPENDIX D

### Results of EDAX analysis for Pd contents of Pd/MCM-41 samples.

| **Sample** | Aug. 29-05 | Oct. 13-05-A | |
|---|---|---|---|
| **Calc. Pd Content % by mass** | 2% | 1% | 5% |
| **EDAX results:** | not analyzed | 0.55 | 3.46 |
| | | 0.87 | 2.93 |
| | | 0.22 | 2.83 |
| | | 1.10 | - |
| **Maximum** | - | 1.1 | 3.46 |
| **Minimum** | - | 0.22 | 2.83 |
| **Average** | - | 0.69 | 3.07 |
| **Standard Deviation** | - | 0.38 | 0.34 |

| **Sample** | Oct. 13-05-B | Aug. 22-06 | | |
|---|---|---|---|---|
| **Calc. Pd Content % by mass** | 5% | 0.1% | 1% | 5% |
| **EDAX results:** | 2.38 | 0.39 | 0.99 | 2.94 |
| | 1.55 | 0.33 | 1.60 | 1.25 |
| | 1.88 | 0.37 | 1.10 | 3.77 |
| | 3.19 | 1.01 | | |
| | 2.19 | 0.88 | | |
| | | 0.00 | | |
| **Maximum** | 3.19 | 1.01 | 1.60 | 3.77 |
| **Minimum** | 1.55 | 0.00 | 0.99 | 1.25 |
| **Average** | 2.24 | 0.50 | 1.23 | 2.65 |
| **Standard Deviation** | 0.62 | 0.38 | 0.33 | 1.28 |

## APPENDIX E

### Analysis results of MCM-41 and Pd/MCM-41 batch TCE degradation experiments.

### Unpalladized MCM-41:

| Sample: | Time (min) | TCE (ug/l) | VC (ug/l) | 1,1-DCE (ug/l) | tDCE (ug/l) | cDCE (ug/l) |
|---|---|---|---|---|---|---|
| control | 41 | 7940 | - | - | - | - |
| | 43 | 9088 | - | - | - | - |
| | 46 | 8736 | - | - | - | - |
| | 48 | 8176 | - | - | - | - |
| | 60 | 8624 | - | - | - | - |
| | 121 | 8160 | - | - | - | - |
| duplicate control | 41 | 7648 | - | - | - | - |
| | 43 | 8552 | - | - | - | - |
| | 46 | 8404 | - | - | - | - |
| | 48 | *12096* | - | - | - | - |
| | 60 | 7716 | - | - | - | - |
| | 121 | 8772 | - | - | - | - |
| reactive | 12 | 7736 | - | - | - | - |
| | 14 | 7544 | - | - | - | - |
| | 26 | 7296 | - | - | - | - |
| | 37 | 9196 | - | - | - | - |
| | 57 | 7748 | - | - | - | - |
| | 119 | 7988 | - | - | - | - |
| reactive duplicate | 12 | 8488 | - | - | - | - |
| | 14 | 8012 | - | - | - | - |
| | 26 | 8120 | - | - | - | - |
| | 37 | 7644 | - | - | - | - |
| | 57 | 7944 | - | - | - | - |
| | 119 | 7204 | - | - | - | - |

### 0.1% Pd MCM-41:

| Sample | Time (min) | TCE (ug/l) | VC (ug/l) | 11 DCE (ug/l) | tDCE (ug/l) | cDCE (ug/l) |
|---|---|---|---|---|---|---|
| reactive | 6 | 4200 | 36 | 115.1 | 58.6 | 110.3 |
| | 14 | 3288 | 4.7 | 67.4 | 13.4 | 60.9 |
| | 23 | 2324 | 4.5 | 59.1 | 11.5 | 57.3 |
| | 35 | 1960 | 4.6 | 61.3 | 12.5 | 58.8 |
| | 60 | 1864 | 3.8 | 57.4 | 14.9 | 55.2 |
| | 125 | 1992 | 3.5 | 58.4 | 10.4 | 55.4 |
| reactive duplicate | 6 | 3835 | 37.2 | 102.1 | 48.9 | 98.6 |
| | 14 | 2228 | 5.4 | 72.7 | 16.6 | 65.2 |
| | 23 | 2408 | 5.3 | 71.6 | 15.9 | 63.7 |
| | 35 | 2020 | 49 | 91.3 | 25.6 | 86.1 |
| | 60 | 2124 | 4.4 | 61.9 | 11.3 | 57.1 |
| | 125 | 2052 | 4.4 | 62.7 | 11.5 | 59 |

| Sample | Time (min) | TCE (ug/l) | VC (ug/l) | 11 DCE (ug/l) | tDCE (ug/l) | cDCE (ug/l) |
|---|---|---|---|---|---|---|
| control | 22 | 7344 | 0 | 2.5 | 1.4 | 2.4 |
| | 32 | 6572 | 0 | 1.1 | 0 | 0 |
| | 36 | 6968 | 0 | 1.5 | 0 | 1.6 |
| | 44 | 6220 | 0 | 0 | 0 | 0 |
| | 63 | 6428 | 0 | 0 | 0 | 0 |
| | 127 | 6652 | 0 | 0 | 0 | 0 |
| control duplicate | 22 | 7728 | 0 | 0 | 0 | 0 |
| | 32 | 6780 | 0 | 0 | 0 | 0 |
| | 36 | 6000 | 3.6 | 6.4 | 3.6 | 9.6 |
| | 44 | 6404 | 0 | 0 | 0 | 0 |
| | 63 | 6276 | 0 | 0 | 0 | 0 |
| | 127 | LOST | 0 | 0 | 0 | 0 |

**0.1% Pd/MCM-41 gaseous products:**

| Sample | Time (min) | methane (ug/l) | ethylene (ug/l) | acetylene (ug/l) | ethane (ug/l) |
|---|---|---|---|---|---|
| reactive | 6 | 4.1 | 13.4 | 0 | 554.3 |
| | 14 | 5.8 | 15.1 | 0 | 912.5 |
| | 23 | 2.5 | 11.7 | 0 | 1003.1 |
| | 35 | 3.7 | 13.7 | 0 | 1268.5 |
| | 60 | 4.6 | 13.5 | 0 | 1172.4 |
| | 125 | 5.3 | 11.2 | 0 | 773.1 |
| reactive duplicate | 6 | 4.8 | 12.5 | 0 | 528.5 |
| | 14 | 5 | 14.3 | 0 | 1029.9 |
| | 23 | 2.4 | 13.3 | 0 | 931.4 |
| | 35 | 4.4 | 14 | 0 | 956.3 |
| | 60 | 4.6 | 13.2 | 0 | 899.1 |
| | 125 | 28 | 15 | 0 | 912.6 |
| control | 22 | 5.8 | 1.7 | 0 | 27.3 |
| | 32 | 5.4 | 0.6 | 0 | 20.8 |
| | 36 | 1.9 | 0.8 | 0 | 46.1 |
| | 44 | 3.7 | 0 | 0 | 10.7 |
| | 63 | 4 | 8.3 | 0 | 6 |
| | 127 | 8.3 | 1.6 | 0 | 9.2 |
| control duplicate | 22 | 4.2 | 0 | 0 | 0.9 |
| | 32 | 5.8 | 0 | 0 | 1.8 |
| | 36 | 4.4 | 1.9 | 0 | 50.8 |
| | 44 | 4.6 | 0 | 0 | 1.8 |
| | 63 | 4.6 | 2.4 | 0 | 42.9 |
| | 127 | 2.8 | 0 | 0 | 0 |

**1% Pd/MCM-41:**

| Sample | Time (min) | TCE (ug/l) | VC (ug/l) | 11 DCE (ug/l) | tDCE (ug/l) | cDCE (ug/l) |
|---|---|---|---|---|---|---|
| reactive | 12 | 888 | 0 | 29 | 9 | 88 |
| | 20 | 842 | 0 | 28 | 9 | 42 |
| | 31 | 1035 | 0 | 26 | 8 | 40 |
| | 40 | 305 | 0 | 0 | 0 | 0 |
| | 62 | 676 | 0 | 20 | 6 | 30 |
| | 125 | 640 | 0 | 22 | 5 | 29 |
| reactive duplicate | 12 | 901 | 0 | 32 | 28 | 52 |
| | 20 | 910 | 0 | 32 | 10 | 52 |
| | 31 | 436 | 0 | 0 | 0 | 0 |
| | 40 | 653 | 0 | 24 | 7 | 34 |
| | 62 | 534 | 0 | 20 | 6 | 31 |
| | 125 | 348 | 0 | 0 | 0 | 0 |
| control | 36 | 4014 | 0 | 0 | 0 | 0 |
| | 41 | 4300 | 0 | 0 | 0 | 0 |
| | 45 | 4199 | 0 | 0 | 0 | 0 |
| | 49 | 4550 | 0 | 0 | 0 | 0 |
| | 64 | 4242 | 0 | 0 | 0 | 0 |
| | 127 | 4240 | 0 | 0 | 0 | 0 |
| control duplicate | 36 | 4176 | 0 | 0 | 0 | 0 |
| | 41 | 4460 | 0 | 0 | 0 | 0 |
| | 45 | 4380 | 0 | 0 | 0 | 0 |
| | 49 | *3466* | 0 | 0 | 0 | 0 |
| | 64 | 4475 | 0 | 0 | 0 | 0 |
| | 127 | 4235 | 0 | 0 | 0 | 0 |

**5% Pd/MCM-41:**

| Sample | Time (min) | TCE (ug/l) | VC (ug/l) | 11 DCE (ug/l) | tDCE (ug/l) | cDCE (ug/l) |
|---|---|---|---|---|---|---|
| reactive | 7 | 4934 | 0 | 44 | 22 | 95 |
| | 17 | 4853 | 0 | 33 | 15 | 74 |
| | 28 | 4306 | 0 | 38 | 20 | 93 |
| | 39 | 4368 | 0 | 40 | 22 | 97 |
| | 60 | 4755 | 0 | 22 | 10 | 46 |
| | 133 | - | - | - | - | - |
| reactive duplicate | 7 | 4850 | 0 | 36 | 18 | 87 |
| | 17 | 4617 | 0 | 24 | 8 | 46 |
| | 28 | 4417 | 0 | 30 | 16 | 76 |
| | 39 | 4526 | 0 | 46 | 12 | 98 |
| | 60 | 4547 | 0 | 39 | 20 | 91 |
| | 133 | - | - | - | - | - |
| control | 34 | 5998 | 0 | 0 | 0 | 0 |
| | 38 | 5912 | 0 | 0 | 0 | 0 |
| | 43 | *4936* | 0 | 0 | 0 | 0 |
| | 46 | 5799 | 0 | 0 | 0 | 0 |
| | 62 | 5922 | 0 | 0 | 0 | 0 |
| | 135 | - | - | - | - | - |
| control duplicate | 34 | 5768 | 0 | 0 | 0 | 0 |
| | 38 | 5674 | 0 | 0 | 0 | 0 |
| | 43 | 5940 | 0 | 0 | 0 | 0 |
| | 46 | *4531* | 0 | 0 | 0 | 0 |
| | 62 | 5694 | 0 | 0 | 0 | 0 |
| | 135 | - | - | - | - | - |




*** Calculation of Outlier (calculated using normalized masses):**

normalized mass at time equal to 43 min: 0.84 moles/initial moles TCE

$Q_1 = 0.981592$

$Q_3 = 1.002412$

$IQR = Q_3 - Q_1 = 0.02082$

lower boundary = $Q_1 - 3*IQR = 0.92$

upper boundary = $Q_3 + 3*IQR = 1.07$

The normalized mass value of 0.84 moles/initial moles TCE is lower than the lower boundary and is thus classified as an extreme outlier.

**APPENDIX F**

**A calculation to determine the amount of hydrogen absorbed from solution by the unpalladized, 1, and 5% Pd/MCM-41 samples.**

- Batch experiment results indicate an average initial TCE concentration of 8346.9 ug/l.

(0.04 l) * (0.0083469 g/l / 131.39 g/mol) = $3.0 \times 10^{-6}$ mol of TCE present in solution
→ $9.0 \times 10^{-6}$ mol of H ions needed to reduce TCE

---

**1% by mass Pd/MCM-41**

Note: EDAX analysis indicates real Pd content is between 1 and 1.1 %.

- Solubility of $H_2$ in water is: 0.000863 mol/l (Randall & Failey, 1927)
- 40 ml reaction bottle, with 0.05 g of 1% by mass Pd/MCM-41.
- Hydrogen uptake experiment indicated that 2 mol of $H_2$ can be taken up per 1 mol of Pd.
  → 4 mol H / 1 mol Pd

(40 ml / 1000ml/l) * (0.000863 mol/l) = $3.45 \times 10^{-5}$ mol $H_2$ available per reaction bottle
= $6.9 \times 10^{-5}$ mol of H available per reaction bottle

0.05 g of 1% by mass Pd/MCM-41 → $5 \times 10^{-4}$ g Pd

($5 \times 10^{-4}$ g Pd) * (mol / 106.42 g) = $4.7 \times 10^{-6}$ mol Pd

($4.7 \times 10^{-6}$ mol Pd) * (4 mol H / 1 mol Pd) = $1.9 \times 10^{-5}$ mol H could be taken up by Pd
[($6.9 \times 10^{-5}$ mol H available) – ($1.9 \times 10^{-5}$ mol taken up)]/2 = $2.5 \times 10^{-5}$ mol $H_2$ still available in solution

- still an excess of $H_2$ available for reaction to proceed.
- Batch experiment results indicated an average initial TCE concentration of 4297.4 ug/l.

(0.04 l) * (0.0042974 g/l / 131.39 g/mol) = $1.3 \times 10^{-6}$ mol of TCE present in solution
$3.9 \times 10^{-6}$ mol of H needed to reduce TCE

- There is adequate $H_2$ in solution and H in the Pd to reduce the TCE

**5% by mass Pd/MCM-41**

Note: EDAX analysis indicates real Pd content is between 3 and 5%

(40 ml / 1000ml/l) * (0.000863 mol/l) $= 3.45 \times 10^{-5}$ mol of $H_2$ available per reaction bottle
$= 6.9 \times 10^{-5}$ mol of H available per reaction bottle

---

0.05 g of 5% by mass Pd/MCM-41 → $2.5 \times 10^{-3}$ g Pd

$(2.5 \times 10^{-3}$ g Pd) * (mol / 106.42 g) $= 2.4 \times 10^{-5}$ mol Pd

$[(2.4 \times 10^{-5}$ mol Pd) * (4 mol H / 1 mol Pd)]/2 $= 4.7 \times 10^{-5}$ mol $H_2$ could be taken up by Pd

$4.7 \times 10^{-5}$ mol $H_2$ taken up > $3.45 \times 10^{-5}$ mol $H_2$ available in solution

- Batch experiment results indicated an average initial TCE concentration of 5838.4 ug/l.

(0.04 l)*(0.0058384 g/l / 131.39 g/mol) $= 1.8 \times 10^{-6}$ mol TCE present in solution
→ $5.4 \times 10^{-6}$ mol H needed to reduce TCE

- There would be adequate H in the Pd to reduce the TCE present, but not enough $H_2$ in solution to reduce TCE present.

## REFERENCES


Abramowicz, D.A., M.J. Brennan, H.M. Van Dort and E.L. Gallagher. 1993. Factors Influencing the Rate of Polychlorinated Biphenyl Dechlorination in Hudson River Sediments. *Environmental Science and Technology*, **27**, 1125-1131.

Alvaro M., A. Corma, D. Das, V. Fornes and H. Garcia. 2005. "*Nafion*"-functionalized mesoporous MCM-41 silica shows high activity and selectivity for carboxylic acid esterification and Friedel-Crafts acylation reactions. *Journal of Catalysis*, **231**, 48-55.

Araujo, A.S., M.J.B. Souza, A.O.S. Silva, A.M.G. Pedrosa, J.M.F.B. Aquino and A.C.S.L.S. Coutinho. 2005. Study of the Adsorption Properties of MCM-41 Molecular Sieves Prepared at Different Synthesis Times. *Adsorption*, **11**, 181-186.

Arnold, W.A. and A.L. Roberts. 2000. Pathways and Kinetics of Chlorinated Ethylene and Chlorinated Acetylene Reaction with Fe(0) Particles. *Environmental Science and Technology*, **34**, 1794-1805.

Bai, N., Y. Chi, Y. Zou and W. Pang. 2002. Influence of high pressure on structural property of mesoporous material MCM-41: study of mechanical stability. *Materials Letters*, **54**, 37-42.

Beck, J.S., J.C. Vartuli, W.J. Roth, M.E. Leonowicz, C.T. Kresge, K.D. Schmitt, C. T-W. Chu, D.H. Olson, E.W. Sheppard, S.B. McCullen, J.B. Higgins and J.L. Schienker. 1992. A New Family of Mesoporous Molecular Sieves Prepared with Liquid Crystal Templates. *Journal of the American Chemical Society*, **114**, 10834-10843.

Behrens, S. and G. Spittel. 2005. A new palladium nanoparticle catalyst on mesoporous silica prepared from a molecular cluster precursor. *Dalton Transactions*, 868-873.

Borade, R.B. and A. Clearfield. 1995. Synthesis of aluminum-rich MCM-41. *Catalysis Letters*. **31**, 267-272.

Brar, S.K. and S.K. Gupta. 2000. Biodegradation of trichloroethylene in a rotating biological contactor. *Water Research*, **24**(17), 4207-4214.

Cheng, C., D.H. Park and J. Klinowski. 1997. Optimal Parameters for the synthesis of the mesoporous molecular sieve [Si]-MCM-41. *Journal of the Chemical Society Faraday Transactions*, **93**(1), 193-197.

Cobden, P.D., V.V. Gorodetskii and B.E. Nieuwenhuys. 1999. Field emission microscope study of the initial behaviour of the palladium-hydrogen system at low temperatures. *Surface Science*, **432**, 61-68.

Corma, A., V. Fornes, M.T. Navarro and J. Perez-Pariente. 1994. Acidity and Stability of MCM-41 Crystalline Aluminosilicates. *Journal of Catalysis*, **148**, 569-574.

Corma, A., Q. Kan, M.T. Navarro, J. Perez-Pariente and F. Rey. 1997. Synthesis of MCM-41 with Different Pore Diameters without Addition of Auxiliary Organics. *Chemistry of Materials*, **9**, 2123-2126.

Corma, A. and E. Domine. 2005. Gold supported on a mesoporous $CeO_2$ matrix as an efficient catalyst in the selective aerobic oxidation of aldehydes in the liquid phase. *Chemical Communications*, 4042-4044.

Cothern, C.R., W.A. Coniglio and W.L. Marcus. 1986. Estimating risk to human health. *Environmental Science and Technology*, **20**(2), 111-116.

Crosta, G.F. and M. Dotti. 1998. Volatile halocarbons in a drinking water supply system: forecasting contamination values and estimating health risk. *Chemosphere*, **37**(14-15), 2873-2884.

Day, S. R., S.F. O'Hannesin and L. Mardsen. 1999. Geotechnical techniques for the construction of reactive barriers. *Journal of Hazardous Materials*, **B67**, 285-297.

Decyk, P. 2006. States of transition metal ions in modified mesoporous MCM-41 and in microporous ZSM-5 studied by ESR spectroscopy. *Catalysis Today*, **114**, 142-153.

Dua, M., A. Singh, N. Sethunathan and A.K. Johri. 2002. Biotechnology and bioremediation: successes and limitations. *Applied Microbiology and Biotechnology*, **59**, 143-152.

Eastman, J.A., L.J. Thompson and B.J. Kestel. 1993. Narrowing of the palladium-hydrogen miscibility gap in nanocrystalline palladium. *Physical Review B*, **48**(1), 84-92.

Ewald, G. 1998. Chlorinated Fatty Acids-Environmental Pollutants with Intriguing Properties. *Chemosphere*, **37**(14-15), 2833-2837.

Fortuny, A., C. Bengoa, J. Font and A. Fabregat. 1999. Bimetallic catalysts for continuous catalytic wet air oxidation of phenol. *Journal of Hazardous Materials B*, **64**, 181-193.

Gainza, A.H. 2004. Reaction of Halogenated Hydrocarbon Solvents with Tertiary Amines: Spectrophotometric and Conductimetric Study. *Wiley Interscience (online publication)*, 500-509.

Gavaskar, A.R. 1999. Design and construction techniques for permeable reactive barriers. *Journal of Hazardous Materials*, **68**, 41-71.

Gaydhankar, T.R., V. Samuel and P.N. Joshi. 2005. Hydrothermal synthesis of MCM-41 using differently manufactured amorphous dioxosilicon sources. *Materials Letters*, **60**, 957-961.

Gonzalez-Arellano, C., A. Corma, M. Iglesias and F. Sanchez. 2004. Pd(II)-Schiff Base Complexes Heterogenised on MCM-41 and Delaminated Zeolites as Efficient and Recyclable Catalysts for the Heck Reaction. *Advanced Synthesis & Catalysis*, **346**, 1758-1764.

Gusmao, A. D., T.M. Pereira de Campos, M. de Melo Maia Nobre and E. do Amaral Vargas Jr. 2004. Laboratory tests for reactive barrier design. *Journal of Hazardous Materials*, **110**, 105-112.

Haber, J., J.H. Block and B. Delmon. 1995. Manual of Methods and Procedures for Catalyst Characterization. *Pure and Applied Chemistry*, **67**, **Nos 8/9**, 1257-1306.

Hammond, W., E. Prouzet, S.D. Mahanti and T.J. Pinnavaia. 1999. Structure factor for the periodic walls of mesoporous MCM-41 molecular sieves. *Microporous and Mesoporous Materials*, **27**, 19-25.

Han, S., W. Hou, J. Xu and Z. Li. 2004. Synthesis of hollow spherical silica with MCM-41 mesoporous structure. *Colloid and Polymer Science*, **282**, 1286-1291.

Hanneken, J.W., D.B. Baker, M.S. Conradi and J.A. Eastman. 2002. NMR study of the nanocrystalline palladium-hydrogen system. *Journal of Alloys and Compounds*, **330-332**, 714-717.

Hohener, P., D. Werner, C. Balsiger and G. Pasteris. 2003. Worldwide Occurrence and Fate of Chlorofluorocarbons in Groundwater.*Critical Reviews in Environmental Science and Technology*, **33**(1), 1-29.

Holmes, S.M., V.L. Zholobenko, A. Thursfield, R.J. Plaisted, C.S. Cundy and J. Dwyer. 1998. *In Situ* FTIR study of the formation of MCM-41. *Journal of the American Chemical Society: Faraday Transactions*, **94**(14), 2025-2032.

Horcajada, P., A. Ramila, J. Perez-Pariente and M. Vallet-Regi. 2004. Influence of pore size of MCM-41 matrices on drug delivery rate. *Microporous and Mesoporous Materials*, **68**, 105-109.

Huo, Q., D.I. Margolese, U. Ciesla, D.G. Demuth, P. Feng, T.E. Gier, P. Sieger, A. Firouzi, B.F. Chmelka, F. Schuth and G.D. Stucky. 1994. Organization of Organic Molecules with Inorganic Molecular Species into Nanocomposite Biphase Arrays. *Chemistry of Materials*, **6**, 1176-1191.

Jana, S.K., R. Nishida, K. Shindo, T. Kugita and S. Namba. 2004. Pore size control of mesoporous molecular sieves using different organic auxiliary chemicals. *Microporous and Mesoporous Materials*, **68**, 133-142.

Joschek, S., B. Nies, R. Krotz and A. Goferich. 2000. Chemical and physicochemical characterization of porous hydroxyapatite ceramics made of natural bone. *Biomaterials*, **21**(16), 1645-1658.

Kao, C.M. and S.E. Lei. 2000. Using a peat biobarrier to remediate PCE/TCE contaminated aquifers. *Water Research*, **34**(3), 835-845.

Kim, Y-H and E.R. Carraway. 2003. Dechlorination of chlorinated ethenes and acetylenes by palladized iron. *Environmental Technology*, **24**, 809-819.

Kircheim, R., T. Mutschele, W. Kieninger, H. Gleiter, R. Birringer and T.D. Koble. 1988. Hydrogen in Amorphous and Nanocrystalline Metals. *Materials Science and Engineering*, **99**, 457-462.

Kittaka, S., T. Iwashita, A. Serizawa, M. Kranishi, S. Takahara, Y. Kuroda, T. Mori and T. Yarnaguchi. 2005. Low Temperature Properties of Acetonitrile Confined MCM-41. *Journal of Physical Chemistry B*, **109**, 23162-23169.

Kleestorfer, K., H. Vinek and A. Jentys. 2001. Structure simulation of MCM-41 type materials. *Journal of Molecular Catalysis A: Chemical*, **166**, 53-57.

Koh, C.A., R. Nooney and S. Tahir. 1997. Characterization and catalytic properties of MCM-41 and Pd/MCM-41 materials. *Catalysis Letters*, **47**, 199-203.

Kosslick, H., G. Lischke, B. Parlitz, W. Storek and R. Fricke. 1999. Acidity and active sites of Al-MCM-41. *Applied Catalysis A: General*, **184**, 49-60.

Koutsopoulos, K. 2002. Synthesis and characterization of hydroxyapatite crystals: A review study on the analytical methods. *Journal of Biomedical Materials Research*, **62**(4), 600-612.

Kruk, M., M. Jaroniec and A. Sayari. 1997. Adsorption Study of Surface and Structural Properties of MCM-41 Materials of Different Pore Sizes. *Journal of Physical Chemistry B*, **101**, 583-589.

Kruk, M., M. Jaroniec and A. Sayari. 1999. A Unified Interpretation of High-Temperature Pore Size Expansion Processes in MCM-41 Mesoporous Silicas. *Journal of Physical Chemistry B*, **103**, 4590-4598.

Kumar, D., K. Schumacher, C. du Fresne von Hohenesche, M. Grun and K.K. Unger. 2001. MCM-41, MCM-48 and related mesoporous adsorbents: their synthesis and characterization. *Colloids and Surfaces A: Physicochemical and Engineering Aspects*, **187-188**, 109-116.

Lensveld, D.J., J.G. Mesu, A. Jos van Dillen and K.P. de Jong. 2001. Synthesis and characterization of MCM-41 supported nickel oxide catalysts. *Microporous and Mesoporous Materials*, **44-45**, 401-407.

Lesage, S. 1991. Characterization of groundwater contaminants using dynamic thermal stripping and adsorption/thermal desorption-GC-MS. *Fresenius' Journal of Analytical Chemistry*, **339**, 516-527.

Letellier, F., J. Blanchard, K. Fajerwerg, C. Louis, M. Breysse, D. Guillaume and D. Uzio. 2006. Search for confinement effects in mesoporous supports: hydrogenation of *o*-xylene on $Pt^0$/MCM-41. *Catalysis Letters*, **110**(1-2), 115-124.

Li, W. and K.J. Klabunde. 1998. Ultrafine Zinc and Nickel, Palladium, Silver Coated Zinc Particles Used for Reductive Dehalogenation of Chlorinated Ethylenes in Aqueous Solution. *Croatica Chemica ACTA*, **71**(4), 853-872.

Lim, S., D. Ciuparu, C. Pak, F. Dobek, Y. Chen, D. Harding, L. Pfefferle and G. Haller. 2003. Synthesis and Characterization of Highly Ordered Co-MCM-41 for Production of Aligned Single Walled Carbon Nanotubes (SWNT). *Journal of Physical Chemistry B*, **107**, 11048-11056.

Lin, C.J., S. L. Lo and Y.H. Liou. 2004. Dechlorination of trichloroethylene in aqueous solution by noble metal-modified iron. *Journal of Hazardous Materials B*, **116**, 219-228.

Liu, J., Y. Yu, Y., Mu and H. He. 2006. Mechanism of Heterogeneous Oxidation of Carbonyl Sulfide on $Al_2O_3$: An *in situ* Diffuse Reflectance Infrared Fourier Transform of Spectroscopy Investigation. *Journal of Physical Chemistry B*, **110**, 3225-3230.

Long, R.Q. and R.T. Yang. 1999. Selective Catalytic Reduction of Nitric Oxide with Ethylene on Copper Ion-Exchanged Al-MCM-41 Catalyst. *Industrial and Engineering Chemistry Research*, **38**, 873-878.

Lowry G.V. and M. Reinhard. 1999. Hydrodehalogenation of 1- to 3-Carbon Halogenated Organic Compounds in Water Using a Palladium Catalyst and Hydrogen Gas. *Environmental Science and Technology*, **33**, 1905-1910.

Lowry G.V. and M. Reinhard. 2001. Pd-Catalyzed TCE Dechlorination in Water: Effect of $[H_2](aq)$ and $H_2$-Utilizing Competitive Solutes on the TCE Dechlorination Rate and Product Distribution. *Environmental Science and Technology*, **35**, 696-702.

Mackay, D.M. and J.A. Cherry. 1989. Groundwater contamination: Pump-and-treat remediation. *Environmental Science and Technology*, **23**(6), 630-636.

Mackay, D.M., R.D. Wilson, M.J.Brown, W.P. Ball, G. Xia and D.P. Durfee. 2000. A controlled field evaluation of continuous vs. pulsed pump-and-treat remediation of a VOC-contaminated aquifer: site characterization, experimental setup, and overview of results. *Journal of Contaminant Hydrology*, **41**, 81-131.

Mackenzie, K., H. Frenzel and F.D. Kopinke. 2006. Hydrogenation of halogenated hydrocarbons in water with Pd catalysts: Reaction rates and surface competition. *Applied Catalysis B: Environmental*, **63**, 161-167.

Mansour, F., R.M. Dimeo and H. Peemoeller. 2002. High-resolution inelastic neutron scattering from water in mesoporous silica. *Physical Review E*, **66**, 041307-1 – 041307-7.

Marin-Astorga N., G. Pecchi, J.L.G. Fierro and P. Reyes. 2005. A comparative study of Pd supported on MCM-41 and $SiO_2$ in the liquid phase hydrogenation of phenyl alkyl acetylenes mixtures. *Journal of Molecular Catalysis A: Chemical*, **231**, 67-74.

McNab, W.W. Jr and R. Ruiz. 1998. Palladium-catalyzed reductive dehalogenation of dissolved chlorinated aliphatics using electrolytically-generated hydrogen. *Chemosphere*, **37**(5), 925-936.

Mori, T., Y. Kuroda, Y. Yoshikawa, M. Nagao and S. Kittaka. 2002. Preparation of a Water-Resistant Siliceous MCM-41 Sample, through Improvement of Crystallinity, and Its Prominent Adsorption Features. *Langmuir*, **18**, 1595-1603.

Mukhopadhyay, K., B.R. Sarkar and R.V. Chaudhari. 2002. Anchored Pd Complex in MCM-41 and MCM-41: Novel Heterogeneous Catalysts for Hydrocarboxylation of Aryl Olefins and Alcohols. *Journal of the American Chemical Society*, **124**, 9692, 9693.

Nam, S.S., H. Kim, G. Kishan, M.J. Choi and K.W. Lee. 1999. Catalytic conversion of carbon dioxide into hydrocarbons over iron supported on alkali ion-exchanged Y-zeolite catalysts. *Applied Catalysis A: General*, **179**, 155-163.

Narayanan, M., L.C. Davis and L.E. Erickson. 1995. Fate of Volatile Chlorinated Organic Compounds in a Laboratory Chamber with Alfalfa Plants. *Environmental Science and Technology*, **29**, 2437-2444.

Okumara, K., H. Tokai and M. Niwa. 2003. Structural analysis of Pd loaded MCM-41 catalysts for hydrogenation of benzene by means of XAFS. *Photon Factory Activity Report*, **20**(B).

Page, G.W. 1981. Comparison of Groundwater and Surface Water for Patterns and Levels of Contamination by Toxic Substances. *Journal of the American Chemical Society*, **15**(12), 1475-1481.

Pankow, J.F. and J.A. Cherry. 1996. Dense Chlorinated Solvents and other DNAPLs in Groundwater. *Waterloo Press*. Portland, Oregon.

Panpranot J., K. Pattamakomsan, J. G. Goodwin Jr. and P. Praserthdam. 2004a. A comparative study of $Pd/SiO_2$ and Pd/MCM-41 catalysts in liquid-phase hydrogenation. *Catalysis Communications*, **5**, 583-590.

Panpranot, J., K. Pattamakomsan, P. Praserthdam and J.G. Goodwin Jr. 2004b. Impact of the Silica Support Structure on Liquid-Phase Hydrogenation on Pd Catalysts. *Industrial & Engineering Chemistry Research*, **43**, 6014-6020.

Phillips, D.H., D.B. Watson, Y. Roh and B. Gu. 2003. Mineralogical Characteristics and Transformations during Long-Term Operation of a Zerovalent Iron Reactive Barrier. *Journal of Environmental Quality*, **32**, 2033-2045.

Prati, L. and M. Rossi. 1999. Reductive catalytic dehalogenation of light chlorocarbons. *Applied Catalysis B: Environmental*, **23**, 135-142.

Rahiala, H., I. Beurroies, T. Eklund, K. Hakala, R. Gougeon, P. Trens and J.B. Rosenholm. 1999. Preparation and Characterization of MCM-41 Supported Metallocene Catalysts for Olefin Polymerization. *Journal of Catalysis*, **188**, 14-23.

Rajakovic, V.N., S. Mintova, J. Senker and T. Bein. 2003. Synthesis and characterization of V- and Ti-substituted mesoporous materials. *Materials Science and Engineering*, **C23**, 817-821.

Randall, M. and C.F. Failey. 1927. The Activity Coefficient of Gases in Aqueous Salt Solution. *Chemical Reviews*, **4**(3), 271-284.

Richardson, B.J. and G.J. Zheng. 1999. Chlorinated hydrocarbon contaminants in Hong Kong surficial sediments. *Chemosphere*, **39**(6), 913-923.

Robie, R.A., B.S. Hemingway and J.R. Fisher. 1978. Thermodynamic Properties of Minerals and Related Substances at 298.15 K and 1 Bar ($10^5$ Pascals) Pressure and at Higher Temperatures.*U.S. Geological Survey Bulletin*, **1452**, 456pp.

Run, M., S. Wu and G. Wu. 2004. Ultrasonic synthesis of mesoporous molecular sieve. *Microporous and Mesoporous Materials*, **74**, 37-47.

Sachs, C., A. Pundt, R. Kirchheim, M. Winter, M.T. Reetz and D. Fritsch. 2001. Solubility of hydrogen in single-sized palladium clusters. *Physical Review B*, **64**, 075408-1 – 075408-10.

Sakthivel, A., M. Abrantes, A.S.T. Chiang and F.E. Kuhn. 2006. Grafting ή-Cp(COOMe)MoCl$(CO)_3$ on the surface of mesoporous MCM-41 and MCM-48 materials. *Journal of Organometallic Chemistry*, **691**, 1007-1011.

Saravanamurugan, S., M. Palanichamy, M. Hartmann and V. Murugesan. 2006. Knoevenagel condensation over β and Y zeolites in liquid phase under solvent free conditions. *Applied Catalysis A: General*, **298**, 8-15.

Sayari, A., S. Hamoudi and Y. Yang. 2005. Applications of Pore-Expanded Mesoporous Silica. 1. Removal of Heavy Metal Cations and Organic Pollutants from Wastewater. *Chemistry of Materials*, **17**, 212-216.

Schreier, C.G. and M. Reinhard. 1995. Catalytic hydrodehalogenation of chlorinated ethylenes using palladium and hydrogen for the treatment of contaminated water. *Chemosphere*, **31**(6), 3475-3487.

Schuth, C., S. Disser, F. Schuth and M. Reinhard. 2000. Tailoring catalysts for hydrodechlorinating chlorinated hydrocarbon contaminants in groundwater. *Applied Catalysis B: Environmental*, **28**, 147-152.

Shen S.C. and S. Kawi. 2002. MCM-41 with Improved Hydrothermal Stability: Formation and Prevention of Al Content Dependent Structural Defects. *Langmuir*, **18**, 4720-4728.

Soeteman, S.C.J., E. De Greef and F.J.J. Brinkmann. 1981. Persistency of Organic Contaminants in Groundwater, Lessons from Soil Pollution Incidents in the Netherlands. *The Science of the Total Environment*, **21**, 187-202.

Sriwatanapongse, W., M. Reinhard and C.A. Klug. 2006. Reductive Hydrodechlorination of Trichloroethylene by Palladium-on-Alumina Catalyst: $^{13}C$ Solid-State NMR Study of Surface Reaction Precursors. *Langmuir*, **22**, 4158-4164.

Stumm, W. and J.J. Morgan. 1996. Aquatic Chemistry: Chemical Equilibria and Rates in Natural Waters, 3rd Edition. John Wiley and Sons, New York, USA, 1022 pp.

Takamuku, T., H. Maruyama, S. Kittaka, S. Takahara and T. Yamaguchi. 2005. Structure of Methanol Confined in MCM-41 Investigated by Large-Angle X-ray Scattering Technique. *Journal of Physical Chemistry B*, **109**, 892-899.

Trebosc, J., J.W. Wiench, S. Huh, V.S.Y. Lin and M. Pruski. 2005. Solid-State NMR Study of MCM-41-type Mesoporous Silica Nanoparticles. *Journal of the American Chemical Society*, **127**, 3057-3068.

Walbridge, C.T., J.T. Fiandt, G.L. Phipps and G.W. Holcombe. 1983. Acute Toxicity of Ten Chlorinated Aliphatic Hydrocarbons to the Fathead Minnow (*Pimephales promelas*). *Archives of Environmental Contamination and Toxicology*, **12**, 661-666.

Yu, C.C, S. Ramanathan, F. Sherif and S.T. Oyama. 1994. Structural, Surface, and Catalytic Properties of a New Bimetallic V-Mo Oxynitride Catalyst for Hydrodenitrogenation. *Journal of Physical Chemistry*, **98**, 13038-13041.

Yuan, Z. and W. Zhou. 2001. A novel morphology of mesoporous molecular sieve MCM-41. *Chemical Physics Letters*, **333**, 427-431.

Zeng, W., X.F. Qian, J. Yin and Z.K. Zhua. 2006. The drug delivery system of MCM-41 materials via co-condensation synthesis. *Materials Chemistry and Physics*, **97**, 437-441.

Zhang, W., J. Wang, P.T. Tanev and T.J. Pinnavaia. 1996. Catalytic hydroxylation of benzene over transition-metal substituted hexagonal mesoporous silicas. *Chemical Communications*, 979-980.

Zhang, W., C-B. Wang and H-L. Lien. 1998. Treatment of chlorinated organic contaminants with nanoscale bimetallic particles. *Catalysis Today*, **40**, 387-395.

Zhao, X.S., G.Q. Lu, A.K. Whittaker, G.J. Millar and H.Y. Zhu. 1997. Comprehensive Study of Surface Chemistry of MCM-41 Using $^{29}$Si CP/MAS NMR, FTIR, Pyridine-TPD, and TGA. *Journal of Physical Chemistry B*, **101**, 6525-6531.

Zhao, X.S., F. Audsley and G.Q. Lu. 1998. Irreversible Change of Pore Structure of MCM-41 upon Hydration at Room Temperature. *Journal of Physical Chemistry*, **102**, 4143-4146.

Zheng, J., S. Zhai, Y. Zhang, D. Wu, Y. Sun, Y. Yang, L. Chen and F. Deng. Hydrothermally stable MCM-41 analogue with extensive embedded voids. *Catalysis Today*, **93-95**, 529-534.

Ziolek, M., I. Nowak, B. Kilos, I. Sobezak, P. Decyk, M. Trejda and J.C. Volta. 2004. Template synthesis and characterization of MCM-41 mesoporous molecular sieves containing various transition metal elements – TME (Cu, Fe, Nb, V, Mo). *Journal of Physics and Chemistry of Solids*, **65**, 571-581.